6-30-2016

Ecohydrology And Groundwater Dynamics In A Salt Marsh Island

Andrea L. H. Hughes
University of South Carolina

ECOHYDROLOGY AND GROUNDWATER DYNAMICS IN A SALT MARSH ISLAND

by

Andrea L. H. Hughes

Bachelor of Science
University of Kentucky, 2001

Master of Science
University of Rhode Island, 2006

Submitted in Partial Fulfillment of the Requirements

For the Degree of Doctor of Philosophy in

Geological Sciences

College of Arts and Sciences

University of South Carolina

2016

Accepted by:

Alicia M. Wilson, Major Professor

Willard S. Moore, Committee Member

Howie D. Scher, Committee Member

James T. Morris, Committee Member

Lacy Ford, Senior Vice Provost and Dean of Graduate Studies

DEDICATION

I lost the love of my life, my husband Austin L. Hughes, on October 31, 2015. This work is dedicated entirely to him. His patient understanding, his unwavering love and generous encouragement are what made this possible. His heart was so big, I never thought it would stop beating. I love you, Austin! You are my sunshine.

ACKNOWLEDGEMENTS

I want to thank my advisor, Dr. Alicia M. Wilson, for the opportunity to pursue and complete this work with her guidance. I am grateful for the comments from and conversations with my thesis committee members, Dr. Willard S. Moore, Dr. Howie Scher, and Dr. James. T. Morris. The surveying work of my study site, performed by Dr. Ray Torres and his students as well as the late Dr. Robert Trenkamp, made much of this work possible. I was generously assisted in the field by Nickles Badger, Curtis Gebhard, Katrina Byerly, Weihong Wang, Dr. Scott White, Whitney Kiehn, Ipsita Gupta, Dr. Mei Zhang, Joseph Anderson, Gary Price, and my beloved husband, Dr. Austin L. Hughes. Karen Sundberg was also instrumental to this work by her assistance in the field and laboratory. Chapter One benefited from discussions with the late Dr. L. Robert Gardner and the 2010 Fall Hydro Seminar at Stanford University. Various anonymous reviewers significantly improved Chapters One and Two by their comments. This work is based upon research supported by South Carolina Sea Grant Project R/ER-30 to A.M. Wilson, an NSF Grant to J.T. Morris, and a NOAA NERR Fellowship (Award No. NA09NOS4200050).

ABSTRACT

Tidal salt marshes are extraordinarily productive and valuable ecosystems that provide via groundwater a not insignificant portion of coastal solute and nutrient budgets. Among the many goods and services they provide are habitat for diverse wildlife, protection for coastal communities during storms, and protection for coastal surface waters by filtering anthropogenic pollutants. One threat to the health of tidal salt marshes along the East Coast have been episodes of Acute Marsh Dieback (AMD) from 1999 to 2001. Dieback was observed at North Inlet salt marsh from 2000 to 2001. Since salt marsh hydrology is dominated by the local tidal regime, it is important to understand how variations in hydrology impact marsh ecosystem health as well as how these variations impact both groundwater discharge and the distribution of solutes in the subsurface. In particular, the four naturally-occurring Ra isotopes (^{223}Ra, ^{224}Ra, ^{226}Ra, and ^{228}Ra) are considered valuable tracers of water movement and age in coastal systems but their accuracy has been hindered by their spatial and temporal variability.

From 2007 to 2011, a combined field and modeling study was performed on a marsh island in North Inlet salt marsh near Georgetown, South Carolina to better understand the impact of hydrology. A set of 21 piezometers were installed at depths of 1, 2, and 4 m below the marsh surface to measure in-situ pore pressure, temperature and salinity, and to collect water samples to measure salinity, temperature, pH, redox potential, and the activity of the four Ra isotopes. Along with publically available tide and meteorology data and conservative statistical tests, these measurements were used to

(1) calculate hydraulic head, (2) determine groundwater flow paths and discharge rates, (3) calibrate a numerical groundwater flow model, (4) better understand the relationship between hydrology and AMD, and (5) determine the relationship between marsh hydrology and the temporal and spatial variations in porewater Ra activity to improve its use as a coastal groundwater tracer.

TABLE OF CONTENTS

LIST OF TABLES

LIST OF FIGURES

INTRODUCTION

For centuries, human beings have lived along coastlines to take advantage of coastal waterways and oceans for food, transportation and trade, and recreation. By 2010, approximately 39 percent of the population in the United States lived in counties directly in contact with the coast (NOAA National Ocean Service). This distribution in human population subjects finite coastal resources to increasing stresses (Vernberg and Vernberg, 2001) that include surface and groundwater pollution, eutrophication, increased coastal erosion rates, invasive plant and animal species, and over-fishing of native populations of finfish and invertebrates.

The coastal zone can be defined simply as the transition area between the continents and oceans. Shorelines and habitats in coastal zones vary extensively from rocky shorelines to sandy beaches and may include bays, salt ponds, estuaries, and intertidal wetlands. Among these habitats, salt marsh estuaries are among the most productive ecosystems on the planet with net primary productivity of 200 – 3500 g C m^{-2} y^{-1} (Valiela, 1984). Because of this incredible productivity, tidal marshes are an important source of nutrients to coastal surface waters via run-off at low tide and groundwater discharge. Groundwater-borne nutrient fluxes from South Carolina salt marshes have been shown to equal the nutrient fluxes from the state's four major rivers (Krest et al., 2000).

In addition to their incredible productivity, salt marshes also protect people and property from storms and sea level rise (Arkema et al., 2013), and marshes also play a

role in climate regulation through the $CO_2 - O_2$ balance and production of dimethylsulfide (a gaseous source of sulfur to the atmosphere providing nucleation sites for cloud development) (Costanza et al., 1997; de Groot et al., 2002). By the late 1990s to early 2000s, researchers began to calculate the monetary value of the functions and services provided by salt marshes and all coastal ecosystems (Costanza et al., 1997; de Groot et al., 2002). Around the same time, salt marshes in the S.E. United States experienced several large die-off events that lead to increased interest and research attention to intertidal salt marshes (McKee et al., 2004; Ogburn and Alber, 2006; Alber et al., 2008). Although these southeastern intertidal marshes are typically flooded by tide water twice each day, periods of drought were often associated with these die-off events.

Sometime in 2000 to 2001, South Carolina's salt marshes also experienced smaller die-off episodes (Morris and Walker, 2006). The relatively pristine nature of the North Inlet salt marsh near Georgetown, South Carolina, makes it an ideal location to try to answer some outstanding questions about marsh hydrology and about AMD. The primary goals of this research were to determine: how temporal and spatial variations in coastal hydrology affect groundwater discharge, and by extension, nutrient discharge from highly productive marsh ecosystems; how drought may play a role in marsh die-off events in spite of the fact that these marshes are regularly inundated; and how variations in hydrology and groundwater flow may play a role in the variability and distribution of the four naturally-occurring Ra isotopes (^{223}Ra, ^{224}Ra, ^{226}Ra, and ^{228}Ra)—an isotope considered to be a valuable tracer of water movement and age in coastal systems. This work is presented in the following three chapters in manuscript form.

CHAPTER 1

HYDROLOGIC VARIABILITY IN A SALT MARSH:

ASSESSING THE LINKS BETWEEN DROUGHT AND ACUTE MARSH DIEBACK[1]

[1] Hughes, Andrea L. H., Alicia M. Wilson, and James T. Morris, 2012. Hydrologic variability in a salt marsh: Assessing the links between drought and acute marsh dieback. Estuarine, Coastal and Shelf Science 111(2012) 95-106.

1.1 ABSTRACT

It has been hypothesized that acute marsh dieback (AMD) observed along the Gulf Coast and South Atlantic Bight in the early 2000s was the result of drought-induced changes to porewater and sediment chemistry through hypersalinity or through mobilization of metals and acidification associated with redox changes. The impact of drought on coastal wetlands remains unclear because the hydrology of these wetlands is strongly influenced by regular tidal inundation. In order to test the links between hydrologic variability and changes to marsh groundwater conditions that may be stressful to the salt marsh grass Spartina alterniflora, we installed piezometers and passive diffusion samplers in a salt marsh island at North Inlet, South Carolina, where AMD was observed in fall 2001. Significant variations in tidal inundation, rainfall, evapotranspiration, groundwater dynamics, and porewater chemistry were observed. The island was typically inundated twice daily, but there were occasional 19 - 21 h periods in winter and spring when the marsh was not inundated and a singular event when the marsh was not inundated for three days (March 2008). Enhanced exposure resulted in seasonal redox chemistry changes, as indicated by changes in the ratio of ferrous iron [Fe(II)] to total iron [Fe(II) + Fe(III)], but our observations do not support redox and pH changes as the cause of AMD at this site. Porewater salinity varied from 14 to 40 in the upper 1 m of the marsh. Salinity was most variable near the surface and increased with depth, reflecting root zone transpiration and downward movement of porewater through the marsh mud into the underlying confined sand aquifer. Pearson Correlation tests among porewater constituents and hydrologic parameters indicated significant associations between porewater salinity, tidal inundation, rainfall, and ET, and additional associations

between porewater iron concentration, speciation, and tidal inundation. Linear regression model estimates of porewater salinity for 2001 – 2002 did not indicate the development of hypersalinity during that period. However, these estimates did predict a dramatic increase in salinity that coincided with the beginning of drought conditions just prior to the observation of AMD, suggesting this as a cause for AMD at this site. Drought is predicted to increase over the next century; damage caused by potential increases in the frequency of drought-related AMD may limit the ability of intertidal salt marshes to accommodate sea level rise.

1.2 Introduction

Intertidal salt marshes are highly productive ecosystems of great economic importance for coastal communities (Vernberg and Vernberg, 2001). They perform a variety of ecological functions and services including storage and filtration of water, nutrient cycling, dampening of flood and storm effects, retention of soil, opportunities for recreation, and habitat and nursery space for fish, invertebrates, and marine mammals (Costanza et al., 1997; de Groot et al., 2002; Wieski et al., 2010). The monetary worth of these tidal marsh services was estimated to be nearly \$10,000 ha^{-1} yr^{-1} in 1994 dollars (Costanza et al., 1997). In view of their value, the damage to salt marshes caused by acute marsh dieback (AMD) is a concern to the long-term welfare of coastal communities.

Acute marsh dieback (AMD) principally affects the marsh grass *Spartina alterniflora,* and is discernible by the suddenness and large spatial extent of plant mortality (Mendelssohn and McKee, 1988; Ogburn and Alber, 2006; Smith, 2006; Alber et al., 2008). Beginning in 2000, widespread AMD severely damaged 43,000 ha of salt marsh in the Mississippi River delta plain (McKee et al., 2004). In 2001 – 2002, intertidal

marshes in South Carolina and Georgia also experienced significant areas of acute marsh dieback (Morris and Walker, 2006; Alber et al., 2008). These events brought both greater public attention and increased research efforts to the phenomenon of AMD.

Proposed triggers for dieback have ranged from biological agents to porewater geochemical changes. Herbivory of *S. alterniflora* by periwinkle snails (*Littoraria irrorata*) provided a significant top-down control on plant productivity in a series of snail inclusion/exclusion and plot fertilization experiments (Silliman and Zieman, 2001; Silliman and Bortolus, 2003; Silliman et al., 2005; Gustafson et al., 2006). However, a study conducted at a healthy marsh site without experimental cages showed no significant effect on plant productivity with increasing snail density (Kiehn and Morris, 2009), suggesting that snail herbivory is not a trigger for AMD. Pathogens have also been hypothesized as a biological AMD trigger (Alber et al., 2008). Several species of *Fusarium* fungi cultured from dead and dying plants in Louisiana, as well as from several mid- and north-Atlantic AMD sites, have been found to be strongly associated with *S. alterniflora* at dieback sites. However, Elmer and Marra (2011) concluded that in order for these fungi to be harmful, the plants must already be stressed by some other process. In the southeastern U.S., the recent occurrences of AMD were associated with extraordinary periods of drought, suggesting a link between AMD and marsh hydrology.

Drought has the potential to change marsh porewater chemistry in two ways that could cause dieback. First, drought may dry the marsh surface, allowing air entry to occur, thereby changing the redox state of soil and porewater. Such redox changes have been shown to acidify porewater, which may be directly toxic to the plants (Mendelssohn and Morris, 2000; Brown et al., 2006) and can also mobilize potentially toxic metals such

as Fe, Al, and Mn (Portnoy and Valiela, 1997). However, a prior study indicated that metal uptake by *S. alterniflora* roots was inhibited during soil drying (Brown et al., 2006), suggesting metal toxicity may not trigger AMD under drying conditions. Soil and water chemistry measurements in Louisiana showed that dieback area soils became acidified upon oxidation, but the soil at the control sites in a healthy marsh did not. This difference was caused by greater pyrite concentrations in the dieback soils that oxidized to create acidic soil and water conditions (McKee et al., 2004).

The second way in which drought-induced porewater chemistry may initiate dieback is by increasing porewater salinity when evapotranspiration proceeds during periods with little or no precipitation. *S. alterniflora* is known to be highly salt-tolerant, but it can experience salt stress at sub-lethal salinities less than 40 (Linthurst and Seneca, 1980; Hester et al., 2001); significant mortality occurs at salinities greater than 60 (Phleger, 1971; Linthurst and Seneca, 1980; Webb, 1983; Hester et al., 1998). A combination of drying and high salinity is also possible during a drought. In a study during which *S. alterniflora* plants were subjected to two different salinity treatments (3 – 5 and 35 – 38) and soil drying treatments that lasted 8, 16, and 24 days, the survival rate for *S. alterniflora* fell to below 30 percent during a combined treatment of elevated salinity and soil drying (Brown and Pezeshki, 2007). In addition, a large, rapid increase in porewater salinity can result in marsh plant mortality. In a greenhouse experiment designed to study salt pulses and recovery in an oligohaline marsh, one treatment subjected oligohaline macrophytes (*Eleocharis palustris, Panicum hemitomon, Sagittaria lancifolia,*and *Scirpus americanus*) to a rapid salinity increase (3 days) from 0 to 12 and maintained the elevated salinity for a period of 3 months. Significant loss of aboveground

biomass occurred after the first month, and plant mortality under this treatment was 67% and 100% for *Sagittaria* and *Panicum*, respectively. The authors suggest that mortality and recovery of oligohaline marsh grass species depends on the extent and rapidity of the salt pulse and duration of the elevated salinity (Howard and Mendelssohn, 1999). These greenhouse studies and post-dieback measurements show that prolonged drought does have the potential to trigger AMD, but they did not consider the interaction of drought and tidal inundation experienced in a natural tidal marsh setting. Significant redox changes or hypersaline conditions may not have time to develop in the root zone during the few hours of exposure at each low tide.

This paper presents the results of a field study designed to explore the links between 1) variations in marsh hydrology and 2) porewater redox changes and hypersalinity within the marsh root zone as potential causes of acute marsh dieback. The study was conducted at an AMD site within North Inlet Salt Marsh, Georgetown, South Carolina (Fig. 1.1). At this site, we monitored porewater pressure, salinity, and iron; determined marsh stratigraphy; surveyed marsh elevation; and compiled meteorological and tidal records. Because iron is a redox-sensitive metal, both ferrous [Fe(II)] and total iron [Fe(II) + Fe(III)] were measured as proxies for the redox conditions within the soil and porewater. Hydraulic head was calculated to determine water table elevation and the potential for soil drying. Statistical analyses were then performed to quantify relationships between precipitation, evapotranspiration, tide, and shallow porewater iron and salinity. Finally, a regression model was created to hind-cast porewater salinity to the time of South Carolina's drought and onset of AMD beginning in fall 2001.

1.3 Study Area

The study was conducted on a marsh island within the North Inlet-Winyah Bay National Estuarine Research Reserve near Georgetown, South Carolina (Fig. 1.1a). The reserve consists of 12,000 acres of tidally-dominated marsh and wetland. It experiences a semi-diurnal mixed tide with a period of 12.24 hours, an average range of 1.4 m, and has an average surface water residence time of two days (Palmer et al., 1980; North Inlet-Winyah Bay National Estuarine Research Reserve, 2010a). This intertidal salt marsh represents a Holocene transgression sequence that overlies reworked late Pleistocene beach ridge sands (Gardner and Porter, 2001). Of two acute marsh dieback locations that developed beginning in fall 2001 at North Inlet (Morris and Walker, 2006), the northern site was chosen for this study based on its ease of access and natural hydraulic boundaries at nearby creeks (Fig. 1.1b).

Plant mortality at this site was confined to the center of the marsh and did not affect the plants growing along the creek banks (Fig. 1.1b). We considered three potential reasons for this pattern. First, porewater solute distribution within a salt marsh has been shown to be controlled by differences in tidal flushing caused by differences in distance from marsh creeks (King et al., 1982a; Gardner et al., 1988). Second, subtle topographic differences in the marsh surface could bring about persistent hypersaline tide pools in the center of the marsh. Infiltration of this water in conjunction with evapotranspiration could result in extreme hypersaline porewater confined to that area. Third, marsh stratigraphy has been shown to control groundwater flow patterns and discharge locations that could, in turn, influence the development of both reduced and hypersaline groundwater

conditions in areas of very limited flow. For these reasons, initial site installations included the collection of sediment cores and a survey of the marsh surface.

1.4. METHODS

Site Characterization and Monitoring

Beginning in 2006, seven sediment cores were collected to determine the stratigraphy of the site, and piezometer nests were then installed where the sediment cores were collected (Fig. 1.1b). Each nest contains three piezometers constructed from 1.25-inch internal diameter PVC and screened at depths of 1 m, 2 m, and 4 m, respectively. The top of each piezometer was capped, vented, and stood at least 50 cm above the marsh surface to keep the wells from being overtopped during normal spring tide conditions. Well-bore storage within the piezometers was minimized using internal casings constructed of 0.75-inch internal diameter PVC for the suspension of dataloggers.

Hydraulic head was calculated from in-situ measurements of pore pressure and temperature along with surveyed marsh elevation. Pressure, temperature, and barometric pressure readings were made at 10- or 20-minute intervals beginning in May 2007 and ending in May 2008. Marsh surface and piezometer nest elevations were surveyed using both Differential GPS and Real-Time Kinematic GPS surveying equipment benchmarked to NOAA's Tidal Benchmark "A Tidal" (PID# 1345). All elevations were measured in meters relative to NAVD88. Finally, total hydraulic head was calculated, using in-situ pressure, temperature, and elevation, as $h = z + h_p$, where h is total head, z is elevation head, and h_p is pressure head.

Following piezometer installation, triplicate passive-diffusion samplers were permanently installed within the AMD area of the site, roughly 3 m southeast of

piezometer nest NS2 (Fig. 1.1b). Although installed within the perimeter of the dieback zone, the samplers were surrounded by re-growth of *S. alterniflora* after approximately one year. The samplers are side-vented with removable inner casings constructed of 1.25-inch diameter and 1-inch diameter PVC pipe. Slots in the inner casing hold deionized water-filled scintillation vials (22 mL) capped with 45 μm Nitex screen and aligned with sections of horizontal slots in the outer casing at depths of 10, 25, 50, 75, and 100 cm below the marsh surface. From August 2006 to June 2010, samples were allowed to equilibrate with the surrounding porewater for one month and then sub-sampled for analyses of ferrous iron, total iron, and chloride as a proxy for salinity. Our samplers, therefore, recorded an exponential moving average of the 30 days prior to sample collection. The nutrients sulfide, ammonium, and phosphate were also measured but are not presented here. Chloride concentration was measured by coulometric titration and salinity was calculated using the theory of constancy of seawater composition (Salinity‰=1.80655 x Cl^-). Iron was measured using a modification of a new ferrozine method (Viollier et al., 2000).

Hydrologic data were obtained from the NERR Central Data Management Office database to determine the extent of natural variability in tide, precipitation, evapotranspiration, and surface water salinity during the study period. Meteorological and water quality data were acquired for the Oyster Landing and Clambank Creek stations within the reserve (Fig. 1.1a) (NOAA, 2010). Corresponding tide data were acquired from NOAA's Tides and Currents database for the Oyster Landing station (CO-OP ID 8662245) and the Springmaid Pier station (CO-OP ID 8661070) (National Oceanic and Atmospheric Administration, 2010b). The Oyster Landing tide record began

in May 2001, so the tidal record prior to that date was modeled by adding the tide residuals from the Springmaid Pier site (observed tide – predicted tide = residual) to the Oyster Landing predicted tide record. Model fit was tested by comparing two years of modeled tide with two years of measured tide for Oyster Landing (2006 – 2007), and the regression showed an r^2 value of 0.96. Palmer Drought Severity Index data were obtained from NOAA's Drought Information Center website (National Oceanic and Atmospheric Administration, 2010a).

Potential evapotranspiration was estimated from continuous measurements of air temperature and solar radiation (Oyster Landing station) using a modified Turc method (Turc, 1961; Douglas et al., 2009b):

$$ET=0.013\cdot(23.88\cdot R_S + 50)\cdot(T/(T+15)) \quad (1.1)$$

where ET is potential evapotranspiration in mm/day, R_S is solar radiation in MJ m^{-2} d^{-1}, and T is average daily air temperature (geometric mean daily air temperature).

Statistical Methods

We considered 41 variables derived from surface water salinity, rainfall, tide, and calculated ET (Eq. 1) data as well as porewater salinity, ferrous iron [Fe(II)], and total iron [Fe(II) + Fe(III)] measured at the five sampler depths. The passive-diffusion samplers were deployed for 30-day periods, so hydrologic and tidal data were parsed into sums and means of 1, 15, 30, 60, and 90 day increments just prior to the diffusion sample collection dates. Note that we also considered the possibility that porewater samples might be impacted by past conditions, because our hydraulic head observations indicated

that water entering the marsh surface moves downward through the marsh mud. Therefore, 30-day means or sums were calculated beginning 60 and 90 days prior to collection of the porewater samples to evaluate this possible lag. These variable names end in "30:60" or "30:90". The resulting terms are indicated by the abbreviation for the hydrologic variable followed by a number indicating the length of the period of interest (Table 1.1). Solar radiation data were missing for a portion of 2006, making it impossible to calculate 90-day average ET for use in the statistical analyses (the first porewater sample collection date was 9/11/2006).

Statistical analyses were used to identify links between the hydrologic variables defined in Table 1.1 and porewater salinity and iron. Additional analyses were performed to assess links between vertically adjacent porewater salinity measurements. All data were tested for normality using the Kolmogorov-Smirnov normality test (Dytham, 2003) based on a null-hypothesis (H_0) of normal distribution at a significance level of $\alpha = 0.01$ (if the p value from any test is less than the predetermined significance level, the null-hypothesis is rejected). If any dataset was found to be right-skewed, a geometric, rather than arithmetic, mean was used. Preliminary analyses using multiple one-way ANOVAs indicated a seasonality to most of the data. Seasons were defined as spring (March, April, and May), summer (June, July, and August), fall (September, October, and November), and winter (December, January, and February). Associations between hydrologic variables and porewater salinity and iron were then tested by season using the Pearson Correlation test (H_0 = no correlation, $\alpha = 0.05$) (Dytham, 2003). Next, the correlation results were used as a guide to perform linear regression analyses (Neter et al., 1996) by season between the hydrologic variables and porewater salinity in the root zone (10 and

25 cm depths) (H_0 = no linear relationship, $\alpha = 0.05$). Finally, the regression equations were used to estimate porewater salinity at 10 and 25 cm during 2001 – 2002.

1.5. RESULTS

Stratigraphy and Topography

The sediment cores showed that the marsh is topped with mud and silt of varied thickness (1.5 to 4 m) that overlies a fine-grained, well-sorted sand aquifer at depth (Fig. 1.2). The sand was present in all cores, with the exception of sites EW3 and NS3, and represents the re-worked Pleistocene beach ridge sand described previously by Gardner and Porter (2001). Between 20 and 60 cm of marsh mud containing *S. alterniflora* roots was found at the top of each core. The thinnest root zone was found in the core collected within the dieback zone at the center of the site (NS2) reflecting the impact of dieback on the plants even five years after the event.

The median elevation of the marsh surface was 24 cm (NAVD88, 95% confidence interval from 23.9 to 24.4 cm) or nearly 35 cm above mean sea level. Change in elevation along the N-S transect was 13 cm, and along the E-W transect was only 3 cm (Fig. 1.2). The highest elevations were found atop the levees closest to the largest creeks along the southern and western sides of the site (~35 cm NAVD88 or ~ 46 cm MSL). These results indicate that a persistent tidal pool was unlikely to develop in the central marsh where dieback occurred, and that surface inundation and drainage begin to the north and east of the marsh.

Hydraulic Head

The hydraulic head records show very different behavior when the marsh is inundated than when it is exposed. Typical hydraulic head profiles and corresponding

tidal records are presented in Figure 1.3a – c. During the period of 9/29/2007 to 10/5/2007, there was one spring tide (9/29), and one neap tide (10/5). While the marsh was inundated, hydraulic head in each piezometer closely matched the shape and level of the incoming tide, and consequently closely matched one another, indicating no significant vertical groundwater movement during inundation. Although some recharge occurs during inundation (Hemond et al., 1984), most of this signal reflects the added weight of the water column above the marsh surface.

During marsh exposure, our hydraulic head observations indicated extremely low flow in the central marsh, with much greater porewater drainage near the marsh creeks. This pattern was controlled by both marsh stratigraphy and nest proximity to one of the tidal creeks. During low tide, hydraulic gradients at EW1, EW4, NS1, and EW2 indicated downward movement of groundwater through the marsh mud and a significant connection between the confined sand aquifer and nearby surface water (Fig. 1.3a). These 4 nests are located within 45 m of one of the surrounding creeks, and sediment cores indicated the presence of sand at depth (Fig. 1.2). At nests NS2, EW3, and NS3, the hydraulic head at all depths typically fell to 2 to 3 cm below the marsh surface during low tide, and vertical gradients were small to zero (Fig. 1.3b). The lack of significant drainage at sites NS3 and EW3 can be explained by the absence of sand within the upper 4 m and at NS2 by its location at a maximum distance from any of the surrounding marsh creeks. The small, nearly identical drop in head at these nests reflects either ET (Dacey and Howes, 1984) or evaporation in the locations lacking live plants.

Because drying of the marsh surface is one hypothesized trigger for AMD, we examined the tidal and well data to identify whether there were periods when drying was

likely to be significant, particularly at nest NS2 in the dieback area. These records revealed occasional neap tide events when the marsh was not inundated during the lower, semi-diurnal mixed high tide, leaving the marsh surface exposed for 19 – 21 hours. The frequency of these non-inundating high tides (NIHT) varied seasonally, owing to seasonal variations in MSL, with greater incidence during the winter and spring months than the summer and fall months. The hydraulic head and tidal records for 3/24/2008 – 4/5/2008 contain one neap tide on 3/29 and examples of the 19 – 21 hour periods of exposure between 3/30 and 4/03 (Fig. 1.3d and e). An even more remarkable tidal event occurred in March 2008 when the marsh was not inundated for a period of three days (3/27/2008 – 3/30/2008). During this extended period of marsh exposure, hydraulic head at NS2, EW3, and the 1m piezometer at EW2 dropped to between 8 and 15 cm below the marsh surface. This drop in hydraulic head was far larger than the typical 2 to 3 cm response at these locations. An examination of the tidal record, beginning in January 2001, indicated that no similar period of extended exposure occurred during a span of over 9 years.

Distributions of Porewater Salinity and Iron

Overall, mean porewater salinity was lower and more variable near the marsh surface than at depth (Fig. 1.4a). This observation suggests that rainfall infiltrates the marsh to a greater extent than we originally expected for a marsh that is commonly flooded two times each day. Salinity ranged from 14 (3/16/2009 at 10 cm depth) to 40.1 (9/26/2007 at 75 cm depth) and varied seasonally. The highest salinities were typically measured during the summer and the lowest measured during the spring. The two hypersaline porewater values measured during this study (40.1 at 75 cm in 9/2007; 39.9

at 50 cm in 1/2008) occurred while the site experienced moderate drought, supporting the idea that drought can be stressful for *S. alterniflora*.

Inferences about porewater redox conditions and pH changes may be made via measurements of ferrous iron [Fe(II)] and total iron [Fe(II)+Fe(III)]. The concentration and valence state of iron within porewater is controlled by its abundance within the sediments and the redox state of the sediment and porewater (Kostka and Luther, 1994, 1995; Luther et al., 1996; Portnoy and Valiela, 1997). A common redox reaction within shallow marsh sediments is pyrite oxidation (Eq. 2):

$$FeS_2 + 7/2\ O_2 + H_2O \leftrightarrow Fe^{2+} + 2SO_4^{2-} + 2H^+ \quad (1.2)$$

which reduces porewater pH and releases ferrous iron that can be quickly oxidized (Eq. 3).

$$Fe^{2+} + 1/4\ O_2 + H^+ \leftrightarrow Fe^{3+} + 1/2\ H_2O \quad (1.3)$$

Free ferric iron may be precipitated as iron oxides or oxyhydroxides, or it may aid in further oxidation of pyrite (Eq. 4).

$$FeS_2 + 14Fe^{3+} + 8H_2O \leftrightarrow 15Fe^{2+} + 16H^+ \quad (1.4)$$

These reactions not only reduce the pH, but may also temporarily increase the concentration of ferric iron in porewater, which was seen in the results of the current

study. Once the marsh is re-inundated, pH can begin to return to levels prior to air entry, and the typical reducing conditions return.

Measurements of iron concentration and speciation showed variations with depth and season. Ferrous iron [Fe(II)] ranged from 0.4 μM (75 and 100 cm) to 15 μM (10 cm), and total iron [Fe(II) + Fe(III)] ranged from 0.4 μM (75 and 100 cm) to 16 μM (10 cm). The highest iron concentrations and greatest variability were found at 10 cm and decreased with depth (Fig. 1.4b and c). In addition, mean concentrations of ferrous and total iron were generally higher during winter and spring than in summer and fall. Plots of ferrous versus total iron (Fig. 1.5) indicate that ferrous iron comprised the majority of total iron measured during summer and fall, but during winter and spring, ferric iron [Fe(III)] comprised up to 66% of the total, as indicated by departures from the 1:1 line. Higher iron concentrations and an increase in the oxidized form of iron during the winter and spring months correspond to annual periods of greater marsh surface exposure demonstrating the impact of additional soil and porewater oxidation during these months.

Controls on Porewater Salinity in the Root Zone

Visual inspection of the field data suggests that porewater salinity within the *S. alterniflora* root zone was controlled by interactions between surface water salinity, precipitation, and evapotranspiration, and these interactions were either enhanced or moderated by the frequency of tidal inundation (Fig. 1.6). From February to March 2009, porewater salinity at 10 cm dropped from 20 to 14. Over the 30 days prior to the March 2009 sample collection there were 14 NIHTs and 9 cm of precipitation (65-year monthly average for February is 9 cm (South Carolina State Climate Office, 2012)). This freshening indicates that rainfall infiltration is enhanced during periods with significant

surface exposure. From August to September 2007, porewater salinity at 25 cm increased from 31 to a hypersaline value of 39. During the 30 days prior to sample collection in September 2007, there were no NIHTs, 13 cm of precipitation (1.5 inches more than in February 2009), and ET rates over the prior 90 days that were some of the highest during this study. These observations show that in spite of greater rainfall, when compared with February 2009, regular tidal inundation moderated the effect of increased rainfall, and high ET rates resulted in hypersaline porewater.

Statistical Analyses

Salinity

Correlation test results revealed associations between porewater salinity and hydrology that supported the field observations. Significant test results with the highest correlation coefficients at the 10 and 25 cm sample depths are presented in Table 1.2. At 10 cm for both spring and summer, the number of NIHTs and precipitation (PPT) were negatively correlated with porewater salinity. This supports field data indicating that rainfall infiltration was enhanced during periods of increased marsh exposure (Fig. 1.6: March 2009). During the fall, surface water salinity (SS) and ET were positively correlated with porewater salinity, which corresponds to field results in which porewater salinity exceeded surface water salinity during a period of regular tidal inundation and ET (Fig. 1.6: October 2007). During the winter months, surface water and porewater salinity were positively correlated, which indicates that tidal inundation was the primary control. The strongest association for porewater at 25 cm was with the 10 cm sample, which is consistent with net downward flow of porewater. This association was true for all seasons except winter when no significant associations were found.

Results of linear regression analyses, including equations, are listed in Table 1.3. All equations were significant except for 25 cm during fall (P = 0.082) and winter (P=0.228). Regression equations do not always accurately predict the extremes in the independent variable, in this case porewater salinity. However, model fit by season was good ($r^2 > 0.65$) for seven of the eight model equations, indicating that these equations have strong predictive power (Prairie, 1996) (Fig 1.7). The exception to this result was the 25 cm regression equation for winter ($r^2 = 0.345$), a depth and season combination which also lacked significant associations in the correlation tests as well.

Porewater salinity was estimated using the regression model equations (Table 1.3) to assess whether extreme hypersalinity or large increases in salinity occurred during the 2001 – 2002 drought. Salinity estimates for 10 cm ranged from 4 – 28 and for 25 cm from 11 – 37, which were generally fresher than, but comparable to, field measurements from 2006 – 2010 (Fig. 1.8). Although these results did not indicate that prolonged hypersalinity occurred in the root zone, two sharp salinity increases were predicted.

Between August and September of 2001 and 2002, predicted porewater salinity at 10 and 25 cm increased by 21 and 24 and by 16 and 23, respectively. For three months prior to each increase, porewater salinity estimates were significantly fresher, ranging from 4 to 16 and from 9 to 18 during 2001 and 2002. Note that the lowest porewater salinity measured during 2006 – 2010 was 14. These estimated increases occurred during periods with regular tidal inundation and ET rates between 3.5 and 5 mm/day—conditions under which hypersalinity was observed during the current study. In 2001, the increase in porewater salinity coincided with the beginning of drought conditions and immediately preceded the observation of AMD at this site. In 2002, the increase is

coincident with the return of non-drought conditions. No additional dieback was observed in the fall of 2002 at North Inlet, which may be explained by the fact that the remaining live plants after the fall/winter 2001-2002 event were more resistant to this extraordinary osmotic stress.

Iron

Results of Pearson Correlation tests between porewater iron and hydrology also supported field observations indicating that increased marsh exposure influenced the concentration and speciation of this redox-sensitive metal. During winter and spring, the number of NIHTs was positively correlated with both ferrous [Fe(II)] and total iron [Fe(II)+Fe(III)]. Additional controls on porewater iron concentrations were indicated by the correlation tests. The potential effects of porewater iron dilution by rainfall and low-iron seawater could explain the significant, negative correlation between surface water salinity (SS) and rainfall (PPT) during summer and fall. Conversely, evaporative concentration could explain the significant, positive correlation between ET and ferrous iron at 25 cm during fall.

1.6 Discussion

Salt Marsh Groundwater Dynamics and Marsh Redox Chemistry

Seasonal changes in porewater redox chemistry occurred annually during winter and spring at this site, which, along with the known presence of pyrite within the sediments (Gardner et al., 1988), suggests accompanying changes in pH occurred as well. The hydraulic head record revealed 19-21 hour periods without tidal inundation during winter and spring, but these individual events were not likely to be sufficient to trigger AMD. Prior greenhouse and field studies lasting from four weeks to two years, subjected

S. alterniflora to drainage, oxidation, and subsequent pH reductions. The porewater measurements made during these studies indicated pH values from 1.7 to 4, and none of these researchers reported complete mortality (Linthurst and Blum, 1981; Luther et al., 1996; Portnoy and Valiela, 1997). During all of these studies, *S. alterniflora* was subjected to longer periods of drainage and exposure than any observed in the current study. In addition, our data suggest that seasonal redox changes occur annually at this site during winter and spring, but dieback was limited to fall through winter 2001-2002. This observation suggests that redox chemistry was not an AMD trigger for this site.

Drought, salinity, and AMD

Hypersaline porewater (40.1) was measured in this study during a period of moderate drought, suggesting that drought-induced hypersalinity could have triggered AMD at this site. Recall that our porewater diffusion samplers record a moving average of the preceding 30 days; and therefore, they would not reveal short-term salinity spikes of the sort that may occur over a few dry days in the summer when the marsh is not regularly inundated (Morris, 1995). Regression model estimates of shallow porewater salinity for 2001 – 2002, using equations derived from the diffusion sampler record, never exceeded 37. Again, porewater salinity may have been more variable than would be predicted by regression. These estimates did show two sharp increases in salinity within the root zone—one that was concurrent with the beginning of a drought period and immediately preceded observations of AMD at this site (Fig. 1.8a). Although *S. alterniflora* is known to tolerate high salinity, a dramatic increase in salinity, if it occurred over a short period of time, may have exceeded the plant's capacity for osmoregulation.

Climate change impacts on drought and AMD

Currently measureable and predicted impacts of global climate change include sea level rise, increased stress on fresh water supplies, and more frequent droughts (USGCRP, 1989). *S. alterniflora* marshes were shown to be capable of maintaining relative elevation with rising sea level as long as the rate of sea level rise does not exceed a specific limiting rate for the marsh. For the southeastern United States, this limiting rate was estimated to be 3.5 times the current rate of sea level rise (Morris et al., 2002). Therefore, it appears that salt marshes in the southeastern U.S. should be able to maintain their elevation relative to sea level, but they may be subject to increased drought-triggered episodes of dieback. A 2010 study used climate change models and existing drought and precipitation indices to predict changes in drought frequency for the United States over the next 100 years (Strzepek et al., 2010). The majority of simulated climate change scenarios indicated that the southeastern U.S. and Gulf Coast will experience increasing periods of drought over the next century. If this happens, then marshes may not be able to adjust to rising sea level, causing a major shift in the current coastal morphology in these areas.

1.7 CONCLUSIONS

We observed significant variability in hydrologic forcing factors acting on the marsh, which in turn caused variability in marsh groundwater dynamics, redox chemistry, and porewater salinity. Seasonal departures from the normal semi-diurnal tidal regime were seen during winter and spring when the marsh was occasionally not inundated during high tide. Predictably, evapotranspiration varied seasonally, with the highest rates observed during the summer and the lowest rates during the winter. Rainfall varied with

no observable pattern, and moderate to severe drought conditions prevailed for 10 months of the 47-month study period.

Groundwater dynamics varied in space and time due to changes in tide, variable marsh stratigraphy, and lateral distance to the nearest marsh creek. The very low flow within the central marsh, as indicated by the hydraulic record, was the result of the presence of thick (up to 4 m), low permeability sediments and the maximum distance to the nearest tidal creek. The typical lack of flow seen in this area promotes reduced conditions in soil and porewater and may allow subsurface hypersalinity to persist once established. This spatial variability may also explain the central marsh location of dieback at this site. In contrast, porewater chemistry close to the creeks may experience less variability due to more regular tidal flushing of the sediments.

Redox changes resulting from greater marsh surface exposure during winter and spring were reflected in porewater iron chemistry. The presence of pyrite previously found within the sediments at this site suggests that the observed changes in redox chemistry were accompanied by a reduction in porewater pH. However, it is unlikely that the individual exposure events (19 – 21 hours) were a trigger for AMD at this site. In addition, although redox changes occurred every winter and spring during this study, dieback was only observed during fall 2001.

Porewater and surface water salinity differed because of the effects of precipitation and evapotranspiration, enhanced or moderated by the frequency of tidal inundation. Hypersaline porewater was measured during the current study, but estimates of porewater salinity from January 2001 – December 2002 did not exceed 37, therefore, we do not believe that hypersaline porewater was responsible for triggering AMD at this

site. However, the porewater salinity estimates did indicate a sharp increase in salinity coincident with the beginning of drought conditions in the fall of 2001 just prior to the observation of AMD. Although the rate at which this dramatic increase may have occurred is unknown, a rapid porewater salinity increase (~ 3 days) may have exceeded the capacity of *S. alterniflora* for osmoregulation. Additionally, it should be noted that porewater salinity may be more variable than observed and predicted from the time-averaged measurements and regression equations used in this study. Based on the magnitude of the estimated salinity increase in 2001 and its timing in relation to the observation of AMD, this type of event is the most probable trigger for AMD at this site

Table 1.1. Variables Used in Statistical Analyses

ID	Definition	Data Preparation	No. of Terms
SS*xx*[1], SS*30:yy*[2]	Surface water salinity at Clambank Creek water quality station.	Geometric Mean	7
PPT*xx*, PPT*30:yy*	Precipitation recorded at Oyster Landing meteorological station.	Sum	7
NIHT*xx*, NIHT*30:yy*	The number of Non-Inundating High Tides.	Sum	7
ET*xx*, ET*30:yy*	Calculated maximum daily potential evapotranspiration rate.	Geometric Mean	5

[1]*xx* indicates the number of days over which the geometric mean or sum was calculated. We considered periods of 1, 15, 30, 60, and 90 days for all variables except ET (see text).
[2]*30:yy* indicates the 30-day geometric mean or 30-day sum of the variable beginning yy (60 or 90) days prior to the collection of the diffusion samples.

Table 1.2. Pearson Correlation Test Results –Ferrous Iron, Total Iron and Salinity[1]

Ferrous Iron	*Spring*	*Summer*	*Fall*	*Winter*
Sample Depth	Term / Correlation / Sig.	Term / Correlation / Sig.	Term / Correlation / Sig.	Term / Correlation / Sig.
10 cm	PPT1 0.637 / 0.048	SS30 -0.908 / 0.001 PPT30:60 -0.745 / 0.021	PPT60 -0.874 / 0.005	None
25 cm	NIHT90 0.746 / 0.013	SS1 -0.758 / 0.018	ET30 0.871 / 0.005	NIHT60 0.710 / 0.022
Total Iron	*Spring*	*Summer*	*Fall*	*Winter*
Sample Depth	Term / Correlation / Sig.	Term / Correlation / Sig.	Term / Correlation / Sig.	Term / Correlation / Sig.
10 cm	None	SS30 -0.897 / 0.001 PPT30:60 -0.781 / 0.013	None	None
25 cm	NIHT90 0.740 / 0.014	SS15 -0.759 / 0.018	None	NIHT90 0.878 / 0.001 ET60 -0.749 / 0.013
Salinity	*Spring*	*Summer*	*Fall*	*Winter*
Sample Depth	Term / Correlation / Sig.	Term / Correlation / Sig.	Term / Correlation / Sig.	Term / Correlation / Sig.
10 cm	NIHT30:90 / -0.763 / 0.010 PPT1 / -0.638 / 0.047	NIHT30 / -0.817 / 0.007 PPT90 / -0.718 / 0.029	ET30:60 / 0.705 / 0.034 SS90 / 0.703 / 0.035	SS30 / 0.806 / 0.005
25 cm	10 cm / 0.816 / 0.004	10 cm / 0.783 / 0.013	10 cm / 0.685 / 0.042	NONE

[1]Significance Level ($\alpha = 0.05$). Data presented are basic hydrologic parameters (PPT, ET, NIHT, or SS) with both the strongest correlation and most significant result of all significant results from the Pearson Correlation Tests.

Table 1.3. Regression Model Results[1]

Season	10 cm	25 cm
Spring	25.7 – 6.21 (PPT1) - 0.176 (NIHT90)	10.5 + 0.934 (10 cm)[2]
Summer	31.9 - 1.01 (NIHT30) - 0.197 (PPT60)	9.3 + 0.952 (10 cm) – 1.02 (ET60) + 0.441 (NIHT60)
Fall	-49 + 1.68 (SS30) + 3.62 (ET60)	-48.1 + 0.264 (10 cm) + 2.54 (ET30) + 1.93 (SS1) – 4.55 (NIHT)
Winter	-10.4 + 1.07 (SS30) – 0.254(NIHT30)	-16.8 + 1.18 (SS30:90) + 1.23 (ET30:90)
	Significance / r^2 / Adj. r^2	Significance / r^2 / Adj. r^2
Spring	0.006 / 0.768 / 0.702	0.004 / 0.666 / 0.624
Summer	0.021 / 0.723 / 0.630	0.031 / 0.806 / 0.689
Fall	0.017 / 0.742 / 0.656	0.082 / 0.824 / 0.647
Winter	0.005 / 0.777 / 0.714	0.228 / 0.345 / 0.157

[1]Significance Level ($\alpha = 0.05$).

[2]All '10 cm' terms within the 25 cm equations are derived from the model results in the first column. The top half of table presents the regression equations for salinity at 10 cm and 25 cm depth below land surface for each of the four seasons. The bottom half of the table presents the values for P / r^2 / adjusted r^2 for each for the corresponding equations above.

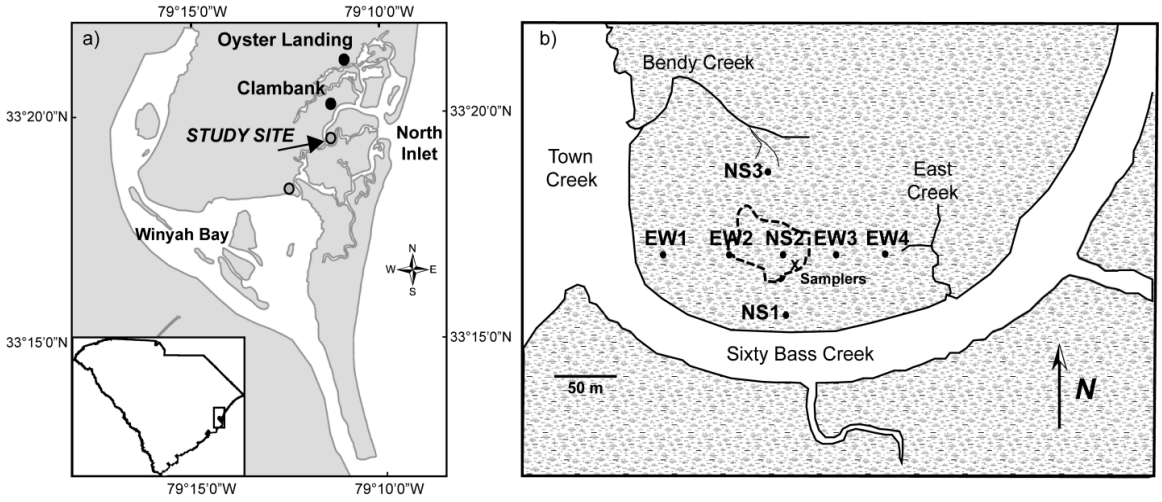

Figure 1.1. Study area: a) North Inlet. The dieback locations are indicated by solid gray circles, an arrow points to the specific study site. Springmaid Pier (33º 39.3' N/78º55.1'W) is located 42 km north of the Oyster Landing station. b) Map of the study site with piezometer nest locations indicated by black circles. A black X shows the approximate location of the passive diffusion samplers. The acute marsh dieback perimeter, as of 9/4/2005, is outlined in the center of the map.

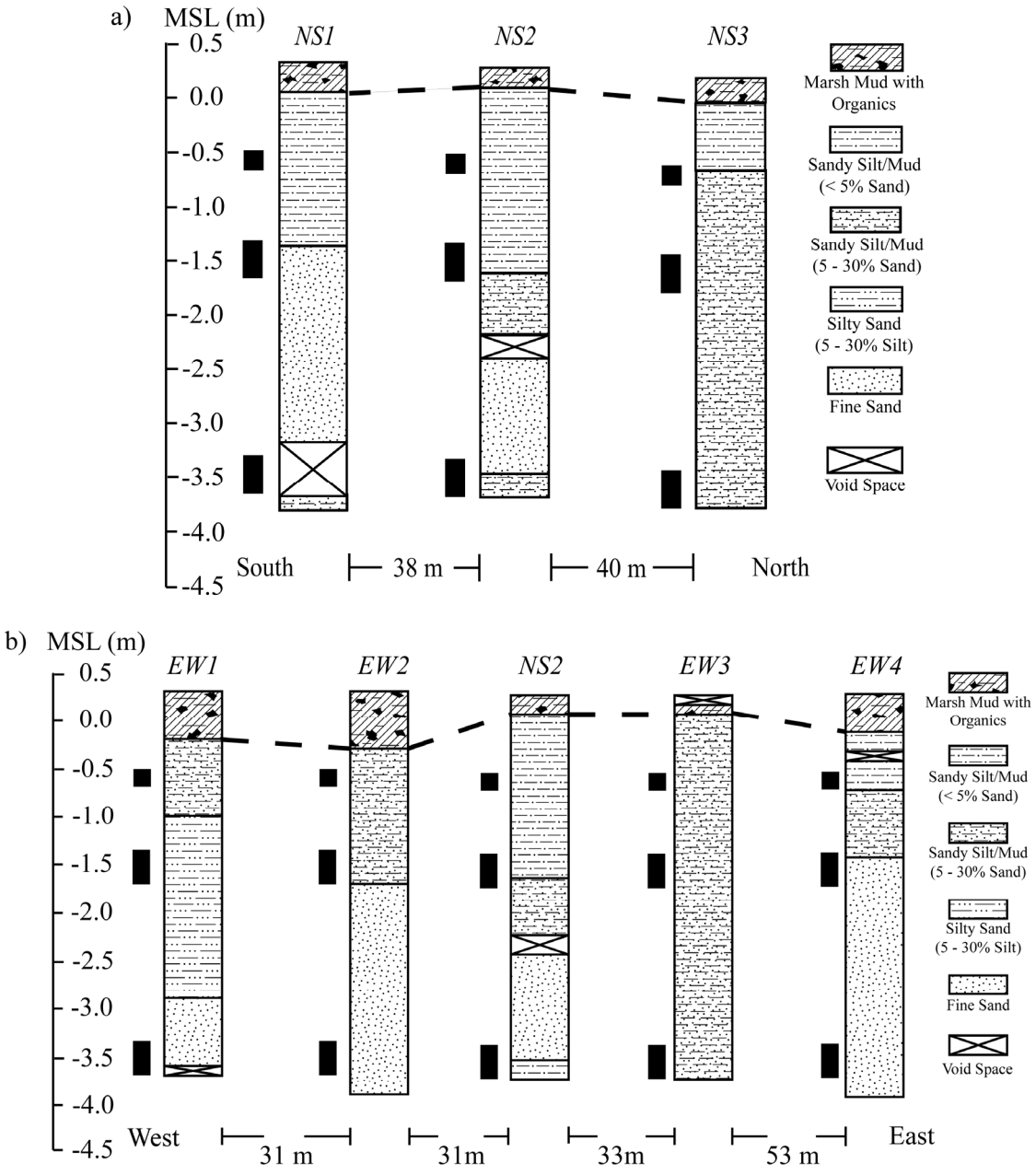

Figure 1.2. Stratigraphy. The results from sediment cores collected prior to piezometer installation along the a) N-S transect and b) E-W transect. Black rectangles near each column represent locations and lengths of piezometer screened intervals.

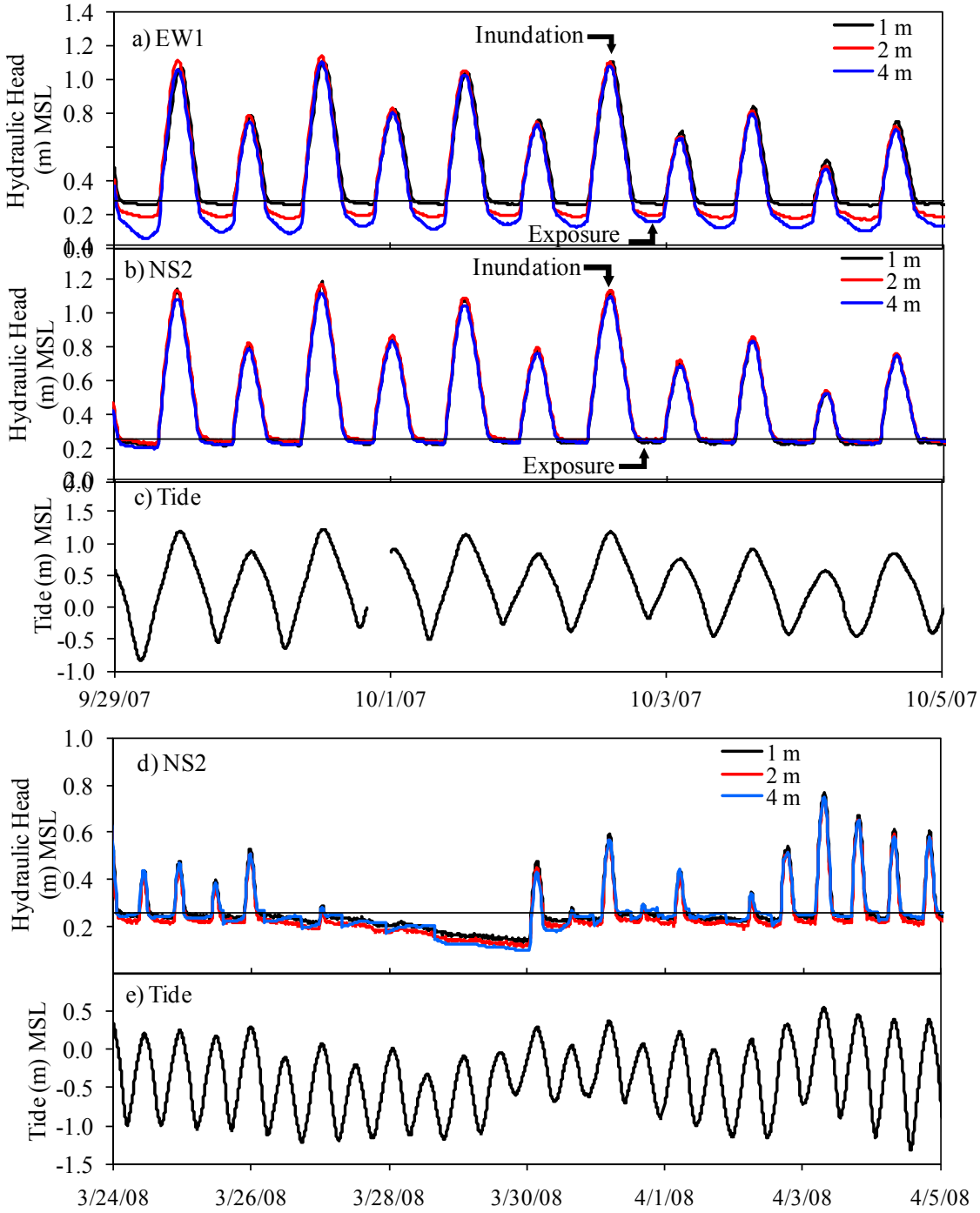

Figure 1.3. Plots showing hydraulic head and accompanying tide. a) and b) Typical hydraulic head profiles from 9/29/2007 – 10/5/2007 and c) accompanying tide for the same period. d) and e) Hydraulic head profile and accompanying tide (3/24/2008 – 4/5/2008) showing additional drainage during non-inundation periods. The horizontal line in each plot represents the marsh surface elevation at that nest.

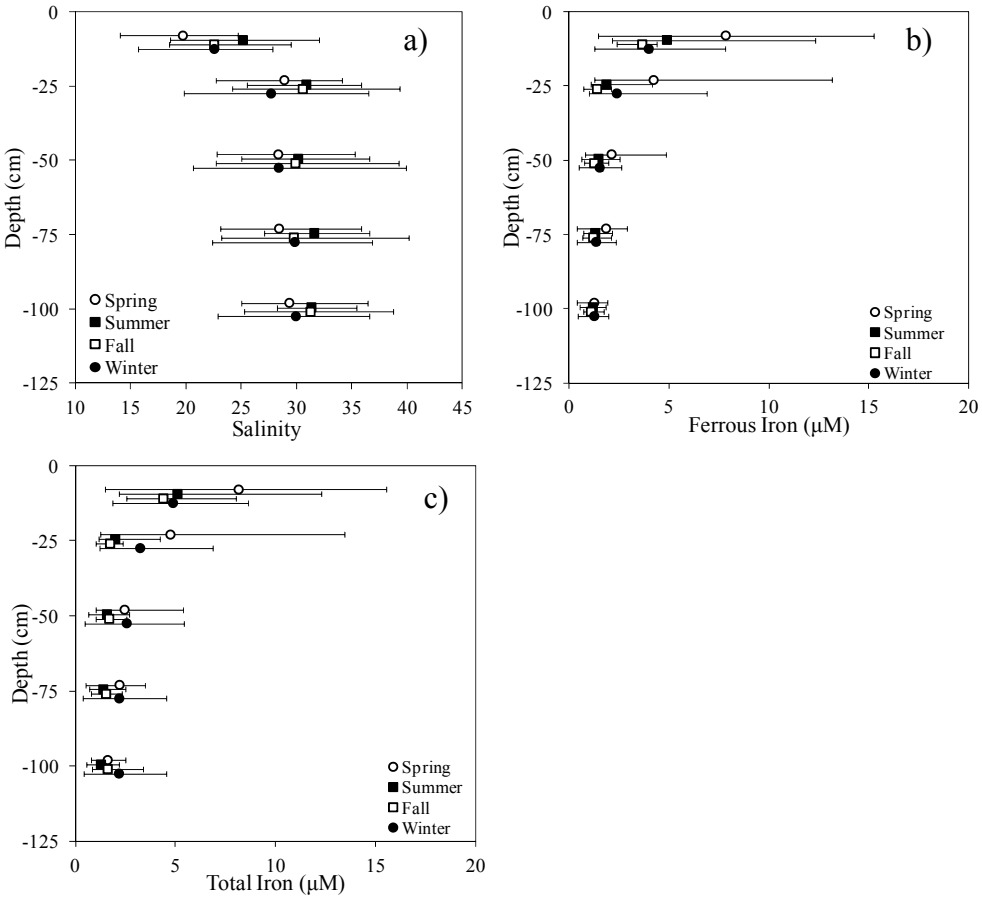

Figure 1.4. Passive-Diffusion Samples from 9/2006 – 6/2010. a) porewater salinity; b) porewater ferrous iron [Fe(II)]; c) porewater total iron [Fe(II) + Fe(III)]. Symbols represent median values by season and bars represent the range of measured values. Sample depths were 10, 25, 50, 75, and 100 cm, and were offset at each depth for clarity.

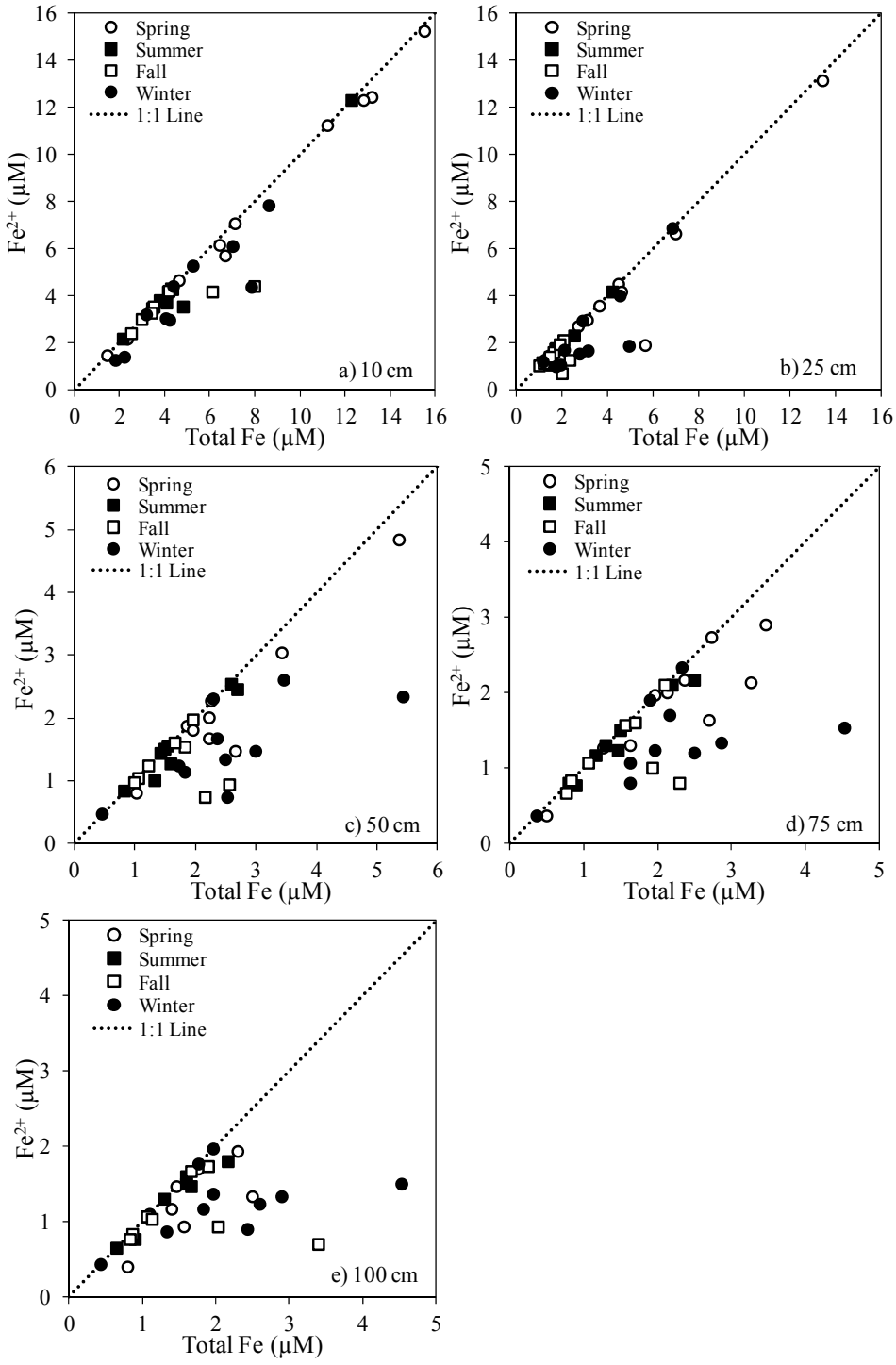

Figure 1.5. Plots of ferrous iron [Fe(II)] vs. total iron [Fe(II) + Fe(III)] at each diffusion sampler depth. Symbols differentiate seasons in which samples were collected. The dashed lines represent 1:1 ratios of ferrous to total iron.

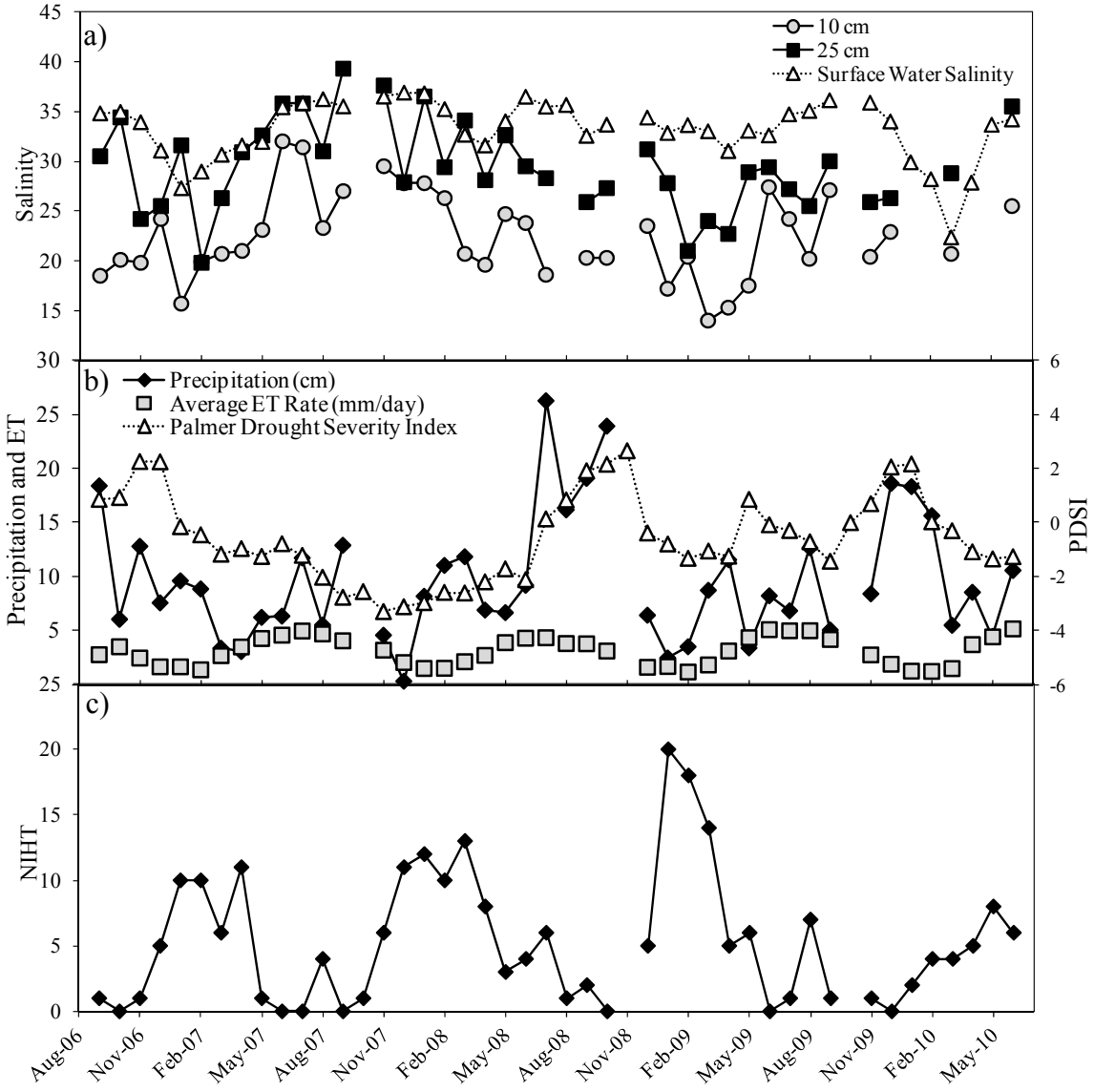

Figure 1.6. Porewater salinity and hydrologic data. Hydrologic data are either the 30-day sums or averages just prior to the porewater sample collection date. a) Porewater salinity at the 10 and 25 cm sample depths along with mean surface water salinity. b) Oyster Landing precipitation data, mean estimated daily maximum potential ET rate, and Palmer Drought Severity Index [Extreme Drought: PDSI ≤ -4; Severe Drought: -3.0 to -3.9; Moderate Drought: -2.0 to -2.9; Near Normal: -1.9 to +1.9; Unusual Moist Spell: +2.0 to +2.9; Very Moist Spell: +3.0 to +3.9; Extremely Moist: PDSI ≥ 4.0]. c) Number of non-inundating high tides.

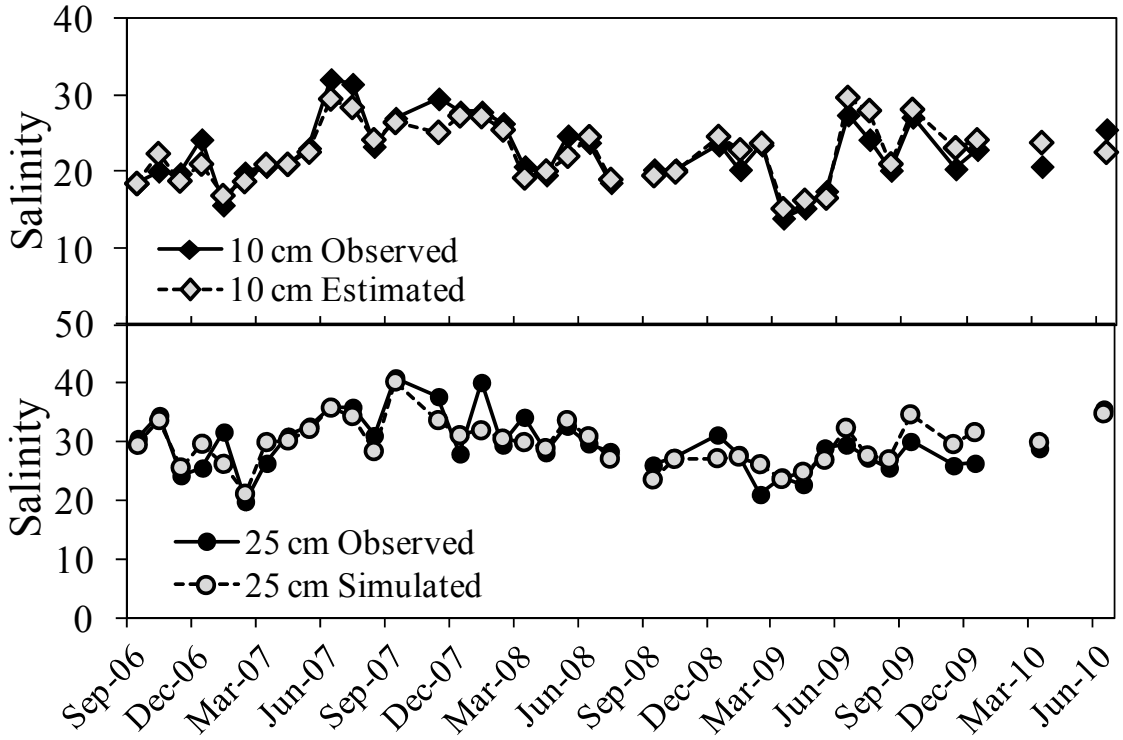

Figure 1.7. Comparison of regression model porewater salinity estimates with measured porewater salinity for the study period at a)10 and b) 25 cm. Salinity at 25 cm was estimated using results of estimated 10 cm porewater salinity. See Table 2 for model equations.

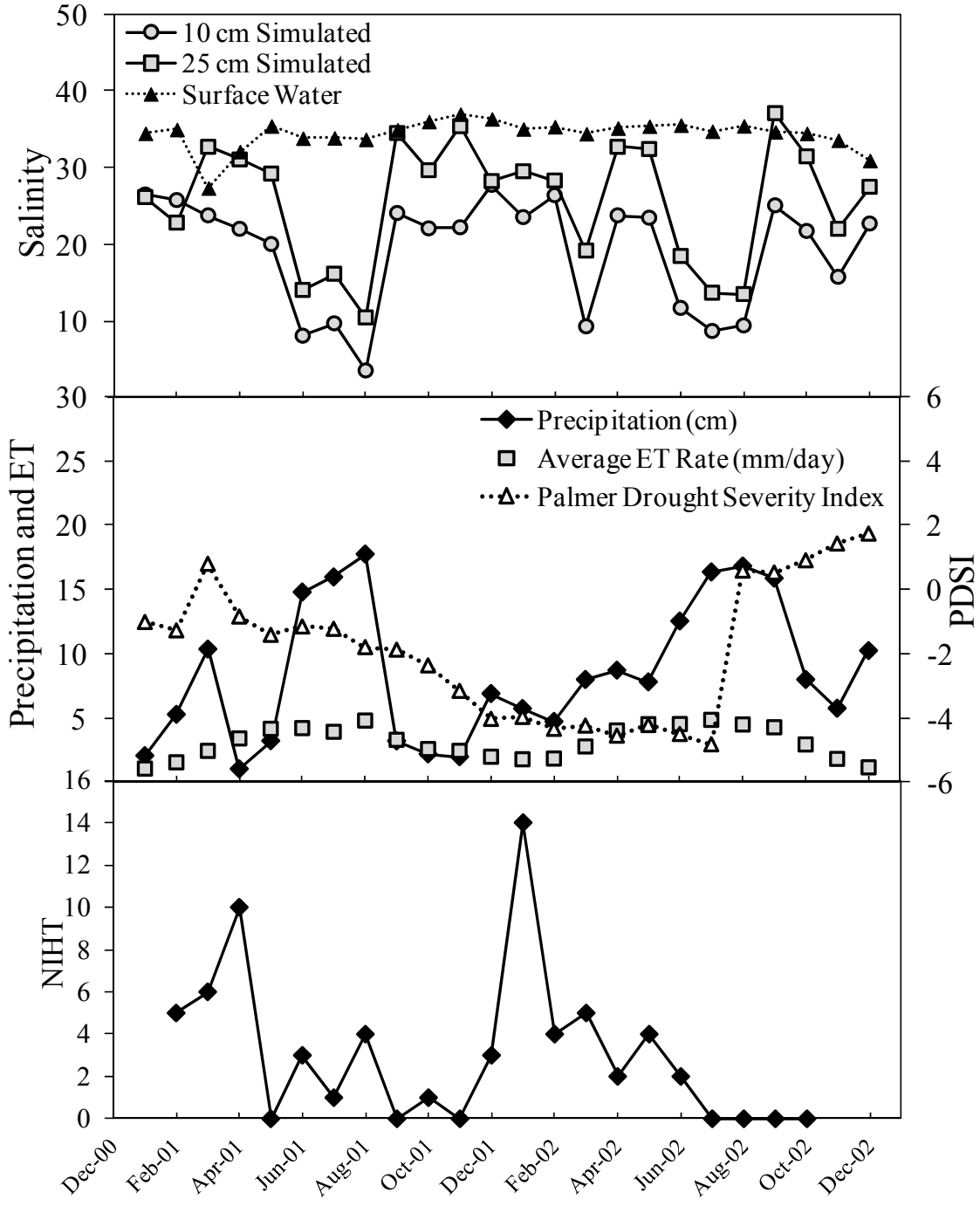

Figure 1.8. Regression model porewater salinity estimates for 2001 – 2002 and the 30-day sum or average hydrologic parameters. a) Porewater salinity estimates at 10 and 25 cm below the marsh surface along with the measured average monthly surface water salinity; b) precipitation data, monthly mean of daily maximum ET rates, and Palmer Drought Severity Index; and c) number of non-inundating high tides.

CHAPTER 2

GROUNDWATER TRANSPORT AND RADIUM VARIABILITY IN COASTAL POREWATERS[2]

[2] Hughes, Andrea L. H., Alicia M. Wilson, Willard S. Moore, 2015. Groundwater and Radium Variability in Coastal Porewaters. Estuarine, Coastal and Shelf Science.164(1): 94-104.

2.1 ABSTRACT

Radium isotopes (^{223}Ra, $t_{1/2}$=11.4 d; ^{224}Ra, $t_{1/2}$=3.66 d; ^{226}Ra, $t_{1/2}$=1600 y; and ^{228}Ra, $t_{1/2}$=5.75 y) are considered excellent tracers of groundwater movement and discharge in coastal systems. However, spatial and temporal variability in porewater radium activity have raised questions about the accuracy of these tracers. To better understand the factors affecting radium variability in coastal systems, measurements of porewater and surface water radium activity were made at an island in North Inlet Salt Marsh in Georgetown, South Carolina, from November 2009 to February 2011. Water salinity, temperature, pH, and redox potential were also recorded, and sediment samples were collected for analysis of bulk ^{228}Ra and ^{226}Ra activity. Hydraulic head observations during 2007 – 2008 from piezometers on the island were used to generate independent estimates of groundwater fluxes.

Porewater radium activities decreased with depth below the marsh surface and increased with distance from the creek banks. Salinity measurements were lower and redox potential higher near the marsh creeks. The stratigraphy of the island is typical of intertidal wetlands in the southeastern U.S., with a mud layer overlying a confined sandy aquifer; the observed patterns in porewater radium, salinity, and redox potential were consistent with (1) shorter porewater residence times in the permeable sand aquifer than in the low-permeability mud, (2) differences in grain size between the mud and sand, and (3) greater tidal exchange near the creeks. Temporal variations in porewater radium activity were not associated with salinity, pH, and redox potential although temperature provided significant control ($P < 0.05$, $r^2 < 0.47$) over variations in ^{228}Ra and ^{226}Ra activity. Lower mean sea water levels resulted in greater calculated groundwater

discharge and were also associated with lower average porewater ^{224}Ra and ^{223}Ra activity, in that groundwater discharge variations strongly affected short-lived radium activity at this site. The $^{228}Ra/^{226}Ra$ activity ratios in the surface water and porewater signified that the confined aquifer, rather than the surficial mud, was the primary source of radium to the surface water. Our results highlight the importance of understanding the hydrology of any coastal system when interpreting radium results. It is also essential to identify and measure the correct porewater end-member(s) (i.e. source aquifers) when calculating radium budgets.

2.2 INTRODUCTION

Groundwater discharge is an increasingly acknowledged and important source of solutes to coastal surface waters (King et al., 1982b; Valiela et al., 1990; Rutkowski et al., 1999; Burnett et al., 2001; Kelly and Moran, 2002; Jahnke et al., 2003; Slomp and Cappellen, 2004; Moore, 2006; Kwon et al., 2014). However, because groundwater discharge is diffuse and spatially variable, it is not easy to directly measure. Radium (Ra) has been used with increasing frequency as a geochemical tracer useful for calculating spatially-integrated estimates of groundwater discharge to coastal waters. The power of this tracer has resulted in a large number of studies using radium-based estimates of groundwater discharge to estimate groundwater-borne solute and nutrient fluxes (Bollinger and Moore, 1984; Rama and Moore, 1996; Hancock et al., 2000; Krest et al., 2000; Charette et al., 2001; Kelly and Moran, 2002; Abraham et al., 2003; Charette et al., 2003; Krest and Harvey, 2003; Charette and Buesseler, 2004; Kim et al., 2005; Charette, 2007; Knee et al., 2008; Gonneea et al., 2013a; Kwon et al., 2014).

Radium is useful as a naturally-occurring tracer in coastal systems for several reasons (Moore, 1987; Webster et al., 1994; Charette et al., 2001; Moore, 2003; Gonneea et al., 2008). Ra isotopes are generated from their respective parent isotopes either within or adsorbed to aquifer solids. The distribution coefficient (K_D) of Ra, the ratio of radium adsorbed to sediment surfaces to radium in solution, decreases with increases in salinity. This leads to higher radium activities in saline coastal porewater. A range of coastal sediment flushing and circulation processes are encompassed by the half-lives of ^{224}Ra and ^{223}Ra (3.66 and 11.4 days), and the half-lives of ^{228}Ra and ^{226}Ra (5.8 and 1600 years) allow them to be considered quasi-conservative tracers. This also means that the activities of ^{228}Ra and ^{226}Ra, once separated from the source aquifer, are affected primarily by dilution in the surface water. Therefore, the ratio of ^{228}Ra/^{226}Ra is largely unaffected because the average residence time of coastal surface waters is much shorter than the half-lives of these isotopes. This allows the source aquifers of water and solutes to coastal surface water to be traced by comparing ^{228}Ra/^{226}Ra activity ratios in groundwater and surface water (Moore, 2003).

Radium-based groundwater discharge studies in coastal systems over the past 30 years have revealed that the final discharge estimate is highly sensitive to variability in measurements of groundwater radium activity. Activity ($N\lambda$) is defined as the number of radium atoms (N) that decay within a specific amount of time (λ t^{-1}). Using radium as a tracer, estimates of groundwater discharge are made by measuring radium activity in the surface water of an embayment of interest and in the nearby ocean and groundwater as end-members. Excess radium in surface water (the contribution exclusively from groundwater inputs) is determined by eliminating radium inputs from other potential

sources. These additional sources include generation of radium from parent isotopes within or adsorbed to surface sediment; molecular and turbulent diffusion of radium from the interstitial water in shallow surface sediment; release of radium via ionic exchange from new sediment deposits to coastal, salt water systems; river discharge; and inputs from near shore surface water at each incoming tide. These measurements are then combined with a simple mixing model to obtain an estimate of groundwater discharge. That is, at what rate will groundwater need to discharge to support the excess radium measured in the surface water?

Radium activity in the porewater of a single aquifer was initially assumed to be constant in space and time, and any changes in excess surface water Ra activity were attributed to changes in groundwater discharge rates. Thus, porewater radium activity was measured only once, or multiple measurements were averaged to a single value for use in the mixing model along with a series of surface water samples collected over an extended period of time (Bollinger and Moore, 1993; Scott and Moran, 2001; Yang et al., 2002; Charette et al., 2003). It is now understood that radium activity in porewater can vary greatly in natural settings, which can produce high variance in radium-based discharge estimates (Gonneea et al., 2008; Hougham et al., 2008; Gonneea et al., 2013a).

Radium activity in porewater is affected by five factors: (1) radioactive production in the sediment as a function of thorium (Th) content; (2) sediment grain size and surface area (Beck and Cochran, 2013), including a strong inverse relationship between sediment grain size and thorium content (Bollinger and Moore, 1993); (3) radioactive decay in the water; (4) groundwater transport (advection and dispersion) and discharge; and (5) sorption as controlled by porewater and sediment chemistry. Porewater

radium activity controlled by generation and decay is isotope-dependent and based upon the half-lives of the Th parent isotopes as well as the individual Ra isotopes, which vary by several orders of magnitude. The porewater radium controls of groundwater transport and discharge, sorption, and differences in sediment grain size are universal across the four Ra isotopes. Measurements of radium activity in sediments include what can be considered immobile as well as mobile fractions. The immobile fraction of radium is generated from thorium held within the sediment grain matrix. This fraction has a greater probability of release into the porewater via alpha recoil if the thorium atom is close to the grain surface (Sun and Semkow, 1998). The mobile fraction may be defined in two parts. Radium may be generated from thorium adsorbed to the sediment grain surfaces or iron- and manganese-oxide grain coatings, and radium may itself be adsorbed to the grain surface or grain coatings.

Changes in porewater and sediment chemistry result in sorption or desorption of both thorium and radium from the sediment surface (mobile sediment radium fraction). Radium sorption to sediment and to Fe and Mn oxide/hydroxide sediment coatings is affected by variations in salinity, temperature, pH, and redox potential (Elsinger and Moore, 1980; King et al., 1982b; Webster et al., 1995; Rama and Moore, 1996; Hancock et al., 2000; Gonneea et al., 2008; Beck and Cochran, 2013). In coastal aquifers, changes in salinity across the fresh water/salt water interface provide the greatest control on distributions of porewater radium (Krest et al., 2000; Gonneea et al., 2008) with increases in radium activity of up to two orders of magnitude as salinity increases from 0 to 25 (Abraham et al., 2003; Gonneea et al., 2008). Thus variations in radium in the surface

water resulting from groundwater discharge can be very difficult to interpret in coastal systems with a mobile fresh water/salt water interface.

The distribution of Ra has also been shown to be variable in coastal aquifers without fresh water/salt water transition areas. Radium activity in porewater still varied by one order of magnitude in space and time in an intertidal salt marsh (North Inlet, South Carolina) where porewater salinity exceeded 17 and porewater was reduced (Krest et al., 2000). In that study, spatial variations in porewater radium were controlled by radium generation, decay, and sediment grain size. Temporal variations in porewater radium were interpreted to be changes in sorption controls (other than salinity) and variable groundwater transport.

Although elevated porewater salinity and reduced conditions are typical of tidal salt marshes along the southeast Atlantic coast (Wiegert and Freeman, 1990), seasonal redox changes in the shallow (0 – 25 cm) porewater and sediment at this site were reflected in porewater iron speciation changes observed to a depth of 100 cm (Hughes et al., 2012). Pyrite oxidation within the shallow marsh sediment during periods of extended marsh surface exposure (winter and early spring) were believed to be the cause of the iron speciation changes and be accompanied by lower porewater pH. However, reduced porewater conditions prevailed for most of the year.

We hypothesize that groundwater transport provides a primary control on porewater Ra distribution in saline systems with generally reduced porewater conditions. To test this hypothesis, we conducted a field and modeling study on a marsh island at North Inlet, South Carolina. High porewater salinities and typically reduced porewater conditions at this site mean that salinity and redox have the potential to be eliminated as

factors affecting porewater radium variability. The overall goal of this study was to investigate the role of groundwater flow on the spatial and temporal distribution of porewater radium activity. In order to determine the controls on spatial and temporal variability, we measured bulk sediment radium activity within the marsh mud and underlying confined sand aquifer. Simultaneous measurements of radium, temperature, salinity, redox potential, and pH were made in the groundwater and surface water. Finally, to investigate the role of groundwater flow and residence time on porewater radium activity, we used previously measured hydraulic head at this site to estimate groundwater discharge rates.

2.3. METHODS

Study Site and Installation

The study site is an island in North Inlet Salt Marsh near Georgetown, South Carolina, in the North Inlet-Winyah Bay National Estuarine Research Reserve (NI-WB NERR; Fig. 2.1). The NI-WB NERR encompasses 32 km^2 of tidally-dominated salt marsh and wetlands populated extensively by the salt marsh cord grass *Spartina alterniflora*. This intertidal salt marsh experiences a semi-diurnal tide with an average range of 1.4 m (Palmer et al., 1980; North Inlet-Winyah Bay National Estuarine Research Reserve, 2010b).

Sediment cores were collected at nine locations (Fig. 2.1B) revealing stratigraphy of 1 – 4 m of marsh mud overlying a fine-grained sand at depth (Fig. 2.2). The upper 25 cm of the marsh mud contains organic detritus and *S. alterniflora* roots. Below that, the marsh mud contains occasional sand inclusions and a small, varying percentage of sand (up to 30% at most). The hydraulic conductivity of the marsh mud is at least one order of

magnitude lower than the underlying sand (Thibodeau, 1997; Gardner, 2005; Gardner and Wilson, 2006). Piezometer nests were then installed at seven locations (Fig. 2.1B) forming N-S and E-W transects. Each piezometer nest contains three piezometers screened at depths of 1, 2, and 4 m below the marsh surface (Fig. 2.2). The 1 and 2 m piezometers are primarily screened within marsh mud, and the 4 m piezometers, except for NS3 and EW3, are screened within the confined sand aquifer (Fig. 2.2). The piezometers were instrumented to record pore pressure, temperature, and salinity during 2007 – 2008 (Hughes et al., 2012), prior to the start of this study. Briefly, these measurements were used, along with surveyed piezometer elevations, to calculate hydraulic head as:

$$H_T = P/(\rho g) + z \tag{2.1}$$

where H_T (m) is total hydraulic head, $P/(\rho g)$ (m) is pressure head (P = pressure; ρ= water density), and z (m) is the elevation of the location of the pressure measurement.

Calculations of hydraulic head were then used to understand groundwater flow paths and discharge variations. Prior interpretations of the hydraulic head dataset indicated that groundwater moves vertically downward through the marsh mud into the underlying sand and then laterally through the sand discharging to nearby marsh creeks (Hughes et al., 2012). Faster groundwater flow rates were found in the higher permeability confined aquifer and were also found near the tidal creeks compared with the marsh interior. For the current work, measurements of hydraulic head and tide were used to determine the hydraulic conductivity of the confined aquifer and ultimately

calculate rates of groundwater discharge from the marsh. Tide data for 2007 – 2008 and for 2009 – 2011 were acquired from NOAA's Tides and Currents database recorded at the Oyster Landing station (Fig. 2.1A; CO-OP ID 8662245) (NOAA/National Ocean Service, 2013). Methods for calculating groundwater discharge are described in Appendix A.

Sample and Data Collection

Piezometers and nearby surface water were sampled quarterly for Ra beginning in November 2009 and ending February 2011. Prior to porewater sample collection (0.5 – 4 L), piezometers were purged. Nearby surface water (26 L) was collected at high tide, low tide, or both at each quarterly sample period. Measurements of temperature and salinity (YSI EC300), as well as pH and redox potential (YSI pH100), were made in the field immediately after sample collection. In order to remove most sediment present in the water samples, the water was either filtered in the field using a 10 μm glass fiber filter or by allowing the sediment to settle to the bottom of the sample container and decanting the liquid into a clean container.

Two sediment collection schemes were used to quantify both temporal and spatial variations in bulk radium activity. Shallow marsh sediment (surface sediment) often reflects seasonal changes in radium sorption to grain surfaces (K_D: distribution coefficient) due to seasonal changes in sediment and porewater chemistry. The previous study at this marsh island indicated that redox changes in shallow marsh (0 – 25 cm) chemistry were strongly associated with changes to the regularity with which the marsh surface was inundated. In particular, when mean tide is at its lowest level annually in the winter and early spring, the marsh surface occasionally remained exposed for as long as

21 hours, compared with the typical average of 8+ hours. This happens because the marsh was not inundated during high tide. One event was recorded when the marsh was not inundated for three days (Hughes et al., 2012). In order to determine if there were changes in bulk sediment radium activity in the surface marsh sediment during periods of extended marsh surface exposure, samples were collected from the top 10 cm of the marsh in February (low MWL) and September 2010 (high MWL). On each of the two dates, six samples were collected from the marsh surface and nearby creek bottom along a line adjacent to the N-S transect of piezometers (Fig. 2.2B). In order to quantify differences in bulk sediment radium activity based on sediment type (marsh mud versus the fine-grained sand of the confined aquifer), five samples were also split from three of the nine sediment cores collected during site installation (Fig. 2.2A).

Statistical tests were used to quantify spatial and temporal differences in measurements of radium, salinity, temperature, pH, and redox potential in porewater and surface water as well as in bulk sediment radium measurements. Statistical tests (Pearson correlations) were also used to analyze the relationships between radium activity in porewater and surface water and simultaneous measurements of salinity, temperature, pH, and redox potential. Regression analyses were used to obtain predictive equations for groundwater discharge for the current study when hydraulic head was not being measured. Finally, partial correlation tests were used to quantify the relationship between porewater radium activity and rates of groundwater discharge. A detailed description of the statistical methods, water and sediment sample preparation methods, and radium analytical techniques are available in the Appendix A.

2.4. RESULTS

Spatial Variability

All measurements of radium, salinity, temperature, pH, and redox potential in the porewater and surface water are listed in Tables A.1 and A.2 in Appendix A. The mean, minimum, and maximum values of all parameters measured in the water, along with the number of samples included in the mean, are available in Tables A.3 and A.4 and presented in Figure 2.3. The aggregate measurements of the four radium isotopes and the $^{228}Ra/^{226}Ra$ and $^{224}Ra/^{223}Ra$ activity ratios varied significantly by sample depth ($P < 0.008$; Table 2.1, Fig. 2.3, Table A.3). When analyzed within each sample date, a variety of patterns emerged with far fewer significant results, largely because the sample sizes were too small to generate statistically significant results. Tukey's multiple comparison tests confirmed variable but consistent decreases with depth (Table 2.1).

Lateral differences in porewater measurements were analyzed by piezometer location (Interior Marsh = EW3, NS2, and EW3; Exterior Marsh = EW1, NS1, NS3, and EW4) in aggregate, at individual depths (1, 2, and 4 m), and within each sample date (Nov 09, Mar 10, Jul 10, Oct 10, Feb 11) (Table 2.2, Figs. A.2 – A.11). Salinity and redox potential were the only overall measurements to vary significantly by piezometer location, with lower salinity and less reduced values near the marsh creeks ($P < 0.001$; Table 2.2). Within the 1 m measurements, there were no significant lateral differences, and within the 2 m measurements, redox potential was the only parameter to vary significantly ($P < 0.0056$), with less reduced values near the marsh creeks (Table 2.2, Fig. A.5 B). In the confined aquifer (4 m), ^{224}Ra activity ($P < 0.0056$) and the $^{228}Ra/^{226}Ra$ activity ratio ($P < 0.001$) were significantly lower at exterior versus interior marsh

locations (Table 2.2, Figs. A.7 C and A.11 C). No significant lateral variations were found in the porewater measurements when analyzed by sample date, again largely due to the small sample size.

Spatial differences in bulk sediment ^{226}Ra and ^{228}Ra activity were observed between the surface samples (0 – 10 cm) and the samples taken from the sediment cores (Tables 2.3 and 2.4, Fig. 2.2). ^{226}Ra and ^{228}Ra activity measured in the surface samples showed slightly but significantly lower activity when compared with samples taken from the sediment cores ($P < 0.01$). Different sediment types from the core samples (marsh mud and sand) did not show significant differences in radium activity.

In general, porewater Ra activity decreased with depth below the marsh surface. Higher radium activity was measured in samples collected from the 1 and 2 m piezometers screened in the marsh mud and lower activity was measured in samples collected from the 4 m piezometers screened in the confined sand aquifer (Fig. 2.2). Contrasting with this result were the nearly constant values of salinity, temperature, pH, and redox potential with depth, which suggests that something other than porewater geochemistry may be controlling the vertical profile of porewater radium activity at 1 m depth and below. Significant lateral variations in Ra activity were limited to ^{224}Ra and the ^{228}Ra/^{226}Ra activity ratio in the confined aquifer (4 m) with higher values measured at the marsh interior. Aggregate measurements of salinity and redox potential, and the 2 m measurements of redox potential, were found to vary between interior and exterior marsh piezometers, with higher salinity values and the most reduced potential measurements found at the marsh interior locations. Finally, the lower bulk sediment ^{226}Ra and ^{228}Ra activity in the upper 10 cm of the marsh and comparatively consistent activity below 10

cm may be the result of the rapid removal of any radium that is generated from surface-bound thorium by semi-diurnal tidal flushing of the marsh surface.

Temporal Variability

Measurement variations by sample date in porewater and surface water, and in the porewater at each sample depth (1, 2, and 4 m), were analyzed using one-way ANOVAs (Table 2.5, Fig. 2.3). The aggregate porewater measurements of the four radium isotopes varied by sample date ($P < 0.0125$), but only ^{226}Ra was also found to vary by date in the surface water ($P < 0.05$) as well as at individual depths (2 m; $P < 0.001$) (Table 2.5). The ratios of $^{224}Ra/^{223}Ra$ and $^{228}Ra/^{226}Ra$ did not vary significantly by sample date in the porewater or surface water ($P > 0.05$) (Table 2.5). Tukey's multiple comparison tests indicated that the highest mean radium activities were typically measured in the fall of 2010 and the lowest in the spring of 2010 (Table 2.5, Table A.3, Fig. 2.3).

Temperature measurements varied predictably in porewater ($P < 0.001$) and surface water ($P < 0.05$) with the highest temperatures measured in July and October 2010 and the lowest in March 2010 (Table 2.5, Table A.4, and Fig. 2.3). Measurements of pH were also found to vary significantly by sample date ($P < 0.0125$) in the porewater but not in the surface water. The highest measurements of pH were made in November 2009 and March 2010. Aggregate porewater salinity varied with time ($P < 0.001$) with the lowest salinity values measured in November 2009. Statistically significant ($P < 0.001$) variations in salinity were also identified in the confined aquifer (4 m) despite the small sample size. There were no significant temporal variations in the porewater or surface water measurements of redox potential ($P > 0.05$), and porewater was strongly reduced compared to the oxidized surface water (Table 2.5, Table A.4, and Fig. 2.3). Finally, bulk

sediment ^{226}Ra and ^{228}Ra activity within the top 10 cm of the marsh did not differ significantly between the two sample dates (two-sample t-test; $P > 0.01$).

At fixed sampling locations in the marsh, the only potential drivers of temporal radium variability are changes in temperature, salinity, pH, redox chemistry and/or variable groundwater flow. Even though the porewater measurements of the four radium isotopes along with the measurements of salinity, temperature, and pH, varied seasonally, their temporal profiles do not match (Fig. 2.3). This suggests that changes in porewater chemistry, which control the Ra distribution coefficient (K_D), were not a primary factor controlling variations in porewater radium at this site over the course of this study. This lack of co-variance in porewater measurements was reflected in the Pearson correlation test results, which indicated no significant relationship between porewater radium and salinity, temperature, pH, or redox potential (Fig. 2.4). The exception to this result was found in the significant, positive correlation between temperature and porewater ^{226}Ra and ^{228}Ra ($P < 0.001$) (Fig. 2.4J and 2.4N). That is, as temperature increased, ^{226}Ra and ^{228}Ra activity in the porewater increased. The r^2 values for these correlations were less than 0.47, indicating that for our measurements, temperature accounted for less than 50% of the temporal variability found in the long-lived radium isotopes. With the exception of temperature controls over the long-lived isotopes, the geochemistry of the porewater and sediment may not play a primary role in temporal variations in porewater radium activity at this site. For the short-lived isotopes (^{223}Ra and ^{224}Ra), variable groundwater flow and discharge may provide a primary control.

Hydrology-based groundwater discharge estimates

The hydrology-based estimates of groundwater discharge during this study (see Appendix A) revealed that groundwater discharge at this site is inversely related to the mean sea water level (Fig. 2.5A). That is, groundwater discharge was higher when mean sea level was low and lower when mean sea level was high. This occurs because a greater hydraulic gradient ($\Delta h/x$) develops between the marsh and creek when the mean water level is lower. The periods of highest calculated discharge occurred in the winter of 2010 and 2011 during low mean sea water level (Fig. 2.5A). This relationship indicates that mean sea water level can be considered a proxy for groundwater discharge from the salt marsh. We also observed that the two periods of lowest surface water radium activity occurred during the two periods of highest calculated groundwater discharge, contrary to the assumption made when using radium as a groundwater tracer (Fig. 2.5A and 2.5C). Based on the violation of this basic assumption, we did not use our radium measurements to estimate groundwater discharge from this site.

Groundwater discharge and porewater radium activity

Partial correlation tests between 1-day, 4-day, and 11-day averages of specific discharge prior to each sample date and porewater radium activity (see Appendix A) revealed significant, negative associations between discharge and porewater ^{223}Ra and ^{224}Ra, but not ^{228}Ra and ^{226}Ra (Table 2.6). Specifically, ^{224}Ra was associated with the 1-day, 4-day, and 11-day discharge averages ($P < 0.05$). ^{223}Ra was associated with the 1-day and 4-day averages ($P < 0.05$), but not the 11-day average. The strongest association for ^{224}Ra was with the 4-day averages of discharge ($P = 0.005$), which closely corresponds to the half-life of the ^{224}Ra isotope (3.66 days). The lack of association

between ^{223}Ra (half-life of 11.4 days) and the 11-day discharge averages may be due to the additional smoothing of the discharge variations over the longer time period. The inverse relationships indicated by the negative r values of the partial correlations, regardless of a significant result, mean that porewater radium activity decreases as discharge rates increase (Table 2.6, Figs. 2.5A and 2.5B).

2.5. DISCUSSION

The decrease in mean porewater radium activity with depth can be explained in two ways. First, it is clear that the hydraulic conductivity of the fine grained mud is lower than that of the underlying sand aquifer. Slower moving porewater in the low permeability marsh mud resides for a longer period of time and allows for a greater accumulation of radium than in the deeper, more permeable sand of the confined aquifer.

Second, increased thorium content associated with fine-grained sediments (Bollinger and Moore, 1993) and may also affect vertical differences in porewater radium activity. The larger surface area associated with the fine-grained marsh mud provides more sites for adsorption and subsequent release of thorium and radium (Beck and Cochran, 2013). The sediment samples collected from the marsh surface were similar to the mud that was found within the sediment cores, yet the bulk sediment ^{228}Ra and ^{226}Ra activities were significantly lower. These differences reflect both greater sediment flushing of the shallow (< 10 cm) sediment and also suggests that a larger inventory of radium and thorium is held in the mobile fraction. If Ra and Th inventories in the marsh mud were held in the immobile fraction (within the grain matrix), it would not be affected by sediment flushing differences. These mechanisms may provide an additional

explanation for the higher radium activity in the porewater in contact with these sediments.

Lateral differences in porewater activities also likely reflect greater tidal flushing of marsh sediment near the creek bank. The overall porewater measurements in this mixing zone showed salinity closer to surface water values and higher redox potentials (in aggregate and at 2 m). In the confined aquifer (4 m), lower ^{224}Ra activity and ^{228}Ra/^{226}Ra activity ratios are also consistent with the greater tidal flushing near the creeks.

Spatial variations in porewater ^{228}Ra/^{226}Ra activity ratios provided additional information about potential sources of radium inputs to surface water. The activity ratios in the interior confined aquifer (^{228}Ra/^{226}Ra = 5 ± 1) were close to those measured in the 1 and 2 m piezometers (^{228}Ra/^{226}Ra = 7 ± 1). This pattern is consistent with vertical downward flow of groundwater from the marsh mud into the confined aquifer below (Hughes et al., 2012). Once groundwater enters the more permeable confined aquifer, greater exchange occurs between surface water and groundwater across the sediment/water boundary due to tidal pumping. This process results in activity ratios in the confined aquifer near the tidal creeks (^{228}Ra/^{226}Ra =3 ± 1) that are much closer to the ratio found in the surface water (^{228}Ra/^{226}Ra = 2 ± 0.3) (Fig. 2.6). If discharge or seepage from the marsh mud were an important source of groundwater and radium to the surface water, then the ^{228}Ra/^{226}Ra ratio in the surface water would more closely match that measured in the 1 and 2 m piezometers. This means that the confined aquifer is the primary volumetric source of groundwater and solutes to the nearby surface water. More

importantly, these results highlight the importance of identifying and sampling the correct porewater end-member when calculating a radium budget for this or any coastal system.

The short-lived Ra isotope activities were correlated with groundwater flow rates, whereas the long-lived Ra isotopes were not. This reflects the wide range of ingrowth rates for the four radium isotopes. Ingrowth rates can be calculated by solving the radioactive production equation [$N_D\lambda_D = N_P\lambda_P(1 - e^{-\lambda_D t})$] for time (t). Assuming just a 20% ingrowth of the daughter (N_D) from the parent (N_P), the ingrowth times are 1.2 d, 3.7 d, 1.8 y, and 515 y for ^{224}Ra, ^{223}Ra, ^{228}Ra, and ^{226}Ra, respectively. Porewater ^{226}Ra and ^{228}Ra activities do not achieve equilibrium with the sediment because the ingrowth rates far exceed the residence time of porewater within the confined aquifer.

Whereas prior laboratory experiments (Gonneea et al., 2008; Beck and Cochran, 2013) found that radium distribution (K_D) varied with changes in pH, our only significant results from the Pearson correlation tests were between porewater ^{226}Ra, ^{228}Ra, and temperature. In the lab studies, the distribution coefficient was found to vary by as much as 2 orders of magnitude as pH ranged from 2 to 10 (Gonneea et al., 2008; Beck and Cochran, 2013). Shallow (< 25 cm) redox chemistry changes were observed previously at this field site (Hughes et al., 2012) resulting in iron speciation changes measurable to 1 m. These sediment chemistry changes had the potential to increase porewater radium activity in the 1 m piezometers through periodic releases of sediment surface-bound radium during the winter. However, the lowest porewater radium activities observed during the study were measured in the winter (February 2011) and early spring (March 2010) (Fig. 2.3).

The lack of association between pH and Ra activity found in the current study may be explained in two ways. Organic matter coatings occupying potential adsorption sites on sediment grain surfaces were considered to be the reason for anomalously low K_D values (~10) in the surface sediment of North Inlet salt marsh (Rama and Moore, 1996). This may reduce the range of possible K_D values as well as the amount of radium adsorbed to and released from sediment surfaces. In addition, the variability in our pH measurements was relatively small (6.5 to 8.2) compared to the experimental range (2 to 10) of the laboratory studies, which may also limit the variability in radium K_D. Although our quarterly sampling scheme may not have been sufficient to capture the rapid nature of redox chemistry changes, it was comparable to the sampling frequency found in many studies in which radium has been used to estimate submarine groundwater discharge. Therefore, even though seasonal pH and redox changes may cause periodic releases of additional Ra to shallow porewater, these changes are not detectable in porewater radium at 1 m depth and below and do not impact the interpretation of these Ra measurements.

The causes of temporal variations in surface water radium activity are more complex. Average porewater and surface water radium activities both increased during periods of high mean water, which seems to suggest that the increases in porewater radium activity contributed to the increases in surface water activity. However, these seasonal increases in surface water radium activity did not coincide with variations in groundwater discharge (Fig. 2.5A and C), which suggests that variable surface water radium activities are controlled by processes not represented on this island.

A similar disconnect between radium activity in surface water, porewater, and variable groundwater discharge was found in a prior study conducted at Waquoit Bay in

Massachusetts (Gonneea et al., 2013a). The porewater radium variability for this prior study was interpreted as the result of net movement of the fresh water/salt water boundary in the aquifer resulting in additional radium releases from aquifer sediment not normally in contact with salt water. The corresponding increases in surface water radium activity, in spite of decreases in terrestrial, fresh groundwater discharge, were considered to be the result of increases in the re-circulated seawater component of SGD in conjunction with the additional release of sediment-bound radium. The relationship between surface water radium activity and mean sea water level found during the current study may be explained by a similar radium input mechanism along the forest/marsh boundary of the North Inlet salt marsh.

2.6. CONCLUSIONS

In spite of the absence of a mobile fresh water/salt water transition zone, radium activity in the porewater during this study varied by up to a factor of 4 in space and time at this salt marsh island site. Variations in groundwater flow and discharge strongly influenced the short-lived radium isotope activities in the porewater. Vertical differences in radium activity reflected longer porewater residence times in the lower-permeability marsh mud, likely augmented by higher thorium activity and a greater pool of thorium and radium in the mobile fraction in the marsh mud than in the underlying sand. Lateral differences in measurements of salinity, redox potential, ^{224}Ra and the $^{228}Ra/^{226}Ra$ activity ratio were the result of enhanced tidal flushing of the marsh sediment and shorter porewater residence times near tidal creeks. Analysis of radium isotope activity ratios indicated that the confined sand aquifer provided the greatest volume of groundwater and solutes (including radium) from this site to the nearby surface water. In layered coastal

systems, using multiple isotope measurements can identify coastal aquifer locations of greatest tidal exchange to sample as the porewater end-member when using radium as a groundwater tracer.

Temporal changes in porewater ^{228}Ra and ^{226}Ra were influenced by seasonal changes in porewater temperature. Also, variations in groundwater flow provided the only quantifiable control for ^{223}Ra and ^{224}Ra during this study. In effect, the very phenomenon we want to quantify using radium provided one of the primary controls on porewater activities of these isotopes.

Ultimately, our results indicate that interpreting radium isotope measurements can be problematic in complex coastal systems, even in the absence of a subsurface fresh water/salt water transition zone. Improving the accuracy of Ra as a geochemical tracer will rely on determining the appropriate groundwater end-members for use in Ra-based estimates of SGD. This will require that spatial and temporal variations in porewater Ra activity be quantified and that radium activity ratios be used to confirm the appropriate source aquifer. We recommend that traditional hydrologic and Ra-based techniques be used together to provide clearer models for coastal groundwater discharge than can be provided by either method alone.

Table 2.1. Porewater ANOVAs by Depth[1] with Tukey's Multiple Comparison Tests[2,3]

Response	All Samples	Nov 09	Mar 10	Jul 10	Oct 10	Feb 11
^{223}Ra	*P < 0.001 (1 m > 2, 4 m)*	NS[4]	NS	*P < 0.008 (1 m > 2, 4 m)*	*P < 0.008 (1 m > 2, 4 m)*	NS
^{224}Ra	*P < 0.001 (All Pairwise)*	NS	NS	*P < 0.008 (1, 2 m > 4 m)*	*P < 0.008 (1 m > 4 m)*	*P < 0.008 (1, 2 m > 4 m)*
^{226}Ra	*P < 0.001 (1 m > 2, 4 m)*	NS	NS	*P < 0.008 (1 m > 2, 4m)*	NS	NS
^{228}Ra	*P < 0.001 (All Pairwise)*	NS	NS	*P < 0.008 (1, 2 m > 4 m)*	*P < 0.008 (1, 2 m > 4 m)*	NS
^{224}Ra/^{223}Ra	*P < 0.008 (2 m > 4 m)*	NS	NS	NS	NS	NS
^{228}Ra/^{226}Ra	*P < 0.008 (1, 2 m > 4 m)*	NS	NS	NS	*P < 0.008 (1, 2 m > 4 m)*	NS
Salinity	NS	NS	NS	NS	NS	NS
Temp	*P < 0.008*[5] *(1 m > 2, 4 m)*	NS	NS	NS	NS	NS
pH	NS	NS	NS	NS	NS	*P < 0.008 (1 m > 2, 4 m)*
Redox Pot	NS	NS	NS	NS	NS	NS

[1]Depth indicates the sample depth at which porewater was collected – 1, 2, and 4 m below the marsh surface.
[2]P values are the overall F-test with Bonferroni correction ($\alpha = 0.05/6 = 0.008$).
[3]Tukey's multiple comparison test results shown in parentheses (experiment-wise error rate of 0.05).
[4]NS = Not Significant
[5]This correlation is a Type I error.

Table 2.2. Porewater and Surface Water ANOVAs by Sample Date[1] with Tukey's Multiple Comparison Tests[2,3]

Response	All Porewater	1 m Samples	2 m Samples	4 m Samples	Surface Water
^{223}Ra	*P < 0.0125 (4, 5 > 2)*	NS[4]	NS	NS	NS
^{224}Ra	*P < 0.0125 (4 > 2)*	NS	NS	NS	NS
^{226}Ra	*P < 0.001 (3, 4 > 1, 2, 5)*	NS	*P < 0.001 (3 > 1, 2, 5) (4 > 2)*	NS	*P < 0.05 (1 > 2, 5)*
^{228}Ra	*P < 0.001 (4 > 1) (3, 4 > 2)*	NS	NS	NS	NS
^{224}Ra/^{223}Ra	NS	NS	NS	NS	NS
^{228}Ra/^{226}Ra	NS	NS	NS	NS	NS
Salinity	*P < 0.001 (4, 5 > 1)*	NS	NS	*P < 0.001 (2, 3, 4, 5 > 1)*	NS
Temp	*P < 0.001 (3, 4 > 1, 2, 5) (1 > 2)*	*P < 0.001 (3, 4 > 1, 5) (3 > 4)*	*P < 0.001 (3, 4 > 1, 2, 5)*	*P < 0.001 (3, 4 > 2) (3 > 5)*	*P < 0.05 (3, 4 > 1, 2, 5)*
pH	*P < 0.001 (1, 2 > 3, 4, 5)*	*P < 0.0125 (1 > 3, 4, 5)*	*P < 0.001 (1, 2 > 3, 4, 5)*	*P < 0.001 (1, 2 > 3, 4, 5)*	NS
Redox Pot	NS	NS	NS	NS	NS

[1]Samples dates are numbered as follows: 1 = Nov 09; 2 = Mar 10; 3 = Jul 10; 4 = Oct 10; 5 = Feb 11

[2]P values for porewater were analyzed using the overall F-test with Bonferroni correction ($\alpha = 0.05/4 = 0.0125$). P values for surface water were analyzed using the overall F-test ($\alpha = 0.05$).

[3]Tukey's multiple comparison test results shown in parentheses (experiment-wise error rate of 0.05).

[4]NS = Not Significant

Table 2.3. Bulk Radium Activity – Surface Sediment[1]

Location	^{226}Ra (dpm/g)		^{228}Ra (dpm/g)	
	Feb 2010	Oct 2010	Feb 2010	Oct 2010
NS3	0.97	1.07	1.07	1.17
NS3-NS2	0.24	0.90	0.81	0.89
NS2	0.96	0.86	0.99	0.99
NS2-NS1	1.26	1.29	1.03	1.22
NS1	0.39	**[2]	0.39	1.15
Channel	1.5	0.82	**	0.96

[1]Sample collection locations shown in Fig. 2.2B.
[2]Indicates result below detection limit.

Table 2.4. Bulk Sediment Radium Activity – Sediment Core Samples[1]

Core No. (Piezometer)	Sample Depth	Sediment Type	^{226}Ra (dpm/g)	^{228}Ra (dpm/g)
6B (EW4)	4 m	Sand	1.57	1.26
7T (EW3)	0.3 m	Mud/Silt	1.16	1.41
7B (EW3)	3 m	Mud/Silt	1.31	1.78
8B (--)	3 m	Mud/Silt	1.23	1.72
9B (--)	3.5 m	Sand	1.68	1.77

[1]Sample locations shown in Fig. 2.2A.

Table 2.5. Porewater and Surface Water ANOVAs by Sample Date[1] with Tukey's Multiple Comparison Tests[2,3]

Response	All Porewater	1 m Samples	2 m Samples	4 m Samples	Surface Water
^{223}Ra	*P < 0.0125 (4, 5 > 2)*	NS[4]	NS	NS	NS
^{224}Ra	*P < 0.0125 (4 > 2)*	NS	NS	NS	NS
^{226}Ra	*P < 0.001 (3, 4 > 1, 2, 5)*	NS	*P < 0.001 (3 > 1, 2, 5) (4 > 2)*	NS	*P < 0.05 (1 > 2, 5)*
^{228}Ra	*P < 0.001 (4 > 1) (3, 4 > 2)*	NS	NS	NS	NS
^{224}Ra/^{223}Ra	NS	NS	NS	NS	NS
^{228}Ra/^{226}Ra	NS	NS	NS	NS	NS
Salinity	*P < 0.001 (4, 5 > 1)*	NS	NS	*P < 0.001 (2, 3, 4, 5 > 1)*	NS
Temp	*P < 0.001 (3, 4 > 1, 2, 5) (1 > 2)*	*P < 0.001 (3, 4 > 1, 5) (3 > 4)*	*P < 0.001 (3, 4 > 1, 2, 5)*	*P < 0.001 (3, 4 > 2) (3 > 5)*	*P < 0.05 (3, 4 > 1, 2, 5)*
pH	*P < 0.001 (1, 2 > 3, 4, 5)*	*P < 0.0125 (1 > 3, 4, 5)*	*P < 0.001 (1, 2 > 3, 4, 5)*	*P < 0.001 (1, 2 > 3, 4, 5)*	NS
Redox Pot	NS	NS	NS	NS	NS

[1]Samples dates are numbered as follows: 1 = Nov 09; 2 = Mar 10; 3 = Jul 10; 4 = Oct 10; 5 = Feb 11

[2]P values for porewater were analyzed using the overall F-test with Bonferroni correction ($\alpha = 0.05/4 = 0.0125$). P values for surface water were analyzed using the overall F-test ($\alpha = 0.05$).

[3]Tukey's multiple comparison test results shown in parentheses (experiment-wise error rate of 0.05).

[4]NS = Not Significant

Table 2.6. Partial Correlation between Specific Discharge and Porewater Radium Activity[1]

Specific Discharge Averaged Over[2]	^{223}Ra	^{224}Ra	^{226}Ra	^{228}Ra
1 Day	*r = -0.263* *P < 0.05*	*r = -0.324* *P < 0.05*	r = -0.090 NS	r = -0.185 NS
4 Days	*r = -0.249* *P < 0.05*	*r = -0.316* *P < 0.01*	r = -0.086 NS	r = -0.181 NS
11 Days	r = -0.177 NS	*r = -0.261* *P < 0.05*	r = -0.003 NS	r = -0.981 NS

[1]P values are the overall F-test ($\alpha = 0.05$).
[2]Please see Appendix A for details on averaging scheme.

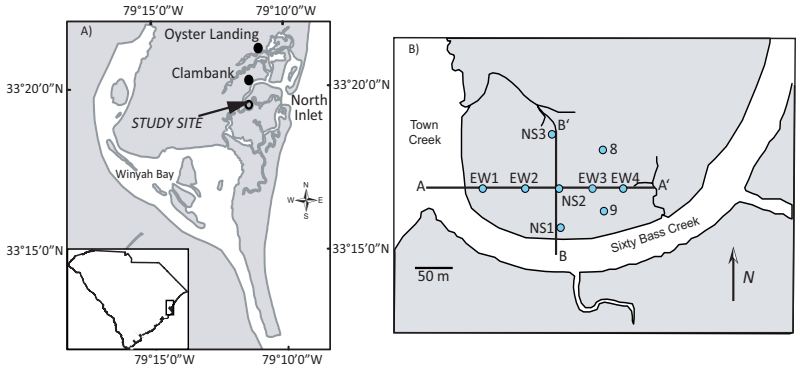

Figure 1

Figure 2.1. Map of Study Area A) North Inlet-Winyah Bay. Tide and meteorological data collected at Oyster Landing. B) Map of the study site with sediment core and piezometer nest locations indicated by circles. Modified from Hughes et al., 2012.

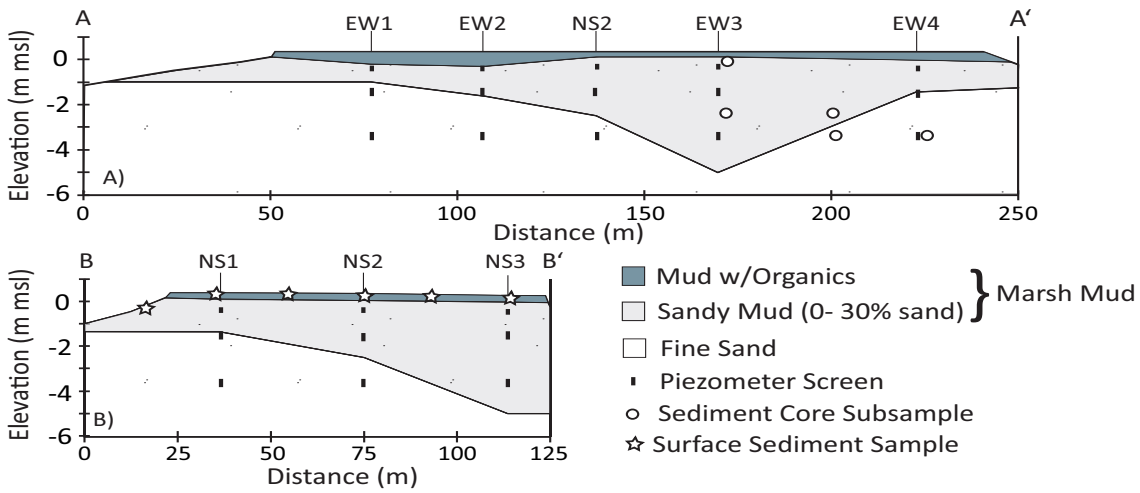

Figure 2

Figure 2.2. Marsh stratigraphy. A) A to A': West to East transect. B) B to B': South to North Transect. The screened interval locations of the piezometers are indicated by vertical dashes. Surface sediment sample collection locations are indicated by stars (2B), and samples split from the sediment cores are indicated by open circles (2A).

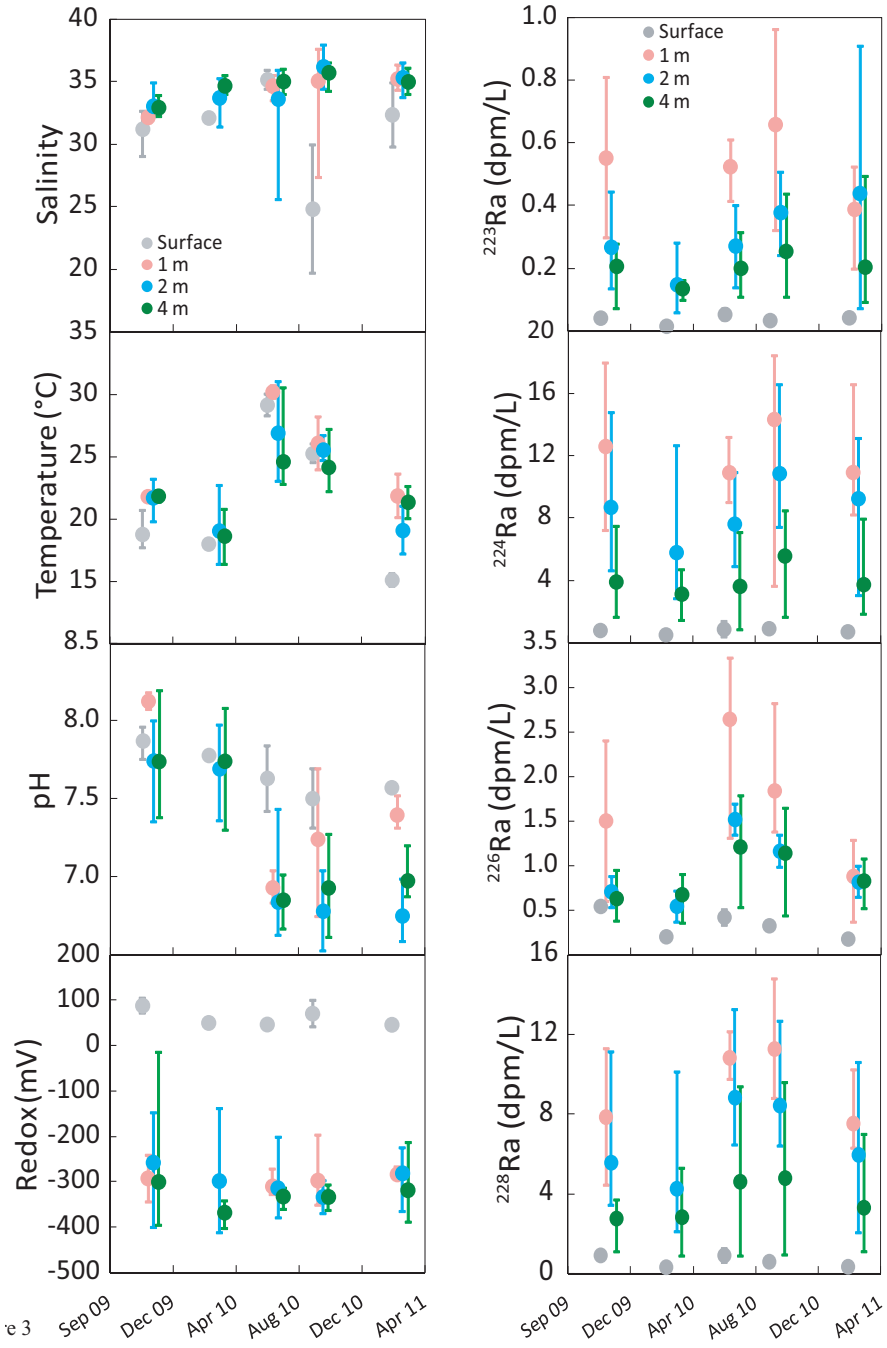

Figure 2.3. E-H) Average salinity, temperature, pH, redox potential, and activities of all four radium isotopes in groundwater and surface water at each sample date. Groundwater values represent an average for all piezometers screened at the specified depth. Error bars indicate the maximum and minimum values. The average and range of these measurements are also listed in Tables A.3 and A.4 in the Appendix. Data points are slightly offset for greater visibility of the error bars.

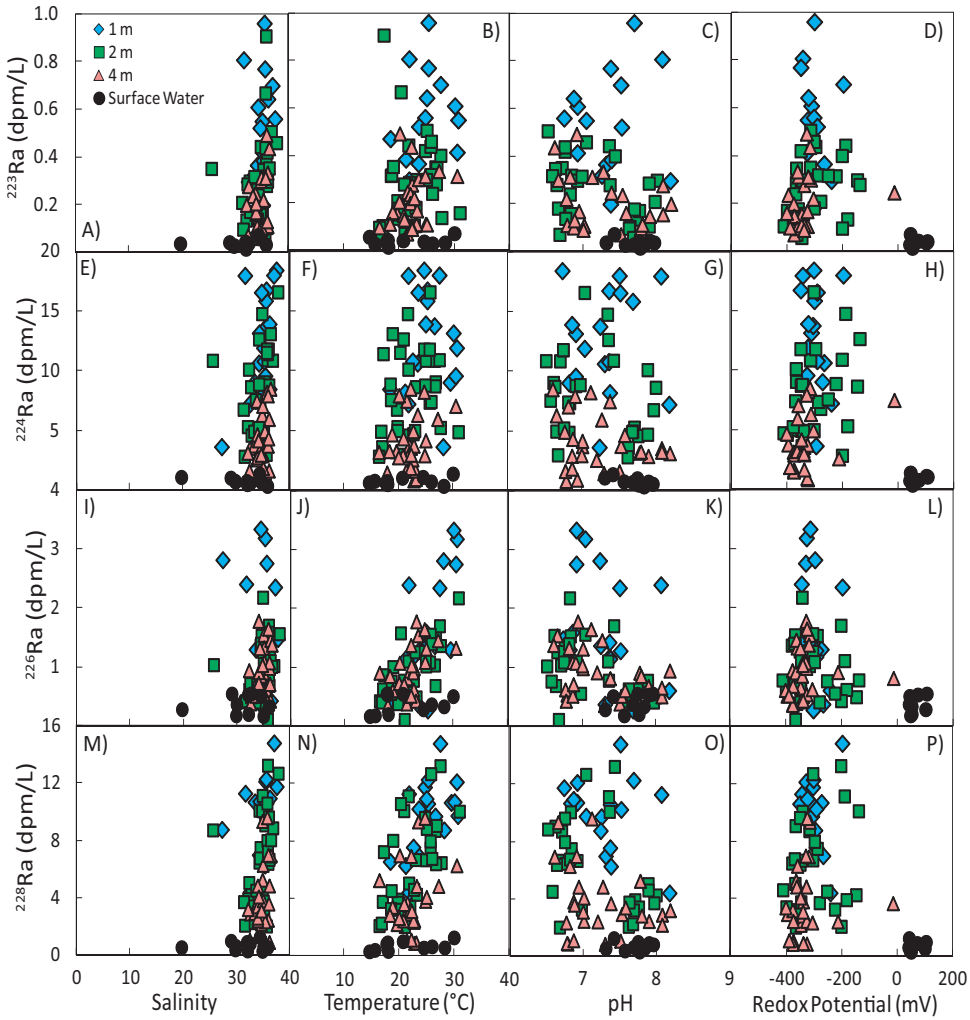

Figure 4

Figure 2..4 Porewater and surface water ^{223}Ra, ^{224}Ra, ^{226}Ra, and ^{228}Ra versus salinity, temperature, pH, and redox potential. Symbols represent measurements made at each piezometer depth and in the surface water.

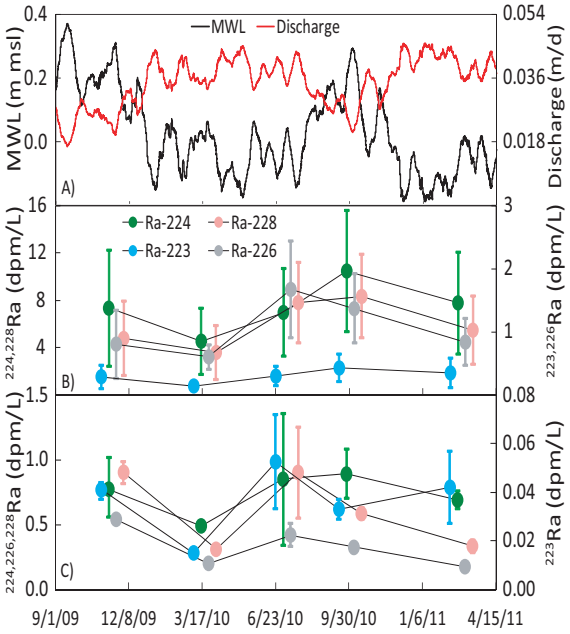

Figure 5

Figure 2.5. A) 14-day averages of tide (m msl) and regression model estimates of specific discharge (m/d per m of shoreline). B) Mean porewater radium activity (± 1 standard deviation), and C) mean surface water radium activity (± minimum and maximum values) by sample date. Data points are slightly offset in Fig. 5B and 5C for clarity.

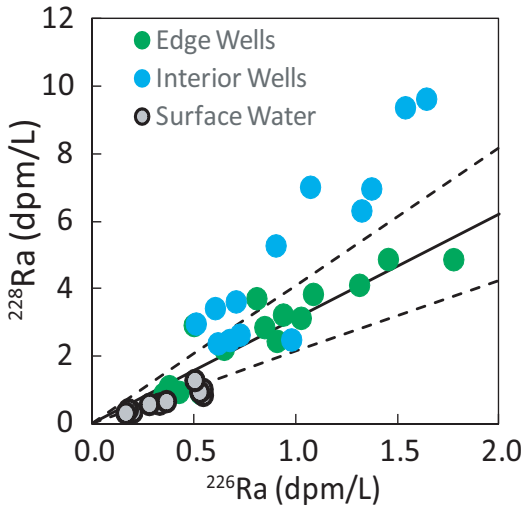

Figure 6

Figure 2.6. Measurements of ^{228}Ra versus ^{226}Ra in the surface water (gray symbols) and in the confined aquifer (4 m piezometers). The solid green symbols represent the interior piezometers (EW2, NS2, and EW3), and the solid blue symbols represent the edge piezometers (EW1, NS1, NS3, and EW4). The solid line and dashed lines are the mean $^{228}Ra/^{226}Ra$ activity ratio measured in the 4 m edge piezometers ± 1 standard deviation about the mean (2.3 ± 0.5).

CHAPTER 3

RECONCILING HYDROLOGIC AND GEOCHEMICAL ESTIMATES OF SUBMARINE GROUNDWATER DISCHARGE: A COUPLED MODEL OF GROUNDWATER FLOW AND RADIUM TRANSPORT[3]

[3] Hughes, A.L.H., A.M. Wilson, and W.S. Moore, Unpublished

3.1 ABSTRACT

Submarine groundwater discharge (SGD) is an important source of carbon, nutrients and other solutes from coastal aquifers to estuaries and coastal oceans. The four isotopes of radium and associated radon daughter products have been essential tracers for estimating SGD from coastal aquifers, but spatial and temporal variations in groundwater tracer compositions can make it difficult to determine the groundwater endmember for these methods. In this study, we developed a groundwater flow and transport model to calculate SGD and identify controls on observed spatial and temporal variations Ra isotope activities in groundwater at a salt marsh island at North Inlet, South Carolina. Groundwater age was also simulated to provide an independent measure of groundwater transport. A primary goal of the modeling was to test prior statistical correlations that suggested that spatial and temporal variations in Ra activity are controlled by variations in groundwater transport. Model experiments confirmed that groundwater transport is an important control on spatial variations in Ra activity, particularly through lower flow rates in a surficial mud layer than in an underlying sandy aquifer and greater tidal exchange near the marsh creeks than in the marsh interior. Spatial variations in Ra activity were also influenced by variations in sediment grain size, which affects the fraction of Ra that becomes mobile. Simulations showed that decreased SGD during seasonal highs in sea level caused measurable increases in groundwater age, but these variations failed to reproduce observed temporal variations in Ra activity. Instead, results from this marsh island suggest that temporal variations in measurements of ^{223}Ra and ^{224}Ra were largely caused by variations in Ra sorption coefficients. Temporal variability in Ra activities was largely captured by the model when the distribution coefficient that

governs Ra sorption was allowed to vary as a function of temperature. The remaining discrepancies between simulated and measured Ra over time suggest that temporal variations in Ra activities are influenced by redox-controlled variations in Ra sorption. Calculated SGD fell within one order of magnitude of other SGD estimates from East Coast salt marshes despite diverse locations and techniques. Our results corroborate existing conceptual models of flow within layered intertidal salt marshes and highlight the value of combining numerical and tracer methods to estimate SGD.

3.2 Introduction

Estuaries and intertidal salt marshes rank among the most productive ecosystems on Earth (Wiegert and Freeman, 1990; Vernberg and Vernberg, 2001). These coastal ecosystems support a wide range of ecological functions, ranging from nutrient cycling to hosting sheltered nurseries for a variety of economically important shell fish and fin fish species. Salt marshes also sequester more carbon per unit area per year than forest ecosystems (Chmura et al., 2003; Duarte et al., 2005; Mcleod et al., 2011). Ecological productivity and biogeochemical cycling in these systems are influenced by a wide range of biotic factors, including competition between species, but abiotic factors provide a framework within which biotic factors operate. In particular, surface-water/groundwater interactions drive significant export of nutrients, carbon, and other dissolved constituents from coastal aquifers to estuaries and the coastal ocean.

Surface-water/groundwater interactions in coastal settings have been widely studied in the context of submarine groundwater discharge (SGD). SGD drives export of nutrients, carbon and other dissolved constituents from coastal sediments to the ocean in coastal systems around the world (Burnett et al., 2003; Moore, 2010; Santos et al., 2011)

and particularly in salt marsh systems (Whiting and Childers, 1989; Krest et al., 2000; Morris, 2000; Charette et al., 2003; Charette and Buesseler, 2004). Previous studies of submarine groundwater discharge have used a variety of methods to determine groundwater discharge rates in coastal ecosystems (Burnett et al., 2002; Burnett et al., 2006). Geochemical tracers are among the most powerful of these methods.

Of the potential geochemical tracers of groundwater, the naturally-occurring isotopes of radium (Ra) have proven extremely useful in the coastal zone (Burnett et al., 2003; Moore, 2010; Santos et al., 2012). However, activity of Ra in groundwater can be quite variable in space and time, which introduces an equivalent uncertainty in tracer-based calculations of groundwater discharge (Gonneea et al., 2008; Hougham et al., 2008; Gonneea et al., 2013). One of the primary goals of this paper is to develop a process-based understanding of variations in porewater activities of Ra.

Several factors affect Ra activity in porewater. The primary control is the rate of Ra generation and decay, which differs among the four Ra isotopes. Geochemically-driven changes to the Ra distribution coefficient (K_d) also control porewater radium activity by altering the extent of sorption to sediments. Several laboratory and field studies have shown that radium activity is affected by changes in K_d due to changes in salinity, temperature, pH, and redox potential, with the greatest control on Ra sorption provided by variable porewater salinity (King et al., 1982; Krest et al., 2000; Gonneea et al., 2013). Porewater Ra activities can also be affected by groundwater transport and aquifer sediment grain size. In a salt marsh island at North Inlet, SC, clear spatial patterns in Ra activity were linked qualitatively to sediment heterogeneity, which included differences in permeability and reactive surface area, and tidally-driven groundwater flow

patterns, which included greater tidal exchange near the creek banks than in the interior of the marsh island (Hughes et al., 2015). This prior study also indicated a statistically significant relationship between temporal variations in porewater Ra activity and seasonal groundwater discharge. The activity of ^{228}Ra and ^{226}Ra in porewater was also statistically correlated with temperature, which also varied seasonally. Although these relationships were statistically significant, they were established using only a few Ra samples from quarterly sampling events. Here we seek a quantitative, process-based explanation for the observed correlations between temperature, groundwater discharge, and Ra activity using numerical models of groundwater flow and transport.

Groundwater models have been developed to simulate rates of SGD, but they have not always generated results that agree with radioisotope tracer results (Burnett et al., 2003). Models can be affected by uncertainty in physical parameters, particularly sediment permeability, and by conceptual errors, in which important flow processes are not included in the model (Oreskes et al., 1994). A very effective way to resolve these issues is to calibrate the model to naturally-occurring tracer data.

In the current study, we took advantage of a salt marsh island in which the factors driving groundwater flow and Ra transport are well-conceptualized and where models can be calibrated to observed hydraulic head and Ra data. We then used those models to map groundwater flow patterns, calculate time-varying groundwater discharge, calculate groundwater age, and test prior conceptual models describing the controls of discharge, tidal exchange, residence time, and temperature over spatial and temporal variations in the porewater Ra activity (Hughes et al., 2015).

3.3 Conceptual Model for Groundwater Flow in Salt Marshes with Layered Stratigraphy

Groundwater flow in salt marshes is driven by tidal fluctuations, evapotranspiration, infiltration of fresh rainwater and saline creek water, and discharge of fresh groundwater from adjacent uplands. Together, these flow processes drive net flow from the uplands to tidal creeks and estuaries (Harvey et al., 1987; Thibodeau et al., 1998; Gardner and Reeves, 2002; Hughes et al., 2012; Wilson and Morris, 2012; Wilson et al., 2015b). Salt marshes in the southeastern U.S. and around the world commonly exhibit layered stratigraphy, in which fine-grained marsh muds overlie older, more permeable sand layers (Wiegert and Freeman, 1990; Hughes et al., 1998; Gardner and Porter, 2001; Grewell et al., 2007). This creates a confined aquifer system, in which groundwater flow in the mud layer has been conceptualized as essentially vertical (Hemond and Fifield, 1982; Hughes et al., 2012; Wilson et al., 2015b), and flow through the sand is largely horizontal (Harvey et al., 1987; Wilson et al., 2011).

Groundwater exchange between the sediments and surface water is also heavily influenced by variations in sea level, which occur over time scales ranging from one tidal cycle to centuries. A recent field study of a layered marsh confirmed that groundwater discharge per tidal cycle is proportional to the amplitude of tidal fluctuations (Wilson et al., 2015a), consistent with analytical models for confined aquifers. Groundwater discharge has also been found to be significantly inversely related to seasonal variations in MWL (Harvey et al., 1987; Hughes et al., 2015; Wilson et al., 2015a), so that marshes that are unable to accrete quickly enough to maintain their current elevation relative to rising sea level will see decreasing volumes of SGD.

3.4 Field Site

The study site is an island in North Inlet Salt Marsh near Georgetown, South Carolina, in the North Inlet-Winyah Bay National Estuarine Research Reserve (NI-WB NERR; Fig. 3.1). This study site has been the subject of two prior hydrogeologic investigations (Hughes et al., 2012; Hughes et al., 2015). The NI-WB NERR covers 32 km^2 of tidally-dominated salt marsh and wetlands extensively populated by the salt marsh cord grass *Spartina alterniflora*. Nine sediment cores revealed stratigraphy of 1 – 4 m of marsh mud overlying fine-grained sand (Fig. 3.2A). The top 25 cm of the marsh mud contains organic detritus and *S. alterniflora* roots. Below the top 25 cm, the marsh mud contains occasional sand inclusions and a small (< 30%), varying percentage of sand. The sands underlying the surficial mud at this site are non-calcareous, muddy, fine- to medium-grained sand that was reworked from Pleistocene beach ridges (Gardner and Porter, 2001).

Previous studies show that the hydrogeology of the island conforms to the conceptual model described above for layered salt marshes (Hughes et al., 2012; Hughes et al., 2015) including a relationship between MWL and discharge estimates from the confined sand made using Darcy's Law (Hughes et al., 2015). The lack of a freshwater upland immediately adjacent to the island is an advantage of the site, because it greatly simplifies groundwater flow. In particular, the average porewater salinity below the root zone is essentially constant at 30 ppt (Hughes et al., 2012). Within the root zone, the average salinity increases with depth owing to infiltration of fresh rainwater at the surface and transpiration from the root zone (Hughes et al., 2012), which creates a stable density configuration. This removes the need to consider variable density groundwater flow or

salinity-related changes in Ra sorption because ionic exchange of Ra in salt water is considered to reach its maximum extent at salinities of roughly 10 ppt and over (Webster et al., 1995).

Prior analyses at the site suggested clear links between stratigraphy, groundwater flow patterns, and spatial variations in Ra activities (Hughes et al., 2015). The highest Ra activities were found in the surficial mud layer. Ra activities were lower in the underlying sandy aquifer and declined further near the creek bank, where tidal exchange with low-Ra creek water occurred. The relatively high Ra activities observed in the surficial mud layer were attributed to relatively long residence times in the low-permeability mud and to the small grain size of the mud. It was suggested that grain size influenced Ra activities primarily through increased reactive surface area, which should support a greater pool of sorbed Th parent isotopes.

This prior work also reported that small temporal changes in porewater ^{223}Ra and ^{224}Ra activity coincided with seasonal changes in groundwater discharge (Hughes et al., 2015). A statistically significant relationship was found between temporal variations in Ra activity and seasonal variations in SGD. A statistically significant relationship was also found between temporal variations in Ra activity and seasonal variations in temperature. These results left several remaining questions, however, because the statistical analyses were limited by small sample sizes, and statistical relationships do not establish causality. The estimates of SGD were also calculated using Darcy's Law rather than a 2- or 3-D model, raising questions about their accuracy. In this paper we present process-based models that were used to test the controls on spatial and temporal variations in Ra that were proposed by Hughes et al. (2015).

3.5 Materials and Methods

Field Installation and Observations

Piezometer nests were installed at seven of the nine core locations (Fig. 3.1B) forming N-S and E-W transects with three piezometers per nest screened at depths of 1, 2, and 4 m below the marsh surface (Fig. 3.2A). The piezometers were instrumented to record pore pressure, temperature, and salinity during 2007 – 2008 (Hughes et al., 2012). These measurements were used, along with surveyed piezometer elevations, to calculate hydraulic head as:

$$H_T = P/(\rho g) + z \tag{3.1}$$

where H_T (m) is total hydraulic head, $P/(\rho g)$ (m) is pressure head (P = pressure; ρ= water density, g is gravity: [9.81 m s^{-2}]), and z (m) is the elevation of the location of the pressure measurement. We measured radium activity in the porewater and surface water quarterly from November 2009 to February 2011. Bulk sediment radium activity was measured in samples collected from the marsh surface as well as split from the sediment cores. Tide, meteorological, surface water temperature and salinity data recorded at the Oyster Landing station (Fig. 3.1A; CO-OP ID 8662245), were obtained from the NOAA Tides & Currents webpage and the NOAA NERRS Central Data Management System (NOAA, 2012, 2013; Hughes et al., 2015).

Numerical Models

We simulated groundwater flow and transport of ^{223}Ra, ^{224}Ra, and ^{228}Ra using the saturated/unsaturated groundwater flow and solute transport code SUTRA (Voss and

Provost, 2002), and all terms are in kg, m, and s. ^{226}Ra was excluded from the Ra transport models because the time it takes for this isotope to achieve secular equilibrium in the marsh, roughly 5 to 6 times the half-life of 1600 y, is equivalent to the age of this Holocene marsh. Model parameters are listed in Table 3.1. This version of SUTRA was modified to incorporate changes in total stress (Reeves et al., 2000):

$$\nabla \cdot |K(\psi)\nabla h| = S_w S_s \frac{\partial h}{\partial t} + \phi \frac{\partial S_w}{\partial t} - S_w \alpha_s \frac{\partial \sigma_T}{\partial t} \quad (3.2)$$

where K is hydraulic conductivity as a function of pressure (ψ), h is total hydraulic head, S_w is saturation, S_s is specific storage, ϕ is porosity, α_s is the compressibility of the solids, σ_T is total stress, and t is time. SUTRA was also modified to use the standard form of the specific storage equation:

$$S_s = \rho g(\alpha_s + \phi\beta) \quad (3.3)$$

where ρ is fluid density, g is gravity (9.81 m s^{-2}), ϕ is porosity, and β is the compressibility of water.

The relative permeability of unsaturated sediment was based on calculations of sediment saturation using the van Genuchten equation (van Genuchten, 1980):

$$S_w = S_{wr} + \frac{(S - S_{wr})}{[1+(\alpha|\psi|)^n]^m} \quad (3.4)$$

where S_{wr} is the residual saturation of the sediment, α is the inverse of the capillary rise (m^{-1}), ψ is suction pressure head, and n and m are fit parameters. The inverse capillary rise is:

$$\alpha = \frac{1}{h_b}\left(2^{1/m} - 1\right)^{1-m} \tag{3.5}$$

where h_b is the air entry pressure. The fit parameters of m and n are related as:

$$m = 1 - {}^{1}/_{n} \tag{3.6}$$

Radium transport, generation, and decay were simulated using the advection-dispersion equation (Voss and Provost, 2002):

$$\frac{\partial C_{Tot}}{\partial t} = \nabla \cdot D\nabla C_{aq} - v \cdot \nabla C_{aq} - \lambda\left(C_{aq} + C_s\right) + \gamma \tag{3.7}$$

where $C_{Tot} = C_{aq}+C_s$, C_{aq} is the number of Ra atoms in the pore fluid and C_s is the number of Ra atoms adsorbed to the sediment surface, D is the hydrodynamic dispersion coefficient, v is the fluid flow velocity, λ is the first-order isotope-specific decay constant, and γ is a zero-order production term that can be either an isotope specific generation rate of Ra in the sediment or a source term to simulate groundwater age. The half-lives (and decay constants) of ^{223}Ra, ^{224}Ra, and ^{228}Ra are 11.4 d (7.0358 x 10^{-7} s), 3.66 d (2.1919 x 10^{-6} s), and 5.75 y (3.8225 x 10^{-9} s), respectively.

Radium generation rates were assigned based on laboratory analyses of the sediments (Table 3.1). The sediment generation rate for ^{224}Ra was based on the average bulk sediment ^{228}Th activity. The generation rate for ^{228}Ra was based on the average bulk sediment ^{228}Ra activity assumed to be in equilibrium with sediment ^{232}Th activity. The generation rate of ^{223}Ra was assumed to be 1/22 of the bulk sediment activity of ^{226}Ra (based on an assumption that ^{227}Ac activity is 1/22 of ^{230}Th activity) (Rama and Moore, 1996). The Ra generation rates were then reduced based on the assumption that only 40% of bulk sediment activity is exchangeable with the porewater (Krest et al., 2000). Finally, a multiplication factor based on published, standard grain size data (Horowitz, 1991) was applied to the sediment generation rates of Ra in order to account for the differences in grain surface area between the mud and sand.

Ra sorption to sediment was modeled using the linear sorption isotherm, which was modified to allow the distribution coefficient to vary with time. The Sutra equation for linear sorption isotherm is:

$$\frac{\partial C_s}{\partial t} = (K_d \rho) \frac{\partial C_{aq}}{\partial t} \tag{3.8}$$

where C_s is the activity of Ra sorbed per unit mass of solid, C is the activity of Ra in solution, t is time, K_d is the distribution coefficient of Ra (m^3/kg), and ρ is fluid density. The dependence of K_d on temperature was determined from field data (Rama and Moore, 1996; Hughes et al., 2015), as described in the Appendix. The resulting regression equation was substituted in Equation 3.8:

$$K_d(t) = -0.21 \times ln\big(T(t)\big) + 0.7739 \tag{3.9}$$

Seasonal changes in the distribution of porewater temperature were modeled using an analytical solution to the heat equation (Carslaw and Jaeger, 1959). The analytical temperature equation used in the model is described in the Appendix.

This version of Sutra does not accurately account for the full equation allowing the distribution coefficient to vary with time, which is as follows:

$$\frac{\partial C_s}{\partial t} = \frac{\partial}{\partial t}\left(K_d C_{aq}\right) = K_d \frac{\partial C_{aq}}{\partial_t} + C_{aq} \frac{\partial K_d}{\partial t} \frac{\partial T}{\partial t} \tag{3.10}$$

An analysis of the importance of the second term in Equation 3.10 indicated that for ^{223}Ra and ^{224}Ra, this excluded term is not important when compared to the remainder of the terms in Equation 3.7. However, for ^{228}Ra, this term is equivalent to the generation rate term. Therefore, we have excluded ^{228}Ra from further discussion. Please see the Appendix for a discussion of this analysis.

Groundwater age was also simulated for the 2007 – 2008 period for comparison with patterns of groundwater flow and changes in MWL. Groundwater age was simulated by treating age as if it were a solute subject to transport, dispersion, and mixing with surface water. This was accomplished by setting the zero-order production term in Eq. 3.7 to 1 s^{-1}. The surface water "age concentration" was set to zero and the initial "age" throughout the domain was set to zero.

Model Domain

In order to capture the 3D nature of the study site, we chose a cylindrical model domain where X = 0 was the approximate center of the marsh island (Fig. 3.2B). The domain has a radius of 125 m, representing the average distance from the center of the marsh to the center of the tidal creek. The elevation of the top of the marsh platform was 0.30 m (Y = 0.30 m) above mean sea level based on field observations (Hughes et al., 2012). The bottom of the domain was set at -10.0 m (Y = -10.0 m). Three sediment types were defined within the model: surficial mud with crab burrows, mud below the crab burrows, and fine sand (Table 3.1). A crab burrow layer occupied the upper 20 cm of the marsh platform and was assigned a higher porosity and air entry pressure than the bulk mud below 20 cm (Hughes et al., 1998). The total thickness of mud varied based on field observations, and a layer of mud too thin to represent in Figure 3.2B (20 – 25 cm) covers the sand aquifer along the creek bottom (A to the Sand/Mud boundary). Time varying specified pressure and specified flux boundaries were assigned to the surface of the domain (A to A', Fig. 3.2B) to account for tidal variations as well as precipitation and evapotranspiration (ET). The remaining domain edges were defined as no flow boundaries. Observation nodes were chosen to correspond to the piezometers within nests EW1, EW2, and NS2 (Fig. 3.1B and 3.2B), for a total of 9 observation nodes.

Boundary conditions along the top of the model domain were allowed to vary with time. For areas of the marsh surface that were inundated, the water pressure was specified based on the depth and density of the surface water. All of the time-varying boundary conditions were tidal height, surface water salinity and density, precipitation, and calculations of ET based on meteorological and surface water data obtained from the

NOAA Tides and Currents and the NOAA NERRs Central Data Management Office websites (NOAA, 2012, 2013). Evapotranspiration was calculated using a modification of the Turc equation using solar radiation and average daily temperature (Turc, 1961; Douglas et al., 2009):

$$ET(mm/d) = 0.013 \times \left((23.88 \times TSR) + 50\right) \times \left(\frac{ADT}{ADT+15}\right) \quad (3.11)$$

where ET is evapotranspiration, TSR is total solar radiation (MJ/m^2 d), and ADT is average daily temperature (°C).

Initial Conditions and Steady State Runs

We generated the initial conditions for the model in two steps. First, the groundwater flow model, using a simple sinusoidal tide, was allowed to run until hydraulic heads reached a repeatable tidal cycle. Then Ra transport was added to the tidal flow models and run until a steady-state distribution of Ra activities was obtained.

Model Calibration and Fit

The groundwater flow model was calibrated using hydraulic head data calculated from in-situ pressure, temperature, and salinity measurements from 2007 – 2008 (Hughes et al., 2012). Following the groundwater flow model calibrations, the simulations were run forward to the 2009 – 2011 period when Ra data were collected. The Ra transport component of the model was calibrated next using porewater Ra measurements from 2009 – 2011 (Hughes et al., 2015). Pearson correlation tests were then used to quantify the fit between the continuous records of hydraulic head measurements and simulation results ($\alpha = 0.05$).

Once the groundwater flow model was calibrated to hydraulic head and Ra measurements, further tests were conducted to determine if the model produced unique groundwater flow and Ra results. This was accomplished by maintaining a constant hydraulic diffusivity value while altering the model parameters of intrinsic permeability (k) and sediment compressibility (α_s). Hydraulic conductivity (K) and specific storage (S_s: Eq. 3.3) are related to hydraulic diffusivity (D^*) by the equation (Freeze and Cherry, 1979):

$$D^* = \frac{K}{S_s} \tag{3.12}$$

and hydraulic conductivity (K) is related to intrinsic permeability (k) as:

$$K = k\left(\frac{\rho g}{\mu}\right) \tag{3.13}$$

where μ (0.001 kg m^{-1} s^{-1}) is dynamic viscosity. The range of sediment compressibility and intrinsic permeability values used in these additional tests are also reported in Table 3.1.

3.6 Results

Groundwater Flow

The calibrated porosity, permeability, compressibility, and van Genuchten equation parameters (Eqs. 3.4 through 3.6) of the different sediment regions are presented in Table 3.1. The resulting groundwater flow model produced hydraulic heads very similar to field observations (Fig. 3.3). Pearson correlation tests used to compare the

simulation results with the hydraulic head data set from 2007 – 2008 produced an average r^2 value of 0.9 for nest NS2, 0.8 for nest EW2, and 0.8 for EW1. Sensitivity studies in which sediment compressibility and permeability were varied independently caused the simulated hydraulic head and Ra activity to depart substantially from the calibrated results, indicating that the model results were unique.

The groundwater flow simulations showed patterns similar to those of an earlier modeling study in which an idealized two-layer marsh (mud overlying sand) was subjected to tidal forces (Wilson and Morris, 2012). Examples of typical groundwater flow vectors at high and low tide are shown in Figure 3.4. At high tide, groundwater moved from the channel toward the marsh interior with the lowest groundwater velocities at slack high tide (maximum value typically 0.50 cm/d) (Fig. 3.4A). At low tide, groundwater flow reversed direction and moved from the marsh interior to discharge at the tidal channel (Fig. 3.4B). The simulated flow velocities were greatest in the sand aquifer near the tidal creek, where the velocity occasionally exceeded 90 cm/d.

The average groundwater flow over one tidal cycle shows that the net movement of water within the marsh is vertically downward through the confining marsh mud into the sand aquifer below (Fig. 3.4C). From there, groundwater travels laterally through the sand aquifer to discharge at the marsh creek. The average velocities ranged from 0.03 to 30 cm/d. Generally, groundwater flow was faster within the underlying, higher permeability sand than within the marsh mud, and the greatest velocities occurred near the marsh creek, similar to the pattern of groundwater flow observed at each low tide. This net pattern of groundwater movement corroborates prior interpretations of net

groundwater movement based on hydraulic head data collected at this site during 2007 – 2008 (Hughes et al., 2012).

Simulations showed that groundwater discharge across the sediment/water interface was affected by the daily tide, seasonal changes in mean water level, and the differences in flow velocity between the mud and the sand. On a daily basis, volumetric discharge across the marsh channel reflects semi-diurnal tidal fluctuations (Fig. 3.5A). Discharge rates (positive values) ranged from 0 to 9 m^3/d/m creek bank, and recharge rates (negative values) ranged from 0 to 1.5 m^3/d/m creek bank (Fig. 3.5A). The discharge rates across the creek bank were higher than the recharge rates because the remainder of the recharge occurred across the top of the marsh through precipitation as well as tidal infiltration. The highest modeled creek bank discharge and recharge rates occurred in the month of December 2008 during a period of low mean water level and large tidal range (greater than 2 m). Seasonal changes in MWL (28-day average tide) were inversely related to simulated groundwater discharge averaged over the same period (Fig. 3.5B). Up to four times as much groundwater discharged from the sand aquifer as from the mud layer. These results are also consistent with prior interpretations of hydraulic head and radium data collected from this site (Hughes et al., 2012; Hughes et al., 2015).

Simulated groundwater ages were consistent with the general pattern of downward groundwater flow through the mud followed by lateral movement through the sand (Fig. 3.6A). Age increased downward through the marsh, with the highest values found near the marsh center and at depth. The lowest values were observed at the marsh surface, where net groundwater recharge occurred (Fig. 3.4C), and near the tidal creek,

where the greatest discharge and exchange with surface water occurred. Reduced net flow rates at the marsh center (Fig. 3.4C) explain the high groundwater ages in the central marsh. Temporal variations in water age at EW1 and EW2 corresponded with changes in MWL (Fig. 3.6B and C). That is, decreased discharge during periods of high MWL caused simulated groundwater age to increase. The groundwater age maximums lagged behind the MWL peaks by 45 to 60 days, an indication of the time required for the flow system to respond to the seasonal changes in MWL.

Radium – Spatial Variations

In general, the spatial differences observed in porewater Ra activity from 2009 – 2011 were captured by the Ra transport model. Measured porewater Ra activity and variability generally decreased with depth with occasional periods when the activity inverted, or was greater at the 2 m or 4 m depths than at the 1 m depth (Fig. 3.7). Simulated porewater Ra was consistent with the overall distribution of measured Ra activity (Figs. 3.7 and 3.8). The average simulated porewater Ra activity at the 2 m and 4 m observation nodes for the EW1, EW2, and NS2 locations was consistent with the previously measured values. However, the average Ra simulation values at the 1 m observation nodes at EW1, EW2, and NS2 were less than the measured values (Table 3.2). This included periods of time when temperature was higher at 4 m than at 1 m. Changes in porewater temperature seemed to provide a control on the spatial variations in simulated ^{223}Ra and ^{224}Ra activity. The seasonal inversions in porewater temperature, along with the constant downward flow of groundwater within the marsh mud, may also account for the occasional measurement periods when the Ra activity at deeper depths was greater than at the 1 m depth (Fig. 3.9). Model results also indicate a

shallow layer of higher Ra activity along the creek bottom (Fig. 3.8) which was caused by the thin mud layer included in the model domain. This mud layer had the same hydraulic and radium generation properties as the bulk surficial mud.

Radium – Temporal Variations

Simulations of porewater ^{223}Ra and ^{224}Ra activity captured the general seasonal variations observed in Ra measurements from 2009 - 2011 (Fig. 3.7) when thermal variations in temperature were included. However, measured porewater Ra activity at the EW1, EW2, and NS2 piezometer nests was generally highest in July and October 2010 and lowest in March 2010. In contrast, temporal patterns in simulated ^{223}Ra and ^{224}Ra activity were similar to those in simulated temperature (Fig. 3.9A and B). Simulated ^{223}Ra and ^{224}Ra activities and temperature were highest in August 2010 and not in October 2010, and the lowest simulated activities were in the months of February 2010 and 2011. The timing of the peak in simulated Ra activity did not match the MWL peak, but the maximum measured porewater Ra activity was close to the peak in MWL in October 2010 (Fig. 3.9). However, the maximum measured Ra values did not correspond with the maximum groundwater age, indicated by the red box in Figure 3.9.

3.7 DISCUSSION

The modeling results confirm the inverse relationship between average simulated discharge and MWL that has been reported in a variety of other coastal groundwater studies (Portnoy et al., 1998; Gonneea et al., 2013; Wilson et al., 2015a) and further confirm that Darcy's Law can be an effective way to estimate groundwater discharge from layered salt marshes. Hughes et al. (2015) estimated hydraulic conductivity at this site using two different tidal efficiency methods, then used Darcy's Law to estimate

groundwater discharge and recharge from the confined aquifer. These Darcy's Law calculations resulted in average discharge and recharge estimates of 0.9 (range 0 to 8.3) and 0.2 (range 0 to 1.5) m^3/d/m shoreline, respectively. This compares well with the average discharge and recharge values of the current study of 2.8 (range 0 to 9) and 0.3 (range 0 to 1.5) m^3/d per m of shoreline. This comparison supports the validity of the prior Darcy's Law discharge estimates.

It is important to quantify the seasonality of groundwater discharge and to consider what role these variations might play in the timing of groundwater-borne solute inputs to coastal surface water. Quantifying this seasonality in discharge using methods independent of Ra isotope measurements has lead to the observation that there are certain periods when maximum groundwater discharge and maximum Ra activity in local surface water are not in sync (Gonneea et al., 2013; Hughes et al., 2015). The maximum simulated porewater Ra activity in the current study (August) did not correspond to the period of greatest discharge (January – March), supporting the Ra/discharge discrepancies found in prior studies. The timing and mechanisms of groundwater-borne solutes is crucial to further understanding the seasonality of nutrient fluxes to coastal surface waters. Several studies of porewater nutrient concentrations in tidal salt marshes observed maximum concentrations of ammonium and DOC in the summer when organic detritus begins to degrade after the spring 'growing season'(Howes and Goehringer, 1994; Portnoy and Giblin, 1997). In a study in North-Inlet Winyah Bay estuary, maximum nutrient fluxes from the marsh occurred in the fall (Gardner and Kjerfve, 2006). Since minimum groundwater discharge from this site occurs in the fall appears to correspond to the maximum nutrient flux found in the prior study, the nutrient

concentration in the porewater must be elevated enough to overcome the lower groundwater discharge.

The results of this study compare favorably with prior discharge estimates for tidal salt marshes on the East Coast (Table 3.3), despite differences in methods, observation periods, and geomorphology between study sites. Variations among these results can be explained primarily by the simplifying assumptions used to calculate the estimates. For example, when using a salt/water balance, it is possible that measurements of shallow porewater surface salinity may be underestimated during undersaturated conditions (Morris, 1995). As described in the introduction, Ra-based calculations of groundwater discharge are sometimes hampered by the variability of Ra activities in the porewater end-member, which can contribute to uncertainties of up to 200% (Charette et al., 2003; Hougham et al., 2008). It should also be noted that the stratigraphy of New England salt marshes is typically comprised of coarser, glacial till material versus the sand and mud aquifers underlying southeastern salt marshes. Even though there are uncertainties associated with each method and differences in marsh geomorphologies, the estimates are all within one order of magnitude of one another except for a seepage meter study from Philips Creek Marsh in Virginia (Chambers et al., 1992), with an estimate 3 orders of magnitude less than the other studies. Of note, the average groundwater discharge value from the current study is in good agreement with the results of a prior Ra-based discharge study at North Inlet (Krest et al., 2000), although the discharge estimates from the prior study used Ra samples collected across a greater area than the current study.

The model results also suggest that groundwater flow did not provide a substantial control over the porewater Ra activity for the short-lived isotopes except for locations near the marsh creek. Greater flushing near the creek and differences in flow velocity between the marsh mud and sand caused spatial variations in Ra activity of roughly a factor of two. The short half-lives of ^{223}Ra and ^{224}Ra along with their faster generation rates when compared with the simulated groundwater ages at interior marsh locations (Fig. 3.6B) suggests that these two isotopes generate and decay at a greater rate than would be affected by the seasonal changes in age or residence time.

The maximum Ra activity measured in October 2010, particularly in the 1 m piezometers (Fig. 3.7A - F), did not coincide with the August 2010 Ra activity peak in the simulation results. The most obvious explanation for this discrepancy may be that if Ra measurements had been made in August 2010, the values would have been higher than those of October 2010. However, three other potential explanations for the model's inability to capture this October activity peak. It should be noted that these may not include all of the processes occurring within this intertidal marsh. Prior Ra budget research has suggested that deeper aquifer sources of Ra may provide inputs into the shallow porewater of this system (Rama and Moore, 1996). The observed groundwater flow patterns at our field site indicate that deep aquifer sources cannot discharge through the surficial marsh muds, so additional shallow sediment processes may be active.

First, prior laboratory studies have shown that the distribution coefficient of Ra can be affected by changes in porewater salinity, pH, and redox potential (Krest et al., 2000; Gonneea et al., 2008; Beck and Cochran, 2013). However, analyses of prior, concurrent measurements of Ra and temperature, salinity, pH, and redox potential at this

site did not indicate a significant relationship between Ra and any of these geochemical factors with the exception of temperature (Hughes et al., 2015). An increased sampling frequency, other than the quarterly collections taken in the prior study, may have revealed a significant relationship between these geochemical factors and porewater Ra activity, which are not accounted for in the model. In addition a greater sampling frequency may have revealed a different timing for the porewater Ra activity maximum.

Second, the October 2010 Ra measurement peak was closer to the peak in MWL for 2010 (Fig. 3.9A and C) than for the temperature maximum. It was hypothesized previously that increased residence time during high MWL would increase the activity of short-lived Ra isotopes in porewater (Hughes et al., 2015). However, our groundwater age results indicate that the maximum age typically lags 45 to 60 days behind the peak in MWL, suggesting that groundwater age, or residence time, is not a likely explanation for the high Ra activity in the October 2010 measurements.

Third, sediment heterogeneity with respect to hydraulic conductivity and Ra generation may also contribute to the discrepancies between the simulated Ra results and field measurements. The sediment layers in the model are assigned homogeneous and isotropic permeabilities as well as uniform Ra generation rates. Contrary to the homogeneous sediment assumption made when using the model, natural variability in permeability for a single aquifer can be as much as 3 to 4 orders of magnitude. Large variations in permeability over small spatial scales can result in local flow velocity differences which affect solute dispersion and measurement variability in the aquifer (Sudicky, 1986; Boggs et al., 1992; Tonina and Bellin, 2008; Sudicky et al., 2010) unaccounted for when assuming homogeneous permeability in a numerical simulation.

One other consideration at this site may be the effect of channelized, rapid movement of water and solutes via crab burrows on variations in Ra measurements beyond what would be expected from the bulk permeability of the marsh mud. Prior research at North Inlet indicates that in central marsh locations of short *S. alterniflora*, crab burrows reach an average depth of 8 cm below the surface, and up to 20 cm near the creek banks (Sharma et al., 1987). Since these burrows do not typically reach the depths of the shallowest piezometers (1 m), this is unlikely to be a factor.

Natural variations in sediment Ra and Th activity measured in prior North Inlet studies could also contribute to the variability in observed field measurements of Ra not observed in the model results. Bulk sediment ^{226}Ra and ^{228}Ra activity within the shallow surface sediment (top 10 cm) varied laterally by as much as a factor of 3, but did not vary significantly vertically between samples collected at individual locations (Hughes et al., 2015). Three North Inlet sediment cores collected at creek bank, medium form *S. alterniflora*, and short form *S. alterniflora* locations also revealed strong lateral differences in Ra parent isotope activity (^{228}Th, ^{230}Th, and ^{232}Th) as well as Ra isotope activity (^{228}Ra, ^{226}Ra) (Bollinger and Moore, 1984). The Th isotopes varied laterally by up to an order of magnitude, and the Ra isotopes varied by as much as a factor of seven. However, this large variability was not observed with depth within each core (~ 30 cm). The simplifying assumptions of sediment homogeneity and constant Ra generation rates across each model layer (sand and mud), compared with the spatial differences in measured sediment Ra generation rates, are the likely reason that the model does not capture certain aspects in temporal variations of porewater ^{223}Ra and ^{224}Ra activity.

Prior hydraulic head calculations indicated that the greatest source of water discharging from this marsh island was the confined aquifer (Hughes et al., 2012). A closer correspondence was also found between Ra activity ratios in the underlying sand and the surface water, when compared with the Ra activity ratios in the surficial marsh mud, supporting the interpretation of earlier hydraulic head calculations (Hughes et al., 2015). Spatial and temporal variations in our model results for porewater ^{223}Ra and ^{224}Ra activity capture the same variations found in the Ra measurements. These results clearly indicate that the best sample location for porewater Ra measurements in a layered coastal system for use in Ra budget discharge calculations is within the confined aquifer near the point of discharge to the nearby surface water. In addition, the temporal variability in porewater Ra activity indicates that a monthly sampling schedule over the course of one year would be ideal for capturing the seasonal trends in porewater Ra variability in any coastal system.

3.8 CONCLUSIONS

New numerical models of groundwater flow in a salt marsh island, which are the first to simulate Ra transport in a coastal system, allowed us to identify important controls on spatial and temporal variations in Ra tracer activities. We found that groundwater flow models could be calibrated to hydraulic head observations from the marsh, arriving at unique values for the sediment compressibility and permeability. The models confirmed prior conceptual models for groundwater flow in layered intertidal salt marshes. Specifically, simulation results showed that the net movement of groundwater in the marsh was downward through the confining mud layer into the underlying sand and lateral through the sand to discharge at the tidal creek. Net groundwater flow rates

varied spatially across the marsh from near zero at the marsh center to flow velocities that at times reached nearly 1 m/day in the fine-grained sand aquifer near the tidal creek. Average groundwater discharge from the marsh fell by a factor of nearly 2.5 in response to seasonal increases in MWL, which spanned approximately 45 cm. These seasonal declines in average groundwater discharge caused groundwater ages to vary by as much as 50 days, but they did not, when simulated assuming that Ra sorption parameters remained constant, cause variations in Ra activities.

The development of a well calibrated groundwater flow model allowed us to identify controls on Ra activities. Although prior statistical models had shown that temporal variations in Ra activities were associated with temporal variations in temperature and groundwater discharge, the Ra transport model results show that most of the temporal variability in porewater ^{223}Ra and ^{224}Ra at this site can be explained by thermal controls on the distribution coefficient of Ra. The simplifying assumption of sediment homogeneity within the mud and sand layers may also, in part, explain the other discrepancies between Ra measurements and model results.

Finally, this study highlights the importance of choosing the location and timing of porewater sampling when calculating Ra-based estimates of groundwater discharge for a system of interest. At this site, the differences in groundwater flow and discharge along the creek bank, along with differences in sediment grain size and surface area between the mud and sand, control the spatial variability of porewater radium activity. In what might be called a 'radium budget tautology', higher radium activity porewater sampled from the marsh mud would lead to lower radium-based discharge estimates and lower radium activity sampled from the sand aquifer would lead to higher radium-based

discharge estimates for the same average Ra inventory in the surface water. In addition, the timing of maximum porewater Ra activity and maximum discharge may not coincide, which is important to understand when calculating Ra budgets in coastal systems. Results indicate that groundwater and surface water Ra activities should be measured monthly in order to obtain an accurate picture of Ra seasonality. In the case of layered salt marshes, porewater Ra samples should be drawn from the confined sandy aquifer below the marsh platform, but this location may vary for other tidally-influenced systems. Numerical groundwater flow simulations calibrated to both hydraulic head and porewater Ra measurements are a powerful way to understand coastal groundwater flow patterns and interpret porewater measurements of Ra activity, as well as nutrients and other solutes in coastal ecosystems.

Table 3.1 Groundwater Flow Model Parameters

Model Parameter	Mud (burrows)	Mud	Sand
Porosity ∅	0.8	0.7	0.425
Sediment Compressibility α_s (m s^2 kg^{-1})	10^{-6} (10^{-8} – 10^{-4})[a]	10^{-6} (10^{-8} – 10^{-4})[a]	10^{-8} (10^{-10} – 10^{-6})[a]
Permeability k (m^2)	4×10^{-13} (4×10^{-15} – 4×10^{-11})[a]	4×10^{-13} (4×10^{-15} – 4×10^{-11})[a]	1×10^{-11} (1×10^{-9} – 3×10^{-13})[a]
Hydraulic Diffusivity D^* (m^2/s)	4×10^{-4}	4×10^{-4}	1.0
Residual Saturation S_{wr}	0.1	0.1	0.06
Air Entry Pressure h_b (Pa)	-15,000	-15,000	-5000
Van Genuchten Fit Parameters m, n	0.3, 1.5	0.3, 1.5	0.7, 3.2
Capillary Rise α (m^{-1})	2.44	2.44	2.38
Water Compressibility β (m s^2 kg^{-1})	4.47×10^{-10}		
Water Density ρ (kg m^{-3})	1026.7		
Longitudinal Dispersivity α_L (m)	1		
Transverse Dispersivity α_T (m)	0.1		
Sediment Density (kg m^{-3})	2600		
^{223}Ra Generation Rate (atoms kg^{-1} s^{-1})	0.4[b]	0.4[b]	0.4
^{224}Ra Generation Rate (atoms kg^{-1} s^{-1})	9.0[b]	9.0[b]	9.0
Ra Generation Rate Multiplier[b]	2.85	1.9	1.0

[a]The range of values for intrinsic permeability and sediment compressibility used in the sensitivity studies are shown in parentheses.
[b] A multiplication factor based on sediment radii was used to account for grain size/surface differences. Please see text for explanation. Surface water Ra activities used in the model are: ^{223}Ra = 0.04 dpm/L; ^{224}Ra = 0.7 dpm/L.

Table 3.2 Average Measured and Modeled Porewater Radium Activity

^{223}Ra (dpm/L)	1 m Meas / Sim / Tot[a]	2 m Meas / Sim / Tot	4 m Meas / Sim / Tot
EW1	0.3 / 0.3 / 0.5	0.3 / 0.3 / 0.3	0.2 / 0.3 / 0.2
EW2	0.5 / 0.3 / 0.5	0.5 / 0.3 / 0.3	0.2 / 0.2 / 0.2
NS2	0.5 / 0.3 / 0.5	0.3 / 0.3 / 0.3	0.3 / 0.2 / 0.2
^{224}Ra (dpm/L)	1 m	2 m	4 m
EW1	9.2 / 7.0 / 12.2	8.8 / 6.9 / 8.4	3.3 / 3.7 / 4.0
EW2	13.5 / 7.0 / 12.2	9.1 / 6.9 / 8.4	3.5 / 3.7 / 4.0
NS2	10.1 / 7.0 / 12.2	6.7 / 6.9 / 8.4	5.3 / 3.7 / 4.0

[a]Values listed are: average measured porewater Ra activity for that piezometer, simulated porewater Ra activity for the equivalent observation node, and the average porewater Ra activity for all 1 m, 2 m, and 4 m measurements.

Table 3.3. Summary of Tidal Marsh Discharge Estimates

Source	Location	Discharge[a] ($m^3/m/d$)[b]	Method
Krest et al. (2000)	NI Salt Marsh, SC	1.7	^{228}Ra Balance
		2.8	^{226}Ra Balance
Charette et al. (2003)	Great Sippewissett Marsh, MA	0.4	^{226}Ra Balance
Chambers et al. (1992)	Philips Creek Marsh, VA	7.7×10^{-4}	Darcy's Law
Nuttle and Harvey (1995)	Phillips Creek Marsh, VA	0.2	Water-Salt Balance
Portnoy et al. (1998)	Nauset Marsh, Cape Cod, MA	0.1 – 0.2	Seepage Meter
Howes and Goehringer (1994)	Great Sippewissett Marsh, MA	0.02	Seepage Meter
Harvey et al. (1987)	Carter Creek Marsh, VA	0.3	Darcy's Law
Morris (1995)	NI Salt Marsh, SC	0.4 – 0.7[c]	Water-Salt Balance
Whiting and Childers (1989)	NI Salt Marsh, SC	0.1 – 0.9	Seepage Meter
Wilson et al. (2015a)	Sapelo Island, GA	0.3 – 5.0	Darcy's Law
Hughes et al. (2015)	NI Salt Marsh, SC	0.9	Darcy's Law/ Statistical Model
Current Study	NI Salt Marsh, SC	2.8	Numerical Model

[a]For a discussion of the method differences that should be considered when comparing discharge estimates, please see the Discussion section of the text.
[b]Units are m^3/d per m of shoreline. Literature values reported in units of L/m^2 d were converted using an average creek density of 0.013 m creek/m^2 marsh surface.
[c]The author used an area of 17.5 km^2 of *S. alterniflora* marsh surface based on LIDAR data (Morris et al., 2005). Total area of the intertidal wetland (water, *Juncus*, and *Spartina*) was reported as 40.5 km^2.

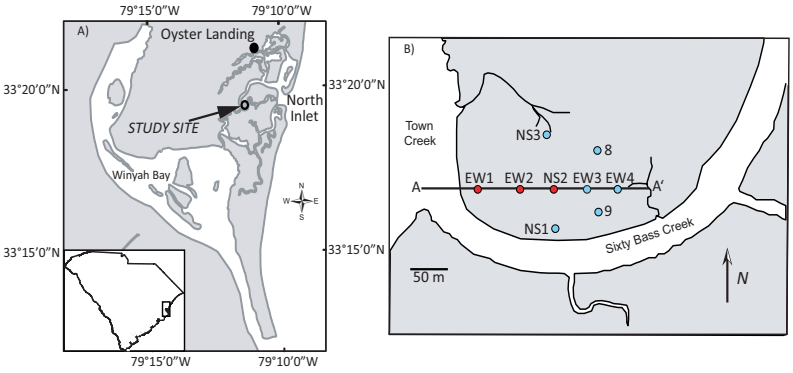

Figure 1

Figure 3.1 Map of study setting (modified from Hughes, et al., 2012). A) North Inlet salt marsh with the locations of the study site and Oyster Landing tide and meteorological station indicated. B) Enlarged map of the study site with the locations of sediment cores and piezometer nests marked with filled circles. Data from piezometer nests used to calibrate the radial model are shown in red.

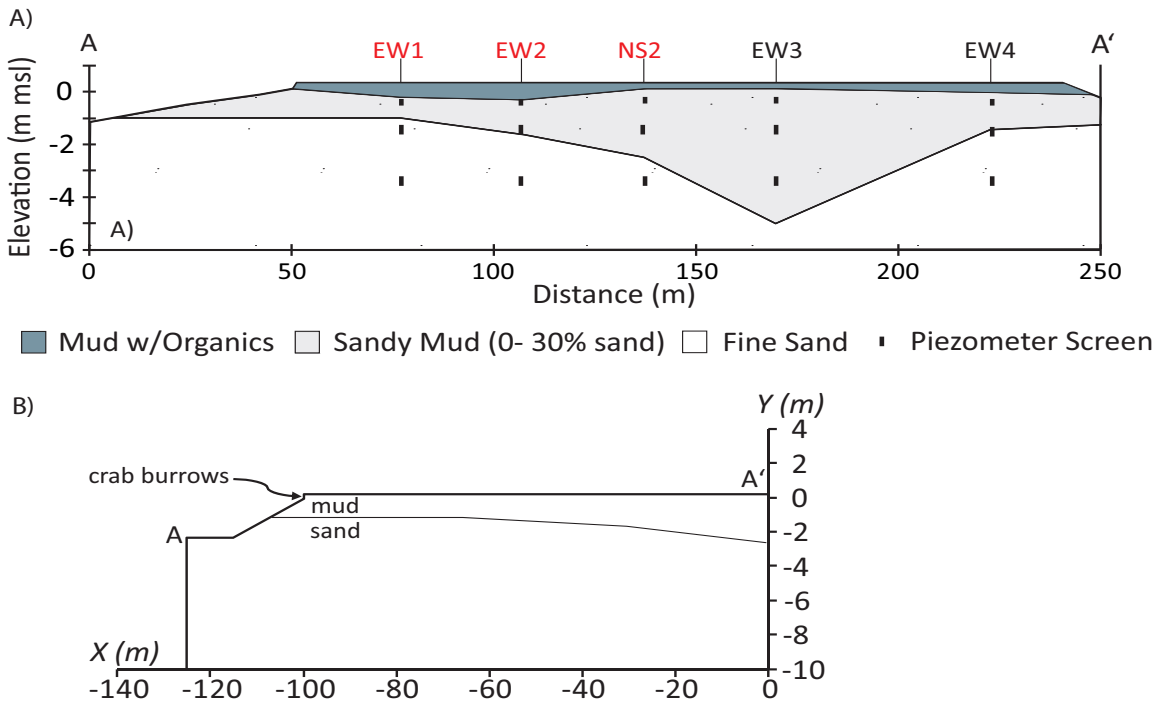

Figure 2

Figure 3.2 Marsh stratigraphy from sediment cores (modified from Hughes, et al., 2015). A) Stratigraphy along the E-W transect of the marsh. Piezometer screened intervals are indicated by short, vertical lines. B) Outline of radial model domain. Specified pressure and specified flux boundary along the top of the domain (A to A'). Remaining boundaries are no-flow boundaries. A thin layer of mud (20 to 25 cm) extends across the sand along the creek bottom (A to sand/mud boundary).

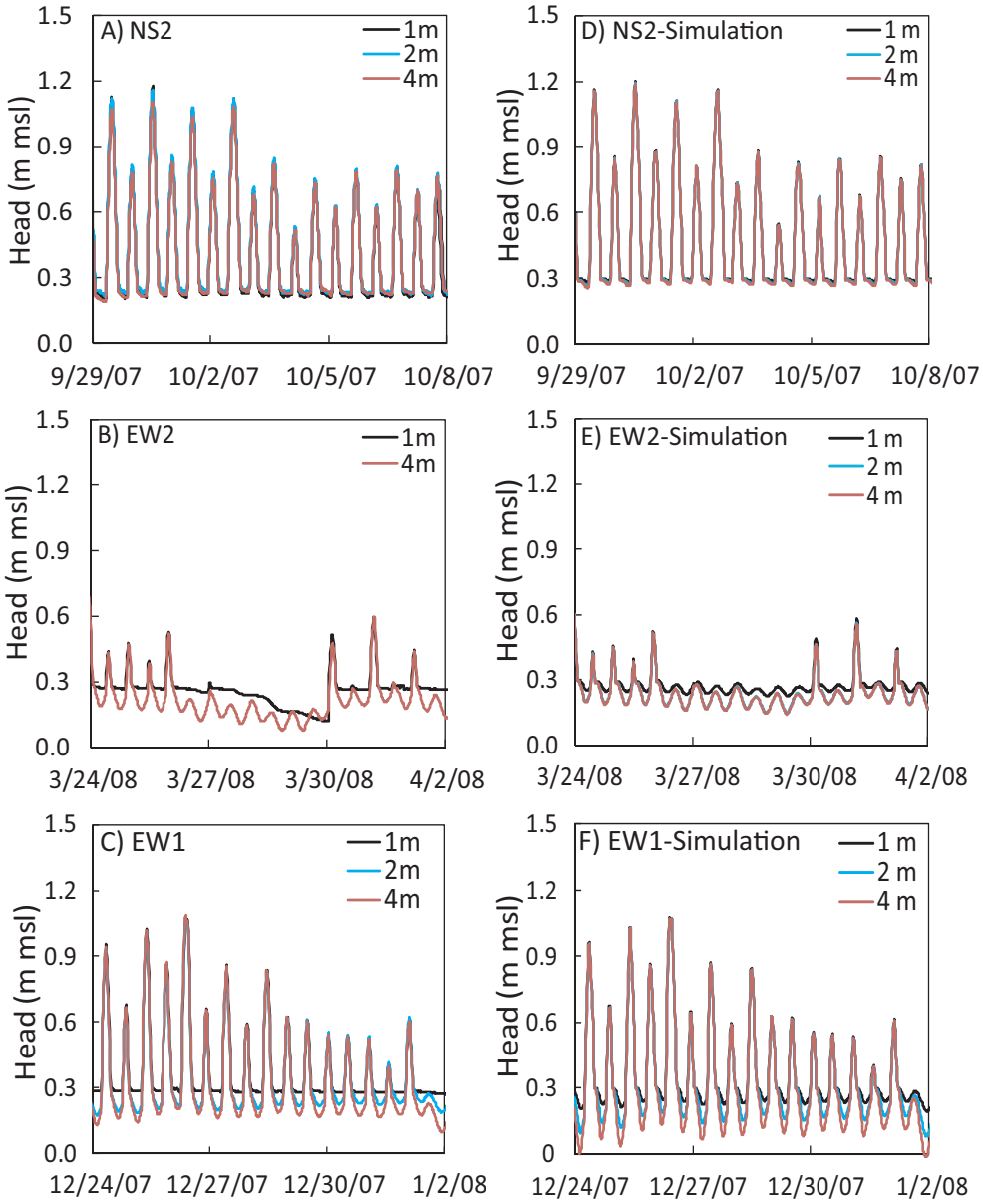

Figure 3

Figure 3.3 Hydraulic head: field measurements and simulation results. A – C) Representative hydraulic head data from piezometers nests NS2, EW2, and EW1. D – F) Simulation results from the same time period shown in plots A – C.

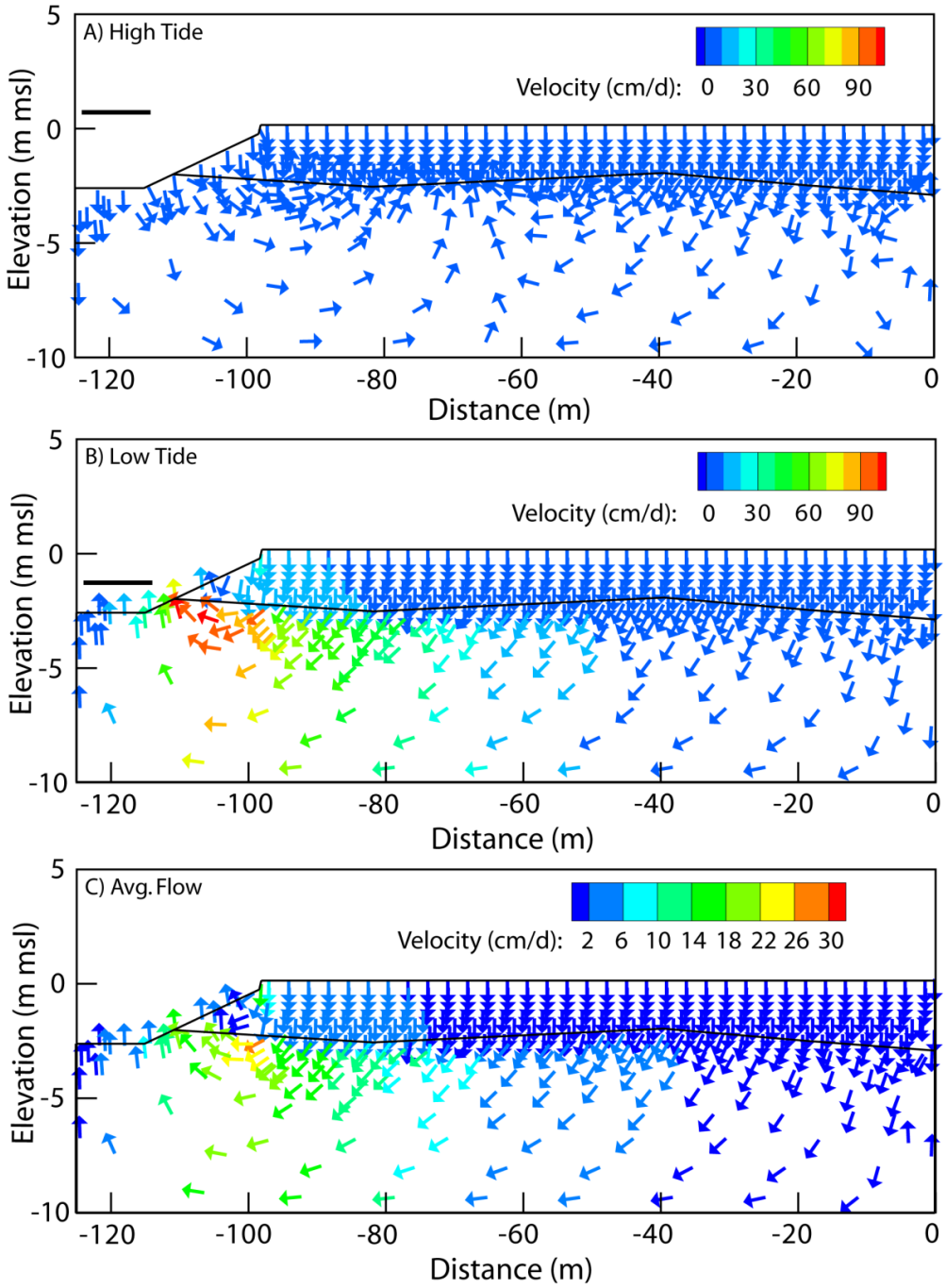

Figure 3.4 Simulated groundwater flow velocities and directions. A and B) Groundwater flow patterns and velocities typical of high and low tide. C) Net groundwater flow direction and velocity over a single tidal cycle.

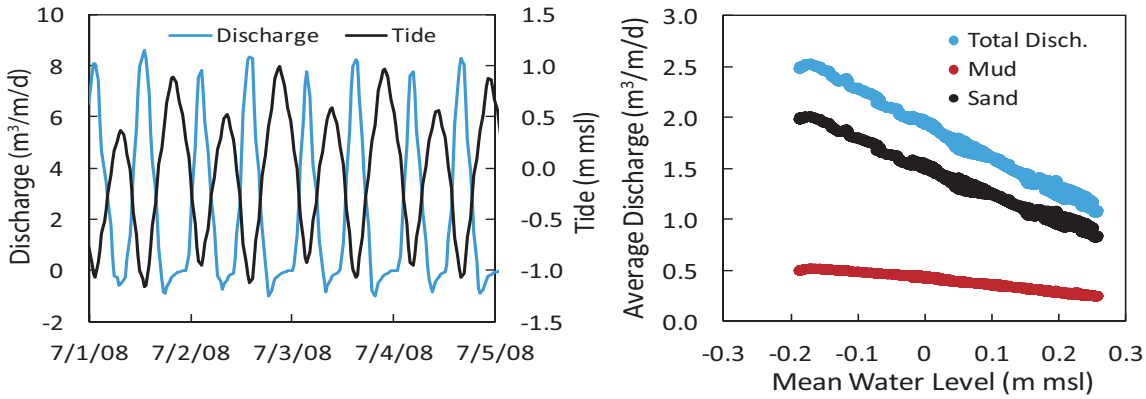

Figure 6

Figure 3.5 Simulated groundwater discharge and tide. A) Variations in simulated groundwater discharge across the tidal creek with daily tidal cycles from 7/1 to 7/5/2008. B) 28-day averages of discharge and tide over the 6-month period from 7/1/2008 to 1/1/2009. The blue points represent all discharge across the creek bank, the black points represent discharge from the sand, and the red points indicate discharge from the surficial marsh mud.

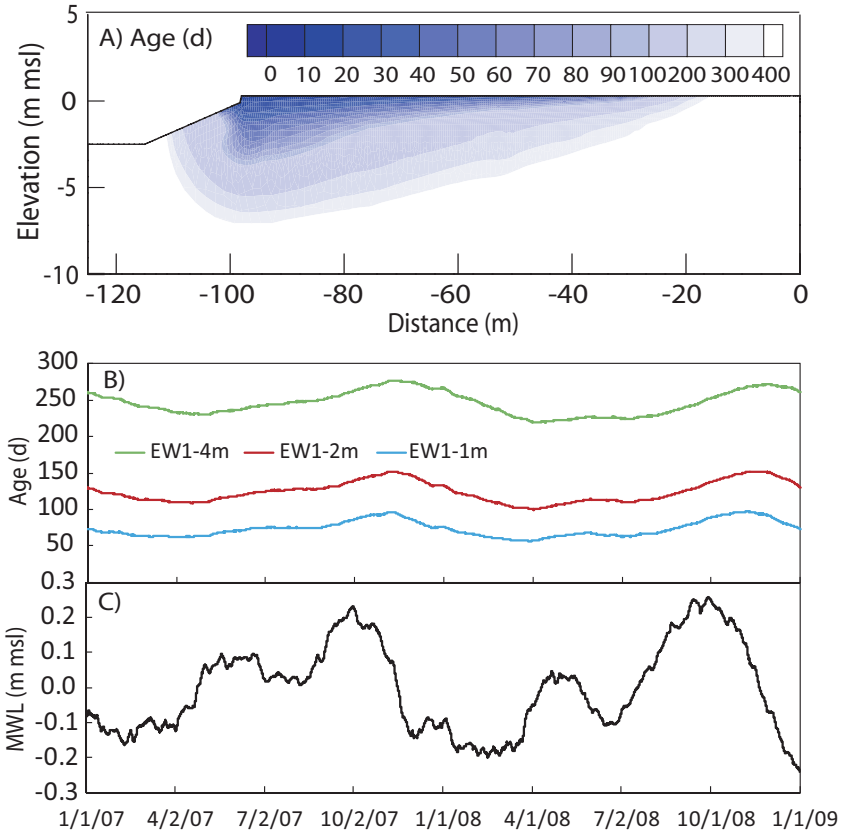

Figure 5

Figure 3.6 Simulated groundwater age. A) Profile of groundwater age. B) Simulated groundwater age through time from the observation nodes representing piezometer nest EW1 at the 1, 2, and 4 m depths below the marsh surface. C) The 28-day average tide for the 2007 – 2008 period. Note the lag (45 to 60 days) between the MWL maximums and the age maximums.

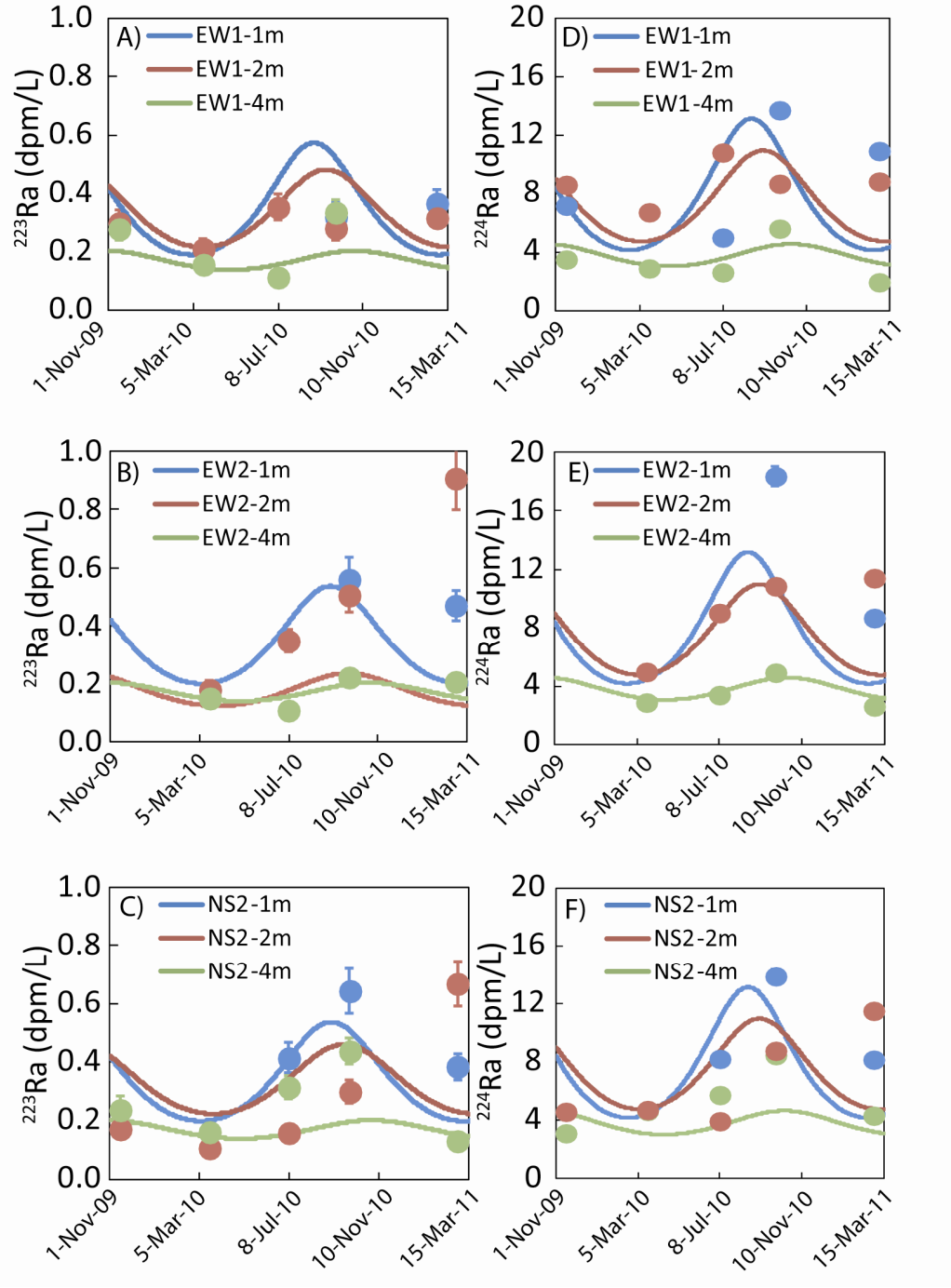

Figure 3.7. Measured and simulated ^{224}Ra and ^{223}Ra for EW1, EW2, and NS2 piezometers. The symbols represent the average radium activity measured in all 1, 2, and 4 m piezometers on each sample date, and the bars represent the range in activity across the three nests at each depth/sample period. The lines represent the modeled Ra activity at observations nodes corresponding to the piezometer screened interval locations.

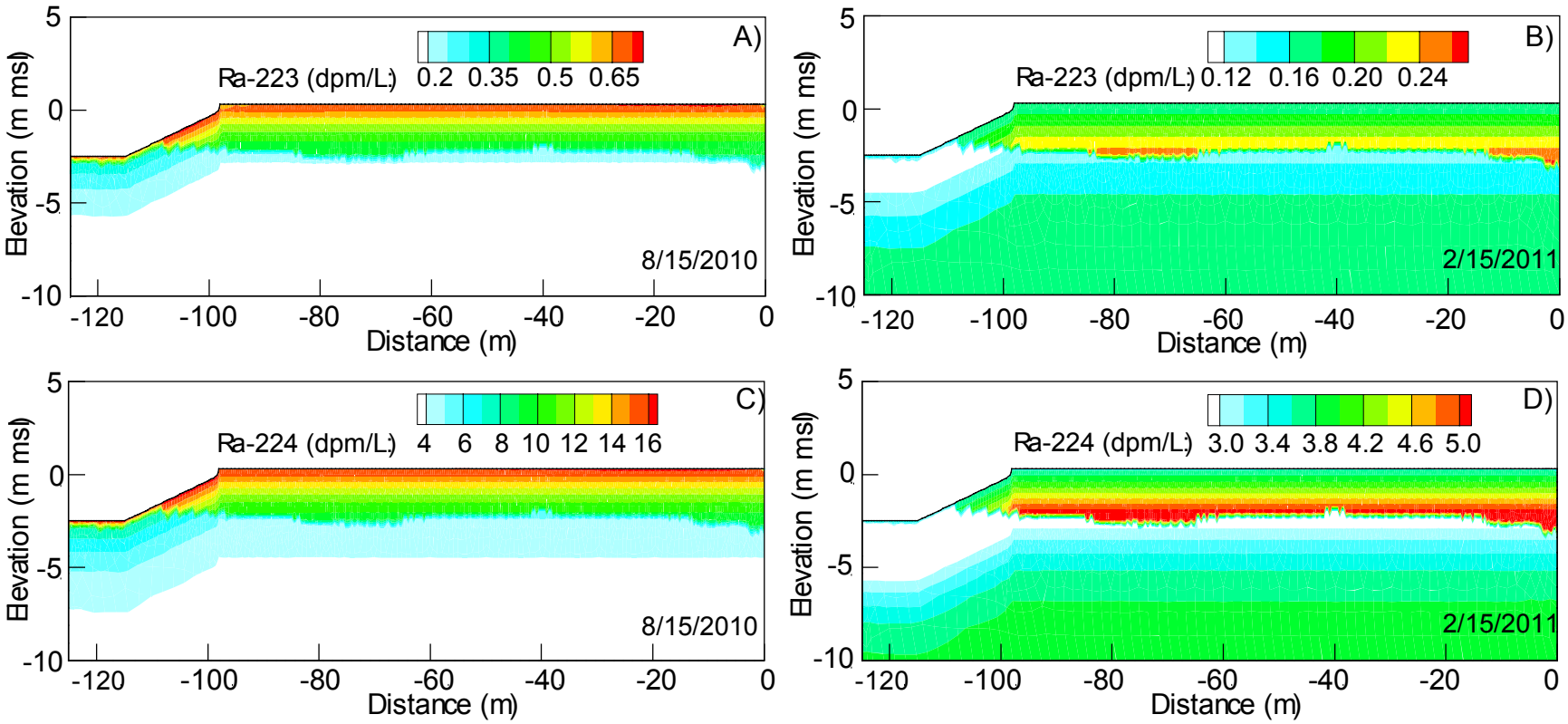

Figure 3.8 Contour profiles of select Ra simulation results. A and B) ^{224}Ra activity and C and D) ^{223}Ra activity during periods of high (August 15, 2010) and low (February 15, 2011) mean water level. The lowest simulated ^{223}Ra values were 0.16 dpm/L (August 2010) and 0.09 dpm/L (February 2011). The lowest simulated ^{224}Ra values were 3.6 dpm/L (August 2010) and 2.0 dpm/L (February 2011).

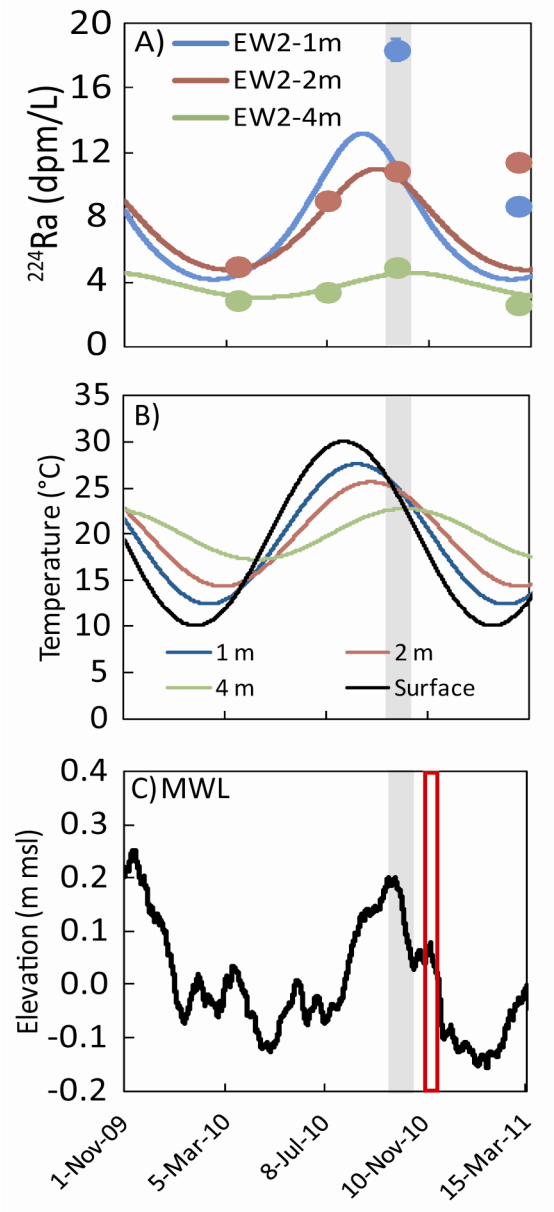

Figure 3.9 Comparison of temporal Ra results with simulated temperature and MWL. A) 224Ra measurements and simulation results at piezometer nest EW2. B) Simulated temperature results using an analytical solution to the heat transport equation used in the model. C) The 28-day average tide (MWL) measured at the Oyster Landing location. The grey shaded bar highlights the October 1, 2010 Ra samples and the equivalent period in the temperature and MWL records and simulation results. The red box in plot C) indicates the position of maximum groundwater age 45 days after the peak in MWL. Please see the text for a full explanation.

BIBLIOGRAPHY

Abraham, D.M., Charette, M.A., Allen, M.C., Rago, A. and Kroeger, K.D., 2003. Radiochemical estimates of submarine groundwater discharge to Waquoit Bay, Massachusetts. Biological Bulletin, 205: 246-247.

Alber, M., Swenson, E.M., Adamowicz, S.C. and Mendelssohn, I.A., 2008a. Salt Marsh Dieback: An overview of recent events in the US. Estuarine, Coastal and Shelf Science, 80(2008): 1-11.

Alber, M., Swenson, E.M., Adamowicz, S.C. and Mendelssohn, I.A., 2008b. Salt Marsh Dieback: An overview of recent events in the US. Estuarine, Coastal and Shelf Science, 80: 1-11.

Arkema, K.K. et al., 2013. Coastal habitats shield people and property from sea-level rise and storms. Nature Climate Finish, 3: 913 - 918. 10.1038/NCLIMATE1944.

Beck, A.J. and Cochran, M.A., 2013. Controls on solid-solution partitioning of radium in saturated marine sands. Marine Chemistry, 156(2013): 38 - 48.

Boggs, J.M. et al., 1992. Field Study of Dispersion in a Heterogeneous Aquifer 1. Overview and Site Description. Water Resources Research, 28(12): 3281-3291.

Bollinger, M.S. and Moore, W.S., 1984. Radium fluxes from a salt marsh. Nature, 309: 444-446.

Bollinger, M.S. and Moore, W.S., 1993. Evaluation of salt marsh hydrology using radium as a tracer. Geochimica et Cosmochimica Acta, 57: 2203-2212.

Bradley, P.M. and Morris, J.T., 1990. Physical characteristics of salt marsh sediments; ecological implications. marine Ecology Progress Series, 61: 245-252.

Brown, C.E. and Pezeshki, S.R., 2007. Threshhold for recovery in the marsh halophyte *Spartina alterniflora* grown under the combined effects of salinity and soil drying. Journal of Plant Physiology, 164(2007): 274-282.

Brown, C.E., Pezeshki, S.R. and DeLaune, R.D., 2006. The effects of salinity and soil drying on nutrient uptake and growth of *Spartina alterniflora* in a simulated tidal system. Environmental and Experimental Botany, 58(2006): 140-148.

Burnett, W.C. et al., 2006. Quantifying submarine groundwater discharge in the coastal zone via multiple methods, Science of the Total Environment, pp. 498-543.

Burnett, W.C., Bokuniewicz, H., Huettel, M., Moore, W.S. and Taniguchi, M., 2003. Groundwater and pore water inputs to the coastal zone. Biogeochemistry, 66: 3-33.

Burnett, W.C. et al., 2002. Assessing methodologies for measuring groundwater discharge to the ocean. EOS, 83(11): 117, 122-123.

Burnett, W.C., Taniguchi, M. and Oberdorfer, J., 2001. Measurement and significance of the direct discharge of groundwater into the coastal zone. Journal of Sea Research, 46(2): 109-116.

Bye, J.A.T. and Narayan, K.A., 2009. Groundwater response to the tide in wetlands: Observations from the Gillman Marshes, South Australia. Estuarine, Coastal and Shelf Science, 84(2009): 219-226.

Carslaw, H.S. and Jaeger, J.C., 1959. Conduction of Heat in Solids. Oxford University Press, Oxford, England, 510 pp.

Chambers, R.M., Harvey, J.W. and Odum, W.E., 1992. Ammonium and Phosphate Dynamics in a Virginia Salt Marsh. Estuaries, 15(3): 349-359.

Charette, M.A., 2007. Hydrologic forcing of submarine groundwater discharge: Insight from a seasonal study of radium isotopes in a groundwater-dominated salt marsh estuary. Limnology and Oceanography, 52(1): 230-239. doi: 10.4319/lo.2007.52.1.0230.

Charette, M.A. and Buesseler, K.O., 2004. Submarine groundwater discharge of nutrients and copper to an urban subestuary of Chesapeake Bay (Elizabeth River). Limnology and Oceanography, 49(2): 376-385.

Charette, M.A., Buesseler, K.O. and Andrews, J.E., 2001. Utility of radium isotopes for evaluating the input and transport of groundwater-derived nitrogen to a Cape Cod estuary. Limnology and Oceanography, 46(2): 465-470.

Charette, M.A., Splivallo, R., Herbold, C., Bollinger, M.S. and Moore, W.S., 2003. Salt marsh submarine groundwater discharge as traced by radium isotopes. Marine Chemistry, 84(2003): 113-121. doi: 10.1016/j.marchem.2003.07.001.

Chmura, G.L., Anisfeld, S.C., Cahoon, D.R. and Lynch, J.C., 2003. Global Carbon sequestration in tidal, saline wetland soils. Global Biogeochemical Cycles, 17(4): 1111. 10.1029/2002GB001917.

Costanza, R. et al., 1997. The value of the world's ecosystem services and natural capital. Nature, 387: 253-260.

D'Andrea, A.F., Aller, R.C. and Lopez, G.R., 2002. Organic matter flux and reactivity on a South Carolina sandflat: The impacts of porewater advection and macrobiological structures. Limnology and Oceanography, 47(4): 1056-1070.

Dacey, J.W.H. and Howes, B.L., 1984. Water uptake by roots controls water table movement and sediment oxidation in short Spartina marsh. Science, 224(4648): 487-489.

de Groot, R.S., Wilson, M.A. and Boumans, R.M.J., 2002. A typology for the classification, description and valuation of ecosystem functions, goods and services. Ecological Economics, 41(2002): 393-408.

Douglas, E.M., Jacobs, J.M., Summer, D.M. and Ray, R.L., 2009a. A comparison of models for estimating potential evapotranspiration for Florida land cover types. Journal of Hydrology, 373: 366-376. doi: 10.1016/j.jhydrol.2009.04.029.

Douglas, E.M., Jacobs, J.M., Sumner, D.M. and Ray, R.L., 2009b. A comparison of models for estimating potential evapotranspiration for Florida land cover types. Journal of Hydrology, 373(2009): 366-376. 10.1016/j.jhydrol..2009.04.029.

Duarte, C.M., Middelburg, J.J. and Caraco, N., 2005. Major role of marine vegetation on the oceanic carbon cycle. Biogeosciences, 2: 1-8.

Dytham, C., 2003. Choosing and Using Statistics: A Biologist's Guide. Blackwell Publishing, Malden, MA, 248 pp.

Elsinger, R.J. and Moore, W.S., 1980. ^{226}Ra Behavior in the Pee Dee River - Winyah Bay Estuary. Earth and Planetary Science Letters, 48: 239-249.

Ferris, J.G., 1952. Cyclic Fluctuations of Water Level as a Basis for Determining Aquifer Transmissibility, U.S.Geological Survey, Water Resources Division, Washington, DC.

Fetter, C.W., 2000. Applied Hydrogeology. Prentice Hall, 598 pp.

Freeze, R.A. and Cherry, J.A., 1979. Groundwater. Prentice-Hall, Inc., 604 pp.

Gardner, L.R., 2005. A modeling study of the dynamics of pore water seepage from intertidal marsh sediments. Estuarine Coastal and Shelf Science, 62(2005): 691-698.

Gardner, L.R. and Kjerfve, B., 2006. Tidal fluxes of nutrients and suspended sediments at the North Inlet--Winyah Bay National Estuarine Research Reserve. Estuarine, Coastal and Shelf Science, 70: 682-692.

Gardner, L.R. and Porter, D.E., 2001. Stratigraphy and geologic history of a southeastern salt marsh basin, North Inlet, South Carolina, USA. Wetlands Ecology and Management, 9: 371-385.

Gardner, L.R. and Reeves, H.W., 2002. Seasonal Patterns in the Soil Water Balance of a *Spartina* Marsh site at North Inlet, South Carolina, USA. Wetlands, 22(3): 467-477.

Gardner, L.R. and Wilson, A.M., 2006. Comparison of four numerical models for simulating seepage from salt marsh sediments. Estuarine Coastal and Shelf Science, 69(2006): 427-437.

Gardner, L.R., Wolaver, T.G. and Mitchell, M., 1988. Spatial variations in the sulfur chemistry of salt marsh sediments at North Inlet, South Carolina. Journal of Marine Research, 46: 815-836.

Gonneea, M.E., Morris, P.J., Dulaiova, H. and Charette, M.A., 2008. New perspectives on radium behavior within a subterranean estuary. Marine Chemistry, 109(2008): 250-267. 10.1016/j.marchem.2007.12.002.

Gonneea, M.E., Mulligan, A.E. and Charette, M.A., 2013a. Seasonal cycles in radium and barium within a subterranean estuary: Implications for groundwater derived chemical fluxes to surface waters. Geochimica et Cosmochimica Acta, 119(2013): 164-177. doi: 10.1016/j.gca.2013.05.034.

Gonneea, M.E., Mulligan, A.E. and Charette, M.A., 2013b. Seasonal cycles in radium and barium within a subterranean estuary: Implications for groundwater derived chemical fluxes to surface waters. Geochimica et Cosmochimica Acta, 119(2013): 164-177. 10.1016/j.gca.2013.05.034.

Grewell, B.J., Callaway, J.C. and W.R. Ferren, J., 2007. Estuarine Wetlands. In: M.G. Barbour, T. Keeler-Wolf and A.A. Schoenherr (Editors), Terrestrial Vegetation of California. University of California Press, Berkeley, CA, pp. 124-154.

Gustafson, D.J., Kilheffer, J. and Silliman, B.R., 2006. Relative Effects of *Littoraria irrorata* and *Prokelisia marginata* on *Spartina alterniflora*. Estuaries and Coasts, 29(4): 639-644.

Hancock, G.J., Webster, I.T., Ford, P.W. and Moore, W.S., 2000. Using Ra isotopes to examine transport processes controlling benthic fluxes into a shallow estuarine lagoon. Geochimica et Cosmochimica Acta, 64(21): 3685-3699.

Harvey, J.W., Germann, P.F. and Odum, W.E., 1987. Geomorphological Control of Subsurface Hydrology in the Creekbank Zone of Tidal Marshes. Estuarine, Coastal and Shelf Science, 25: 677-691.

Hemond, H.F. and Fifield, J.L., 1982. Subsurface flow in salt marsh peat: A model and field study. Limnology and Oceanography, 27(1): 126-136.

Hemond, H.F., Nuttle, W.K., Burke, R.W. and Stolzenbach, K.D., 1984. Surface Infiltration in Salt Marshes: Theory, Measurement, and Biogeochemical Implications. Water Resources Research, 20(5): 591-600.

Hester, M.W., Mendelssohn, I.A. and McKee, K.L., 1998. Intraspecific Variation in Salt Tolerance and Morphology in *Panicum hemitomon* and *Spartina alterniflora* (poaceae). International Journal of Plant Sciences, 159(1): 127-138.

Hester, M.W., Mendelssohn, I.A. and McKee, K.L., 2001. Species and population variation to salinity stress in *Panicum hemitomon*, *Spartina patens*, and *Spartina alterniflora*: morphological and physiological constraints. Environmental and Experimental Botany, 46(2001): 277-297.

Horowitz, A.J., 1991. A Primer on Sediment-Trace Element Chemistry, U.S. Geological Survey.

Hougham, A.L., Moran, S.B., Masterson, J.P. and Kelly, R.P., 2008. Seasonal changes in submarine groundwater discharge to coastal salt ponds estimated using ^{226}Ra and ^{228}Ra as tracers. Marine Chemistry, 109(2008): 268-278. doi: 10.1016/j.marchem.2007.08.001.

Howard, R.J. and Mendelssohn, I.A., 1999. Salinity as a constrain on growth of oligohaline marsh macrophytes. II. Salt pulses and recovery potential. American Journal of Botany, 86(6): 795-806.

Howes, B.L. and Goehringer, D.D., 1994. Porewater drainage and dissolved organic carbon and nutrient losses through the intertidal creekbanks of a New England salt marsh. Marine Ecology Progress Series, 114: 289-301.

Hughes, A.L.H., Wilson, A.M. and Moore, W.S., 2015. Groundwater Transport and Radium Variability in Coastal Porewaters. Estuarine, Coastal and Shelf Science, 164(1): 94-104.

Hughes, A.L.H., Wilson, A.M. and Morris, J.T., 2012. Hydrologic variability in a salt marsh: Assessing the links between drought and acute marsh dieback. Estuarine, Coastal and Shelf Science, 111(2012): 95-106. doi: 10.1016/j.ecss.2012.06.016.

Hughes, C.E., Binning, P. and Willgoose, G.R., 1998. Characterisation of the hydrology of an estuarine wetland. Journal of Hydrology, 211(1998): 34-49.

Jahnke, R.A., Alexander, C.R. and Kostka, J.E., 2003. Advective pore water input of nutrients to the Satilla River Estuary, Georgia, USA. Estuarine, Coastal and Shelf Science, 56: 641-653. doi: 10.1016/S0272-7714(02)00216-0.

Kelly, R.P. and Moran, S.B., 2002. Seasonal changes in groundwater input to a well-mixed estuary estimated using radium isotopes and implications for coastal nutrient budgets. Limnology and Oceanography, 47(6): 1796-1807.

Kiehn, W.M. and Morris, J.T., 2009. Relationships between *Spartina alterniflora* and *Littoraria irrorata* in a South Carolina salt marsh. Wetlands, 29(3): 818-825.

Kim, G., Ryu, J.-W., Yang, H.-S. and Yun, S.-T., 2005. Submarine groundwater discharge (SGD) into the Yellow Sea revealed by ^{228}Ra and ^{226}Ra isotopes: Implications for global sillicate fluxes. Earth and Planetary Science Letters, 237: 156-166.

King, G.M., Klug, M.J., Wiegert, R.G. and Chalmers, A.G., 1982a. Relation of Soil Water Movement and Sulfide Concentration to *Spartina alterniflora* Production in a Georgia Salt Marsh. Science, 218(4567): 61-63.

King, P.T., Michel, J. and Moore, W.S., 1982b. Ground water geochemistry of ^{228}Ra, ^{226}Ra and ^{222}Rn. Geochimica et Cosmochimica Act, 46: 1173-1182.

Knee, K.L., Layton, B.A., Street, J.H., Boehm, A.B. and Payton, A., 2008. Sources of Nutrients and Fecal Indicator Bacteria to Nearshore Waters on the North Shore of Kaua'i (Hawai'i, USA). Estuaries and Coasts, 31: 607-622. doi: 10.1007/s12237-008-9055-6.

Kostka, J.E. and Luther, G.W., III, 1994. Partitioning and speciation of solid phase iron in saltmarsh sediments. Geochimica et Cosmochimica Acta, 58(7): 1701-1710.

Kostka, J.E. and Luther, G.W., III, 1995. Seasonal cycling of Fe in saltmarsh sediments. Biogeochemistry, 29: 159-181.

Krest, J.M. and Harvey, J.W., 2003. Using natural distributions of short-lived radium isotopes to quantify groundwater discharge and recharge. Limnology and Oceanography: 1-11.

Krest, J.M., Moore, W.S., Gardner, L.R. and Morris, J.T., 2000. Marsh nutrient export supplied by groundwater discharge: Evidence from radium measurements. Global Biogeochemical Cycles, 14(1): 167-176. doi: 10.1029/1999GB001197.

Kwon, E.Y. et al., 2014. Global estimate of submarine groundwater discharge based on an observationally constrained radium isotope model. Geophysical Research Letters, 41: 8438-8444. 10.1002/2014GLl061574.

Linthurst, R.A. and Blum, U., 1981. Growth modification of *Spartina alterniflora* Loisel. by the interaction of pH and salinity under controlled conditions. Journal of Experimental Biology and Ecology, 55: 207-218.

Linthurst, R.A. and Seneca, E.D., 1980. Dieback of Salt-water Cordgrass (*Spartina alterniflora* Loisel.) in the Lower Cape Fear Estuary of NOrth Carolina: An Experimental Approach to Re-establishment. Environmental Conservation, 7(1): 59-66.

Luther, G.W., III, Shellenbarger, P.A. and Brendel, P.J., 1996. Dissolved organic Fe(III) and Fe(II) complexes in salt marsh porewaters. Geochimica et Cosmochimica Acta, 60(6): 951-960.

McKee, K.L., Mendelssohn, I.A. and Materness, M.D., 2004. Acute salt marsh dieback in the Mississippi River deltaic plain: a drought-induced phenomenon? Global Ecology and Biogeography, 13(2004): 65-73.

Mcleod, E. et al., 2011. A blueprint for blue carbon: toward an improved understanding of the role of vegetated coastal habitats in sequestering CO2. Frontiers in Ecology and the Environment, 9(10): 552-560. 10.1890/110004.

Mendelssohn, I.A. and McKee, K.L., 1988. *Spartina alterniflora* Die-Back in Louisiana Time-Course Investigation of Soil Waterlogging Effects. Journal of Ecology, 76: 509-521.

Mendelssohn, I.A. and Morris, J.T., 2000. Eco-Physiological Controls on the Productivity of *Spartina alterniflora* Loisel. In: M.P. Weinstein and D.A. Kreeger (Editors), Concepts and controversies in Tidal Marh Ecology. Kluwer, pp. 875.

Moore, W.S., 1984. Radium isotope measurements using germanium detectors. Nuclear Instruments and Methods in Physics Research, 223(1984): 407-411.

Moore, W.S., 1987. Radium 228 in the South Atlantic Bight. Journal of Geophysical Research, 92(C5): 5177-5190.

Moore, W.S., 2003. Sources and fluxes of submarine groundwater discharge delineated by radium isotopes. Biogeochemistry, 66(2003): 75-93.

Moore, W.S., 2006. The role of submarine groundwater discharge in coastal biogeochemistry. Journal of Geochemical Exploration, 88: 389-393.

Moore, W.S., 2010. A reevaluation of submarine groundwater discharge along the southeastern coast of North America. Global Biogeochemical Cycles, 24. 10.1029/2009GB003747.

Moore, W.S. and Arnold, R., 1996. Measurement of ^{223}Ra and ^{224}Ra in coastal waters using a delayed coincidence counter. Journal of Geophysical Research, 101(C1): 1321-1329.

Morris, J.T., 1995. The Mass Balance of Salt and Water in Intertidal Sediments: Results From North Inlet, South Carolina. Estuaries, 18(4): 556-567.

Morris, J.T., 2000. Effects of sea level anomalies on estuarine processes. In: J. Hobbie (Editor), Estuarine Science: A Synthetic Approach to Research and Practice. Island Press, pp. 539.

Morris, J.T., Sundareshwar, P.V., Nietch, C.T., Kjerfve, P. and Cahoon, D.R., 2002. Responses of coastal wetlands to rising sea level. Ecology, 83(10): 2869-2877.

Morris, J.T. and Walker, S., 2006. E-mail communication of original acute marsh dieback sighting in North Inlet Salt Marsh, SC, Columbia.

National Oceanic and Atmospheric Administration, 2008. NOAA Drought Information Center. NOAA. http://www.drought.noaa.gov/index.html

National Oceanic and Atmospheric Administration, 2006 - 2008. NOAA Tides and Currents. Website. Center for Operational Oceanographic Products and Services. http://tidesandcurrents.noaa.gov/index.shtml

Neter, J., Kutner, M.H., Nachtsheim, C.J. and Wasserman, W., 1996. Applied linear statistical models. WCB McGraw-Hill, Boston, MA, 1408 pp.

NOAA, 2008. NERRS Central Data Management Office. National Oceanic and Atmospheric Administration. http://cdmo.baruch.sc.edu/

NOAA, 2006 - 2015. National Estuarine Research Reserve System-wide Monitoring Program. Internet. CDMO. http://www.nerrsdata.org/

NOAA, 2006 - 2015. NOAA Tides and Currents. Website. Center for Operational Oceanographic Products and Services. http://tidesandcurrents.noaa.gov/stations.html?type=Water+Levels

NOAA National Ocean Service, 2015. National Ocean Service Facts: Population. Website. NOAA. http://oceanservice.noaa.gov/facts/population.html

NOAA/National Ocean Service, 2006-2013. NOAA Tides and Currents. Website Portal. http://tidesandcurrents.noaa.gov/waterlevels.html?id=8662245

North Inlet-Winyah Bay National Estuarine Research Reserve, About North Inlet-Winyah Bay. University of South Carolina. http://www.northinlet.sc.edu/about/niwb.html

North Inlet-Winyah Bay National Estuarine Research Reserve, 2006. About North Inlet-Winyah Bay. University of South Carolina. http://www.northinlet.sc.edu/about/niwb.html

Ogburn, M.B. and Alber, M., 2006. An Investigation of Salt Marsh Dieback in Georgia Using Field Transplants. Estuaries and Coasts, 29(1): 54-62.

Oreskes, N., Shrader-Frenchette, K. and Belitz, K., 1994. Verification, Validation, and Confirmation of Numerical Models in the Earth Sciences. Science, 263.

Palmer, M.A., Kjerfve, B. and Schwing, F.B., 1980. Tidal Analysis and Prediction in a South Carolina Estuary. Contributions in Marine Science, 23(1980).

Pawlowicz, R., Beardsley, B. and Lentz, S., 2002. Classical tidal harmonic analysis including error estimates in MATLAB using T_TIDE. Computers & Geosciences, 28(2002): 929-937.

Phleger, C.F., 1971. Effect of Salinity on Growth of a Salt Marsh Grass. Ecology, 52(5): 908-911.

Portnoy, J.W. and Giblin, A.E., 1997. Effects of historic tidal restrictions on salt marsh sediment chemistry. Biogeochemistry, 36: 275-303.

Portnoy, J.W., Nowicki, B.L., Roman, C.T. and Urish, D.W., 1998. The discharge of nitrate-contaminated groundwater from developed shoreline to marsh-fringed estuary. Water Resources Research, 34(11): 3095-3104.

Portnoy, J.W. and Valiela, I., 1997. Short-Term Effects of Salinity Reduction and Drainage on Salt-Marsh Biogeochemical Cycling and *Spartina* (Cordgrass) Production. Estuaries, 20(3): 569-578.

Prairie, Y.T., 1996. Evaluating the predictive power of regression models. Canadian Journal of Fisheries and Aquatic Science, 53: 490-492.

Rama and Moore, W.S., 1996. Using the radium quartet for evaluating groundwater input and water exchange in salt marshes. Geochimica et Cosmochimica Acta, 60(23): 4645-4652.

Reeves, H.W., Thibodeau, P.M., Underwood, R.G. and Gardner, L.R., 2000. Incorporation of Total Stress Changes into the Ground Water Model SUTRA. Groundwater, 38(1): 89-98.

Rutkowski, C.M., Burnett, W.C., Iverson, R.L. and Chanton, J.P., 1999. The effect of groundwater seepage on nutrient delivery and seagrass distribution in the northeastern Gulf of Mexico. Estuaries, 22(4): 1033-1040.

Santos, I.R. et al., 2011. Uranium and barium cycling in a salt wedge subterranean estuary: The influence of tidal pumping. Chemical Geology, 287(2011): 114-123. 10.1016/j.chemgeo.2011.06.005.

Santos, I.R., Eyre, B.D. and Huettel, M., 2012. The driving forces of porewater and groundwater flow in permeable coastal sediments: A review. Estuarine, Coastal and Shelf Science, 98(2012): 1-15. 10.1016/j.ecss.2011.10.024.

Scott, M.K. and Moran, S.B., 2001. Ground water input to coastal salt ponds of southern Rhode Island estimated using ^{226}Ra as a tracer. Journal of Environmental Radioactivity, 54(2001): 163-174.

Sharma, P., Gardner, L.R., Moore, W.S. and Bollinger, M.S., 1987. Sedimentation and bioturbation in a salt marsh as revealed by ^{210}Pb, ^{137}Cs, and ^{7}Be studies. Limnology and Oceanography, 32(2): 313-326.

Silliman, B.R. and Bortolus, A., 2003. Underestimation of *Spartina* productivity in western Atlantic marshes: marsh invertebrates eat more than just detritus. OIKOS, 101: 549-554.

Silliman, B.R., van de Koppel, J., Bertness, M.D., Stanton, L.E. and Mendelssohn, I.A., 2005. Drought, Snails, and Large-Scale Die-Off of Southern U.S. Salt Marshes. Science, 310: 1803-1806.

Silliman, B.R. and Zieman, J.C., 2001. Top-Down Control of *Spartina alterniflora* Production by Periwinkle Grazing in a Virginia Salt Marsh. Ecology, 82(10): 2830-2845.

Slomp, C.P. and Cappellen, P.V., 2004. Nutrient inputs to the coastal ocean through submarine groundwater discharge: controls and potential impact. Journal of Hydrology, 295: 64-86. doi: 10.1016/j.jhydrol.2004.02.018.

Smith, S.M., 2006. Report on Salt Marsh Dieback on Cape Cod, National Park Service, Cape Cod National Seashore, Wellfleet, MA.

South Carolina State Climate Office, 2012. Georgetown 2 E, South Carolina - Climate Summary. South Carolina DNR. http://www.dnr.sc.gov/cgi-bin/sco/hsums/cliMAINnew.pl?sc3468

Strzepek, K., Yohe, G., Neumann, J. and Boehlert, B., 2010. Characterizing changes in drought risk for the United States from climate change. Environmental Research Letters, 5(2010). 10.1088/1748-9326/5/4/044012.

Sudicky, E.A., 1986. A Natural Gradient Experiment on Solute Transport in a Sand Aquifer: Spatial Variability of Hydraulic Conductivity and Its Role in the Dispersion Process. Water Resources Research, 22(13): 2069-2082.

Sudicky, E.A., Illman, W.A., Goltz, I.K., Adams, J.J. and McLaren, R.G., 2010. Heterogeneity in hydraulic conductivity and its role on the macroscale transport of a solute plume: From measurements to a practical application of stochastic flow and transport theory. Water Resources Research, 46. 10.1029/2008WR007558.

Sun, H. and Semkow, T.M., 1998. Mobilization of thorium, radium and radon radionuclides in ground water by successive alpha-recoils. Journal of Hydrology, 205: 126-136.

Thibodeau, P.M., 1997. Groundwater flow dynamics across the forest-salt marsh interface: North Inlet, South Carolina. Ph.D. Thesis, University of South Carolina, Columbia, South Carolina, 278 pp.

Thibodeau, P.M., Gardner, L.R. and Reeves, H.W., 1998. The role of groundwater flow in controlling the spatial distribution of soil salinity and rooted macrophytes in a southeastern salt marsh, USA. Mangroves and Salt Marshes, 2: 1-13.

Tonina, D. and Bellin, A., 2008. Effects of pore-scale dispersion, degree of heterogeneity, sampling size, and source volume on the concentration moments of conservative solutes in heterogeneous formations. Advances in Water Resources, 31(2008): 339-354. 10.1016/j.advwatres.2007.08.009.

Turc, L., 1961. Évaluation des Besoins en Eau D'Irrigation, Évapotranspiration Potentielle. Annales Agronomiques, 12(1): 13-49.

USGCRP, 2011. United States Global Change Research Program. Website. University Corporation for Atmospheric Research. http://www.globalchange.gov

Valiela, I., 1984. Marine Ecological Processes. Springer Advanced Texts in Life Sciences. Springer-Verlag, Inc., New York, 546 pp.

Valiela, I. et al., 1990. Transport of groundwater-borne nutrients from watersheds and their effects on coastal waters. Biogeochemistry, 10: 177-197.

van Genuchten, M.T., 1980. A Closed-form Equation for Predicting the Hydraulic Conductivity of Unsaturated Soils. Soil Science Society of America Journal, 44(5): 892-898.

Vernberg, F.J. and Vernberg, W.B., 2001. The coastal zone: past, present, and future. University of South Carolina Press, Columbia, SC, 191 pp.

Viollier, E., Inglett, P.W., Hunter, K., Roychoudhury, A.N. and Cappellen, P.V., 2000. The ferrozine method revisited: Fe(II)/Fe(III) determination in natural waters. Applied Geochemistry, 15(6): 785-790.

Voss, C.I. and Provost, A.M., 2002. SUTRA: A Model for Saturated-Unsaturated, Variable-Density Ground-Water Flow with Solute or Energy Transport. WRIR 02-4231, U.S. Geological Survey, Reston, VA.

Webb, J.W., 1983. Soil Water Salinity Variations and their Effects on *Spartina alterniflora*. Contributions in Marine Science, 26: 1-13.

Webster, I.T., Hancock, G.J. and Murray, A.S., 1994. Use of radium isotopes to examine pore-water exchange in an estuary. Limnology and Oceanography, 39(8): 1917-1927.

Webster, I.T., Hancock, G.J. and Murray, A.S., 1995. Modelling the effect of salinity on radium desorption from sediments. Geochimica et Cosmochimica Acta, 59(12): 2469-2476.

Whiting, G.J. and Childers, D.L., 1989. Subtidal advective water flux as a potentially important nutrient input to southeastern U.S.A. Saltmarsh estuaries. Estuarine, Coastal and Shelf Science, 28(4): 417-471. 10.1016/0272-7714(89)90089-9.

Wiegert, R.G. and Freeman, B.J., 1990. Tidal Salt Marshes of the Southeast Atlantic Coast: A Community Profile. Biological Report 85(7.29), Department of Zoology and Institute of Geology, University of Georgia, Athens, Georgia.

Wieski, K., Guo, H., Craft, C.B. and Pennings, S.C., 2010. Ecosystem Functions of Tidal Fresh, Brackish, and Salt Marshes on the Georgia Coast. Estuaries and Coasts, 33(2010): 161-169.

Wilson, A.M., Evans, T., Moore, W., Schutte, C.A. and Joye, S.B., 2015a. What time scales are important for monitoring tidally influenced submarine groundwater discharge? Insights from a salt marsh. Water Resources Research, 51(6): 4198-4207. 10.1002/2014WR015984.

Wilson, A.M. et al., 2015b. Groundwater controls ecological zonation of salt marsh macrophytes. Ecology, 96(3): 840-849.

Wilson, A.M., Moore, W.S., Joye, S.B., Anderson, J.L. and Schutte, C.A., 2011. Storm-driven groundwater flow in a salt marsh. Water Resources Research, 47: 1-11. 10.1029/2010WR009496.

Wilson, A.M. and Morris, J.T., 2012. The influence of tidal forcing on groundwater flow and nutrient exchange in a salt marsh dominated estuary. Biogeochemistry, 108: 27-38. 10.1007/s10533-010-9570-y.

Yang, H.-S., Hwang, D.-W. and Kim, G., 2002. Factors controlling excess radium in the Nakdong River estuary, Korea: submarine groundwater discharge versus desorption from riverine particles. Marine Chemistry, 78: 1-8.

APPENDIX A

STATISTICAL METHODS, WATER AND SEDIMENT SAMPLE PREPARATION METHODS, AND RADIUM ANALYTICAL TECHNIQUES[4]

[4] Hughes, Andrea L. H., Alicia M. Wilson, Willard S. Moore, in press. Groundwater and Radium Variability in Coastal Porewaters. Estuarine, Coastal and Shelf Science.

A.1 Water and Sediment Sample Preparation and Radium Analytical Techniques

Radium was quantitatively removed from all water samples while in the field by passing it through PVC cylinders packed with 15 – 20 g of MnO_2 coated acrylic fiber. Once back at the laboratory, the fibers are rinsed for 1 minute with DI water and partially dried using a stream of air. Next, the fibers were 'fluffed' evenly within the cylinders, and activities of ^{223}Ra and ^{224}Ra were determined using a RaDeCC delayed-coincidence counter (Moore and Arnold, 1996). Samples were then set aside for a minimum of 3 weeks to allow ^{224}Ra to grow in from any ^{228}Th adsorbed to the fiber (supported ^{224}Ra) and were analyzed on the RaDeCC system a second time in order to determine excess ^{224}Ra activity. Once the short-lived isotopes were measured, the long-lived radium isotopes were removed from the Mn-fibers by first leaching the fibers with hydrochloric acid. Radium in the leachate was co-precipitated with $BaSO_4$, and the precipitate was set aside for 2 or more weeks to allow ^{222}Rn and subsequent daughters to equilibrate with ^{226}Ra. Activities of ^{226}Ra and ^{228}Ra were determined using a well-type germanium gamma detector (Moore, 1984). Sediment samples were dried for more than 1 day in a drying oven at 60°C, disaggregated using a mortar and pestle, and thoroughly homogenized prior to analysis. Roughly 50 g of sediment was split from each sample, placed into a plastic dish that was sealed with glue, and bulk ^{226}Ra and ^{228}Ra activity were determined using a planar-type germanium gamma detector after ^{222}Rn had equilibrated with ^{226}Ra.

A.2 Statistical Methods

Spatial variability in the porewater and sediment measurements and temporal variability in the porewater, surface water, and sediment measurements were analyzed

using one-way ANOVAs and two-sample t-tests. Parameters tested for porewater and surface water were salinity, temperature, pH, redox potential (mV), the four Ra isotopes, and the ratios of $^{224}Ra/^{223}Ra$ and $^{228}Ra/^{226}Ra$. Spatial and temporal differences in bulk sediment ^{228}Ra and ^{226}Ra measurements were also tested using two-sample t-tests. The fixed factors for the statistical tests were porewater sample depth (1, 2, and 4 m), porewater and surface water sample date (Nov 09, Mar 10, Jul 10, Oct 10, and Feb 11), and porewater sample piezometer location (Interior: EW2, NS3, and EW3; Exterior: EW1, NS1, NS3, and EW4). Fixed factors for all the sediment samples collected were sample depth (surface samples versus sediment core samples) and sediment type in the core samples (sand versus marsh mud), and sample date was used as a fixed factor for the surface sediment samples (Feb 10 and Oct 10).

One-way ANOVAs were used to analyze the overall porewater measurement differences by sample depth. Additional ANOVAs were used to analyze measurement differences by depth within each of the five sample dates for a total of six tests. The overall F-test with Bonferroni correction was calculated based on an initial significance level of $\alpha=0.05$ and the number of tests (6) for an adjusted significance level of $\alpha = (0.05/6) = 0.008$. If the overall ANOVA results were significant, Tukey's multiple comparison tests with an experiment-wise error rate of 0.05 were then used to analyze pair-wise differences between the three depths. One-way ANOVAs were also used to quantify measurement differences between sample dates for all porewater and between sample dates at each porewater sample depth for a total of four porewater tests. The adjusted significance level for the porewater tests was $\alpha = (0.05/4) = 0.0125$, and the surface water results were analyzed at $\alpha=0.05$. Again, Tukey's multiple comparison tests

with an experiment-wise error rate of 0.05 were performed on all significant ANOVA results.

Two-sample t-tests were used to quantify overall measurement differences between lateral piezometer locations (marsh exterior vs. marsh interior locations). Lateral measurement differences were also analyzed within each of the five sample dates and within each of the three sample depths for a total of nine tests. The overall F-test with Bonferroni Correction was calculated based on an initial significance level of $\alpha=0.05$ and the number of tests (9) for an adjusted significance level of $\alpha=(0.05/9)=0.0056$. Two-sample t-tests were also used to separately quantify the differences in bulk sediment ^{226}Ra and ^{228}Ra activity by sample date in the shallow (10 cm) surface sediment, by depth between the 10 cm and deeper sediment samples split from the sediment cores, by sediment type (marsh mud vs. sand) for all the core sediment samples. Each test was interpreted using a significance level of $\alpha=0.01$ due to the limited number of sediment samples collected.

Associations between porewater and surface water measurements of radium activity and salinity, temperature, pH, and redox potential were quantified using Pearson correlation tests (Neter et al., 1996). The overall F-test with Bonferroni Correction was calculated based on an initial significance level of $\alpha=0.05$, and the number of pairwise comparisons which were calculated using Eq. A.1. The number of parameters (N) used in the Pearson Correlation tests was 8 for a total number of pairwise comparisons of 28 (N_{pc}). The resulting adjusted significance level was $\alpha=(0.05/28)=0.0018$ (Eq. A.2). Associations between groundwater discharge estimates and porewater radium activity were quantified using partial correlation tests (Neter et al., 1996) interpreted using a

significance level of α=0.05. Discharge was averaged for the day on which samples were collected as well as 4 and 11 days leading up to and including each sample collection date. For example, the 4-day average for November 16, 2009 included November 13 through November 16, 2009. The 4-day and 11-day averages were chosen to correspond to the half-lives of ^{224}Ra (3.66 days) and ^{223}Ra (11.4 days). Discharge averages corresponding to the half-lives of ^{228}Ra (5.75 years) and ^{226}Ra (1600 years) were not included because tidal records do not extend to 1600 years, and the residence time of porewater in the marsh, to the depth our measurements were made, is far less than 5.75 years.

A.3 Hydraulic Conductivity Estimates

The hydraulic properties of coastal aquifers can be determined through an analysis of tide and the hydraulic head response within the aquifer. Hydraulic diffusivity for the confined aquifer at this site was estimated by two methods (Ferris, 1952; Bye and Narayan, 2009) using 2007 – 2008 hydraulic head records and concurrent tide recorded at the Oyster Landing location (Fig. 2.1A). The surficial marsh mud aquifer was not included in these analyses due to the basic assumption of horizontal groundwater flow for both methods. Hydraulic head records indicate that groundwater flow is vertical and downward within the surficial aquifer (Hughes et al., 2012).

The hydraulic head signal within all of the piezometers was not a simple sinusoidal curve, as assumed when using the Ferris method, because a hydraulic head peak occurs during semi-diurnal tidal inundation of the marsh (Fig. A.1 A). To remove this peak, hydraulic head values from the 1 m piezometers were subtracted from the 4 m piezometers along the E-W transect (Fig. 2.1B). For example, the hydraulic head record from EW1-1m was subtracted from EW1-4m. This resulted in adjusted hydraulic head

records for the 4 m piezometers that were appropriately sinusoidal for use in these analyses (Fig. A.1 B). Hydraulic diffusivity was estimated by combining Eq. A.3 (Ferris, 1952) with the parameters listed in Table A.5. The resulting diffusivity values were 0.017 m^2/s (transect from EW1 to NS2) and 0.016 m^2/s (transect from EW4 to NS2).

We also estimated hydraulic diffusivity for the confined aquifer at piezometer nest locations EW1 and EW4 (Fig. 2.1B), after Bye and Narayan (2009), for comparison with the Ferris-derived diffusivities. Harmonic analyses of the time series measurements of both tide and hydraulic head were made using the MATLAB program T_TIDE (Pawlowicz et al., 2002). The amplitudes and phases for the two primary semi-diurnal (M2 and S2) and diurnal (K1 and O1) tidal components (Table A.6) were then used to estimate total hydraulic diffusivity for the confined aquifer using a form of the rms equation (Eqs. A.4 – A.7). Using this method, the average hydraulic diffusivity was 0.041 (range from 0.021 – 0.058) m^2/s (Table A.7).

Hydraulic diffusivity estimates from both methods were next used to estimate hydraulic conductivity based on the relationship between diffusivity, hydraulic conductivity, and specific storage (Eqs. A.8 and A.9) (Fetter, 2000). For the specific storage equation (Eq. A.9), specific weight was determined from salinity and temperature measurements made during this study, resulting in an average density of 1023.7 kg/m^3 and a specific weight of 10^4 $kg/m^2 \cdot s^2$. The value used for compressibility of water was 4.4 x 10^{-10} $m \cdot s^2/kg$ and the sediment compressibility was assumed to be 10^{-7} $m \cdot s^2/kg$. A porosity of 0.43 was used for the confined sand aquifer (Bradley and Morris, 1990; D'Andrea et al., 2002). Specific storage was calculated as 1.0 x 10^{-3} m^{-1}. For the Ferris method, hydraulic conductivity was 2 x 10^{-5} m/s, and for the Bye and Narayan method,

the mean was 4 x 10^{-5} m/s with a range from 2 x 10^{-5} to 6 x 10^{-5} m/s. The median value of all the hydraulic conductivity estimates was 3 x 10^{-5} m/s.

A.4 Groundwater Discharge Estimates

Because hydraulic head measurements were not made during radium sampling, we used a linear regression model equation to predict groundwater discharge based on a running average of mean water level during 2009 – 2011. Volumetric discharge (Q: Eq. 2.10) and specific discharge (q: Eq. 2.11) were calculated using 4 m piezometer hydraulic head measurements at EW1 and EW4 with concurrent tide records from September 2007 to March 2008, resulting in 5 separate piezometer location/time period combinations. First, change in hydraulic head (dh; Eqs. A.10 and A.11) was calculated as the difference between hydraulic head in the piezometers and the simultaneous stream water elevation. Distance (x) from piezometer nest to shore was 25 m for EW1 and 20 m for EW4. The hydraulic gradient (dh/x) is strongly dependent on the lateral distance (x) between measurement points. Therefore, calculations of discharge using this method decrease with increasing distance between points and are considered to be estimates. The discharge area (A; Eq. A.10) was calculated as the average length along the creek bottom from marsh edge to creek center per meter of shoreline (25 m), and the hydraulic conductivity (K) value was the mean of 3 x 10^{-5} m/s described above.

Next, the 14-day running averages of tide and calculated discharge were used to develop a regression model capable of predicting discharge from mean water level. These averages were used in order to capture longer-term trends versus the discharge response to the semi-diurnal tide and were calculated as the average value of the 7 days prior to and following the current date and time (a centered average value). The 14-day scheme

was chosen to correspond to the number of days between neap tides or spring tides. A total of 5 separate regression equations were developed corresponding to the 5 time/location combinations mentioned above. The r^2 values for the individual regression equations ranged from 0.90 to 0.99. The *m* and *b* values (linear equation form $y = mx + b$) from these 5 equations were averaged to develop a single equation to predict discharge from 14-day running averages of tide for 2009 – 2011 (Eq. A.12). Mean water level and estimated specific discharge are presented in Figure 2.5.

A.4 Appendix Symbols

N_{pc}: number of pair-wise comparisons for Bonferroni correction

N: number of test parameters

α: significance level for statistical test

D^*: hydraulic diffusivity (m^2/s)

D_T^*: hydraulic diffusivity (m^2/s) summed over the 4 major tidal components

x: distance (m)

T: tidal period (hours)

a: amplitude of the 'tidal' signal in the well (m)

a_o: amplitude of the tidal signal (m)

a_i: amplitude of the i^{th} component tidal signal in the well (m)

σ_i: tidal phase of i^{th} component (radians/day)

k_i: wave number of the i^{th} component of the tidal signal in the well (m^{-1})

θ: tidal amplitude decay constant within aquifer (m^{-1})

A_i: [θ/k] tidal efficiency within the aquifer (dimensionless)

g: phase of tidal signal in the well from T_TIDE analysis (radians)

g_o: phase of the tidal signal from T_TIDE analysis (radians)

S_s: specific storage

γ: specific weight of the porewater (1 x 10^4 kg/m^2·s^2)

β_s: compressibility of solids (1 x 10^{-7} m·s^2/kg)

β_w: compressibility of water (4.4 x 10^{-10} m·s^2/kg)

η: porosity

K: hydraulic conductivity (m/s)

q: specific discharge or Darcy flux (m^3/m^2·s)

Q: volumetric discharge (m^3/s)

A: unit cross-sectional area of aquifer (m^2)

dh/x: hydraulic gradient, change in hydraulic head (dh) over specified length (dl).

A.5 APPENDIX EQUATIONS:

$$N_{pc} = (N^2 - N)/2 \quad \text{(A.1)}$$

$$\text{Adjusted Significance Level} = \alpha/N_{pc} \quad \text{(A.2)}$$

$$D^* = (\pi x^2)/(T[ln(a/a_0)]^2 \times 3600) \quad \text{(A.3)}$$

$$D_T^* = \sqrt{\sum_{i=1,4}(a_i\sigma_i)^2/\sum_{i=1,4}(a_i(A_i^2+1)k_i^2)^2} \quad \text{(A.4)}$$

$$k = (g - g_0)/x \quad \text{(A.5)}$$

$$\theta = \big(-ln(a/a_0)\big)/x \quad \text{(A.6)}$$

$$A = \theta/k \quad \text{(A.7)}$$

$$D^* = K/S_s \quad \text{(A.8)}$$

$$S_s = \gamma(\beta_s + \eta\beta_w) \quad \text{(A.9)}$$

$$Q = -KA(dh/x) \quad \text{(A.10)}$$

$$q = Q/A = -K(dh/x) \quad \text{(A.11)}$$

$$y = -0.0175X + 0.012 \quad \text{(A.12)}$$

Table A.1 Porewater Measurements

Date	Piezometer	Salinity	Temp	pH	mV
Nov-09	EW1-1m	32.6	21.8	8.18	-241
Nov-09	EW1-2m	32.8	23.2	8	-148
Nov-09	EW1-4m	32.6	22.3	8.08	-339
Nov-09	EW4-2m	32.2	19.8	7.71	-183
Nov-09	EW4-4m	32.5	21.4	7.51	-375
Nov-09	NS1-2m	34.9	21.7	7.35	-190
Nov-09	NS1-4m	33.9	21.5	7.38	-15
Nov-09	NS2-2m	32.9	22	7.76	-400
Nov-09	NS2-4m	33.4	22	7.53	-396
Nov-09	NS3-1m	31.7	21.8	8.07	-344
Nov-09	NS3-2m	32.4	21.8	7.89	-368
Nov-09	NS3-4m	32.2	22	8.19	-377
Mar-10	EW1-2m	31.4	19.7	7.97	-280
Mar-10	EW1-4m	34.7	19.6	8.08	-348
Mar-10	EW2-2m	35.2	19.8	7.69	-361
Mar-10	EW2-4m	34.5	20.8	7.9	-375
Mar-10	EW3-2m	35.1	17	7.63	-347
Mar-10	EW3-4m	34.9	16.4	7.78	-365
Mar-10	EW4-2m	31.6	16.4	7.62	-202
Mar-10	EW4-4m	35.5	17.9	7.3	-376
Mar-10	NS1-2m	34.3	20.9	7.36	-139
Mar-10	NS2-2m	34.9	22.7	7.89	-412
Mar-10	NS2-4m	34	18.8	7.58	-402
Mar-10	NS3-2m	33.4	16.8	7.68	-348
Mar-10	NS3-4m	34.4	18.3	7.8	-342
Jul-10	EW1-1m	33.5	29.5	6.83	-273
Jul-10	EW1-2m	25.6	26.6	6.71	-317
Jul-10	EW1-4m	35	24.8	6.87	-339
Jul-10	EW2-2m	35.4	26.8	6.62	-367
Jul-10	EW2-4m	36	22.8	7.01	-327
Jul-10	EW3-1m	35.2	30.7	7.04	-326
Jul-10	EW3-2m	34.8	23	6.66	-304
Jul-10	EW3-4m	34.9	23.5	6.66	-315
Jul-10	EW4-2m	34.5	25.7	6.84	-288
Jul-10	EW4-4m	35.2	22.8	6.79	-326
Jul-10	NS1-2m	35.9	27.5	7.43	-203
Jul-10	NS2-1m	35.5	30.5	6.92	-329
Jul-10	NS2-2m	34.8	31	6.83	-342
Jul-10	NS2-4m	35	30.5	6.82	-360
Jul-10	NS3-1m	34.4	30.1	6.92	-313
Jul-10	NS3-2m	34.3	27.7	6.76	-379
Jul-10	NS3-4m	34	23.2	6.94	-328

Table A.1 Continued

Date	Piezometer	Salinity	Temp	pH	mV
Oct-10	EW1-1m	35.8	26.6	7.25	-307
Oct-10	EW1-2m	36	26.7	6.64	-350
Oct-10	EW1-4m	36.2	27.2	7.27	-363
Oct-10	EW2-1m	37.6	24.7	6.74	-304
Oct-10	EW2-2m	36.9	25	6.52	-316
Oct-10	EW2-4m	35.4	22.7	6.77	-306
Oct-10	EW3-1m	35.7	25.3	7.37	-351
Oct-10	EW3-2m	36.1	24.7	6.75	-351
Oct-10	EW3-4m	35.8	24.7	7.12	-325
Oct-10	EW4-1m	35.6	25.3	7.69	-302
Oct-10	EW4-2m	35.8	25.7	6.75	-298
Oct-10	EW4-4m	36.2	23.1	6.78	-339
Oct-10	NS1-1m	37.1	27.5	7.51	-198
Oct-10	NS1-2m	37.9	25.8	7.04	-304
Oct-10	NS2-1m	36.3	25	6.87	-324
Oct-10	NS2-2m	36.2	24.9	6.92	-346
Oct-10	NS2-4m	36.5	22.2	6.61	-318
Oct-10	NS3-1m	27.3	28.2	7.24	-296
Oct-10	NS3-2m	34.4	26	6.82	-370
Oct-10	NS3-4m	34.2	25	7.01	-349
Feb-11	EW1-1m	34.3	23.5	7.31	-267
Feb-11	EW1-2m	34.3	18.5	6.98	-225
Feb-11	EW1-4m	34	22.6	7.2	-214
Feb-11	EW2-1m	36.3	18.4		
Feb-11	EW2-2m	35.9	17.2		
Feb-11	EW2-4m	34	20		
Feb-11	EW3-1m	35.3	22.6	7.37	-292
Feb-11	EW3-2m	35.7	21	6.68	-366
Feb-11	EW3-4m	36	20.1	6.91	-330
Feb-11	EW4-1m	34.8	23.6	7.52	-292
Feb-11	EW4-2m	33.7	18.6	6.58	-253
Feb-11	EW4-4m	35.1	22.2	6.87	-390
Feb-11	NS1-2m	36.5	18.9		
Feb-11	NS2-1m	35.4	21.2	7.38	
Feb-11	NS2-2m	35.8	20.3		
Feb-11	NS2-4m	36.1	20.9	6.88	
Feb-11	NS3-4m	34.7	22.3	7	-340

Table A.1 Continued

Date	Piezometer	Ra-223	+/- **	Ra-224	+/- **	Ra-226	+/- **	Ra-228	+/- **	A/R 8/6	A/R 4/3
Nov-09	EW1-1m	0.296	0.047	7.21	0.304	0.60	0.09	4.41	0.07	7.318	24.358
Nov-09	EW1-2m	0.298	0.043	8.64	0.299	0.49	0.03	4.26	0.08	8.676	28.993
Nov-09	EW1-4m	0.277	0.04	3.53	0.159	0.50	0.14	2.89	0.09	5.752	12.744
Nov-09	EW4-2m	0.135	0.028	5.3	0.210	0.61	0.03	3.93	0.12	6.389	39.259
Nov-09	EW4-4m	0.071	0.014	1.6	0.084	0.38	0.03	1.07	0.03	2.810	22.535
Nov-09	NS1-2m	0.443	0.049	14.76	0.372	1.10	0.09	11.13	0.25	10.089	33.318
Nov-09	NS1-4m	0.246	0.044	7.47	0.381	0.81	0.02	3.68	0.07	4.543	30.366
Nov-09	NS2-2m	0.171	0.03	4.59	0.210	0.62	0.02	3.42	0.10	5.480	26.842
Nov-09	NS2-4m	0.236	0.045	3.73	0.179	0.51	0.04	2.93	0.06	5.714	15.805
Nov-09	NS3-1m	0.806	0.102	17.96	0.806	2.40	0.12	11.28	0.16	4.700	22.283
Nov-09	NS3-2m	0.286	0.038	10.11	0.383	0.71	0.04	5.05	0.18	7.084	35.350
Nov-09	NS3-4m	0.199	0.04	3.12	0.167	0.94	0.05	3.20	0.15	3.398	15.678
Mar-10	EW1-2m	0.209	0.037	6.76	0.267	0.40	0.00	3.71	0.02	9.175	32.344
Mar-10	EW1-4m	0.155	0.026	3.24	0.187	0.65	0.03	2.18	0.13	3.354	20.903
Mar-10	EW2-2m	0.177	0.031	4.97	0.205	0.38	0.03	3.22	0.08	8.493	28.079
Mar-10	EW2-4m	0.148	0.023	2.88	0.136	0.68	0.05	2.44	0.07	3.601	19.459
Mar-10	EW3-2m	0.104	0.018	3.61	0.160	0.63	0.02	3.77	0.01	6.007	34.712
Mar-10	EW3-4m	0.097	0.019	3.17	0.136	0.90	0.10	5.25	0.13	5.803	32.680
Mar-10	EW4-2m	0.097	0.017	2.82	0.118	0.43	0.02	2.08	0.01	4.880	29.072
Mar-10	EW4-4m			1.45	0.077	0.35	0.02	0.85	0.01	2.408	
Mar-10	NS1-2m	0.279	0.05	12.64	0.592	0.78	0.02	10.10	0.02	13.001	45.305
Mar-10	NS2-2m	0.106	0.02	4.71	0.220	0.78	0.04	4.61	0.17	5.941	44.434
Mar-10	NS2-4m	0.161	0.028	4.65	0.200	0.61	0.02	3.39	0.03	5.585	28.882
Mar-10	NS3-2m	0.058	0.011	4.91	0.209	0.40	0.01	2.25	0.07	5.559	84.655
Mar-10	NS3-4m	0.112	0.028	3.25	0.161	0.85	0.02	2.82	0.04	3.327	29.018
Jul-10	EW1-1m			9.01	0.360	1.30	0.79	10.68	0.33	8.242	
Jul-10	EW1-2m	0.351	0.045	10.85	0.331	1.03	0.03	8.72	0.09	8.428	30.912
Jul-10	EW1-4m	0.111	0.012	2.9	0.087	1.09	0.04	3.81	0.03	3.501	26.126
Jul-10	EW2-2m	0.347	0.039	9.04	0.282	1.54	0.06	9.07	0.11	5.891	26.052
Jul-10	EW2-4m	0.106	0.014	3.71	0.122	0.98	0.05	2.46	0.14	2.504	35.000
Jul-10	EW3-1m	0.549	0.065	11.9	0.380	3.18	0.20	9.76	0.62	3.069	21.676
Jul-10	EW3-2m	0.181	0.021	4.97	0.142	1.26	0.05	6.69	0.15	5.314	27.459
Jul-10	EW3-4m	0.3	0.039	6.29	0.191	1.54	0.07	9.35	0.05	6.068	20.967
Jul-10	EW4-2m	0.319	0.04	7.35	0.228	1.53	0.04	7.49	0.12	4.899	23.041
Jul-10	EW4-4m			0.8	0.037	0.53	0.03	0.87	0.04	1.633	
Jul-10	NS1-2m	0.4	0.058	10.9	0.372	1.70	0.14	13.24	0.26	7.777	27.250
Jul-10	NS2-1m	0.413	0.052	9.56	0.343	2.75	0.18	12.12	0.15	4.402	23.148
Jul-10	NS2-2m	0.158	0.02	4.87	0.151	2.18	0.04	10.07	0.15	4.624	30.823
Jul-10	NS2-4m	0.313	0.041	7.04	0.222	1.33	0.01	6.28	0.33	4.740	22.492
Jul-10	NS3-1m	0.608	0.083	13.14	0.426	3.33	0.13	10.72	0.25	3.220	21.612
Jul-10	NS3-2m	0.138	0.016	5.23	0.148	1.37	0.10	6.47	0.21	4.741	37.899
Jul-10	NS3-4m	0.168	0.033	0.91	0.040	1.78	0.03	4.84	0.03	2.723	5.417

Table A.1 Continued

Date	Piezometer	Ra-223	+/- **	Ra-224	+/- **	Ra-226	+/- **	Ra-228	+/- **	A/R 8/6	A/R 4/3
Oct-10	EW1-1m	0.319	0.047	13.74	0.485	1.37	0.06	9.72	0.32	7.119	43.072
Oct-10	EW1-2m	0.28	0.039	8.71	0.280	0.69	0.02	6.40	0.01	9.326	31.107
Oct-10	EW1-4m	0.334	0.041	5.94	0.206	1.46	0.05	4.84	0.07	3.327	17.784
Oct-10	EW2-1m	0.559	0.075	18.41	0.691	1.48	0.07	11.75	0.06	7.951	32.934
Oct-10	EW2-2m	0.505	0.056	10.86	0.308	1.02	0.02	8.86	0.02	8.702	21.505
Oct-10	EW2-4m	0.22	0.024	4.92	0.162	0.62	0.04	2.34	0.06	3.777	22.364
Oct-10	EW3-1m	0.768	0.086	16.74	0.550	1.42	0.21	10.60	0.28	7.451	21.797
Oct-10	EW3-2m	0.42	0.059	11.79	0.416	1.26	0.01	9.63	0.01	7.614	28.071
Oct-10	EW3-4m	0.312	0.038	8.22	0.299	1.64	0.02	9.60	0.16	5.841	26.346
Oct-10	EW4-1m	0.959	0.136	15.84	0.609			12.28	0.23		16.517
Oct-10	EW4-2m	0.438	0.046	11.79	0.403	1.09	0.07	7.98	0.05	7.349	26.918
Oct-10	EW4-4m	0.11	0.014	1.63	0.058	0.43	0.02	0.90	0.01	2.108	14.818
Oct-10	NS1-1m	0.698	0.09	17.99	0.601	2.35	0.20	14.79	0.24	6.300	25.774
Oct-10	NS1-2m	0.459	0.058	16.58	0.575	1.56	0.03	12.68	0.47	8.139	36.122
Oct-10	NS2-1m	0.642	0.077	13.9	0.491	1.59	0.12	10.94	0.05	6.866	21.651
Oct-10	NS2-2m	0.298	0.038	8.78	0.293	1.10	0.05	6.67	0.04	6.046	29.463
Oct-10	NS2-4m	0.436	0.045	8.48	0.247	1.37	0.05	6.94	0.09	5.048	19.450
Oct-10	NS3-1m			3.62	0.240	2.81	0.17	8.76	0.43	3.116	
Oct-10	NS3-2m	0.24	0.035	7.4	0.240	1.40	0.04	6.77	0.05	4.844	30.833
Oct-10	NS3-4m	0.109	0.015	4.15	0.145	1.31	0.04	4.08	0.00	3.102	38.073
Feb-11	EW1-1m	0.365	0.047	10.62	0.375	0.37	0.28	6.98	0.32	18.972	29.096
Feb-11	EW1-2m	0.315	0.031	8.86	0.251	0.55	0.03	3.27	0.01	5.894	28.127
Feb-11	EW1-4m			2.56	0.112	0.91	0.02	2.41	0.09	2.654	
Feb-11	EW2-1m	0.47	0.051	8.45	0.268	0.43	0.16	6.55	0.26	15.343	17.979
Feb-11	EW2-2m	0.906	0.108	11.41	0.374	0.87	0.02	7.24	0.15	8.329	12.594
Feb-11	EW2-4m	0.205	0.023	2.73	0.096	0.73	0.02	2.60	0.02	3.574	13.317
Feb-11	EW3-1m	0.198	0.024	10.79	0.373	1.17	0.13	7.56	0.10	6.451	54.495
Feb-11	EW3-2m	0.071	0.009	2.98	0.101	0.11	0.07	2.02	0.01	18.488	41.972
Feb-11	EW3-4m	0.492	0.047	7.92	0.202	1.07	0.01	6.99	0.33	6.507	16.098
Feb-11	EW4-1m	0.521	0.066	16.55	0.582	1.28	0.14	10.24	0.41	8.015	31.766
Feb-11	EW4-2m	0.317	0.032	7.56	0.236	0.76	0.08	4.52	0.22	5.931	23.849
Feb-11	EW4-4m	0.1	0.012	1.83	0.065	0.51	0.02	1.10	0.04	2.140	18.300
Feb-11	NS1-2m	0.353	0.051	13.08	0.439	1.01	0.07	8.03	0.37	7.980	37.054
Feb-11	NS2-1m	0.384	0.045	8.18	0.289	1.14	0.19	6.27	0.19	5.501	21.302
Feb-11	NS2-2m	0.667	0.076	11.52	0.388	1.58	0.17	10.60	0.42	6.700	17.271
Feb-11	NS2-4m	0.13	0.015	4.32	0.147	0.71	0.02	3.58	0.02	5.060	33.231
Feb-11	NS3-4m	0.09	0.011	2.95	0.102	1.03	0.03	3.10	0.06	3.013	32.778

** Radium activity is presented in units of dpm/L, and the '+/-' column lists the counting error calculated as: $\left(\sqrt{No.of\ counts}\,/\,No.of\ counts\right)\times Final\ calculated\ activity$

Table A.2 Surface Water Measurements

Date	Site	Salinity	Temp	pH	mV
9-Nov	SW1	32.6	17.7	7.96	
9-Nov	SW2	29	20.7	7.75	104
9-Nov	SW3	32	17.9	7.9	72
10-Mar	SW1	32.1	18	7.77	50
10-Jul	SW1	34.4	30	7.42	43
10-Jul	SW2	35.9	28.3	7.84	50
10-Oct	SW1	19.7	24.5	7.31	100
10-Oct	SW2	29.9	26	7.69	41
11-Feb	SW1	29.8	15.6	7.57	46
11-Feb	SW2	34.9	14.6		

Table A.2 Continued

Date	Site	Ra-223	+/- **	Ra-224	+/- **	Ra-226	+/- **	Ra-228	+/- **	A/R 8/6	A/R 4/3
9-Nov	SW1	0.037	0.004	0.56	0.017	0.547	0.003	0.814	0.022	1.5	15.1
9-Nov	SW2	0.042	0.006	1.02	0.048	0.546	0.006	0.988	0.028	1.8	24.3
9-Nov	SW3	0.044	0.007	0.74	0.036	0.530	0.003	0.909	0.026	1.7	16.8
10-Mar	SW1	0.015	0.002	0.49	0.022	0.201	0.014	0.309	0.018	1.5	32.7
10-Jul	SW1	0.072	0.009	1.36	0.042	0.506	0.011	1.252	0.034	2.5	18.9
10-Jul	SW2	0.033	0.004	0.34	0.012	0.333	0.007	0.553	0.003	1.7	10.3
10-Oct	SW1	0.037	0.003	1.08	0.031	0.282	0.004	0.542	0.001	1.9	29.2
10-Oct	SW2	0.029	0.003	0.7	0.023	0.366	0.006	0.628	0.006	1.7	24.1
11-Feb	SW1	0.027	0.003	0.76	0.026	0.18	0.00	0.3834	0.0032	2.1	28.1
11-Feb	SW2	0.057	0.005	0.62	0.021	0.17	0.00	0.2846	0.0017	1.7	10.9

** Radium activity is presented in units of dpm/L, and the '+/-' column lists the counting error calculated as: $\left(\sqrt{No.of\ counts}\Big/No.of\ counts\right)\times Final\ calculated\ activity$

Table A.3: Seasonal Radium activity in Surface Water and Porewater (dpm/L; activity ratios are unitless)[1]

^{223}Ra	Nov 2009	Mar 2010	Jul 2010	Oct 2010	Feb 2011
Surface	0.04 (0.037 – 0.044) [3]	0.02 (N/A) [1]	0.05 (0.03 – 0.07) [2]	0.03 (0.029 – 0.037) [2]	0.04 (0.03 – 0.04) [2]
1 m	0.6 (0.3 – 0.8) [2]	N/A	0.5 (0.4 – 0.6) [3]	0.7 (0.3 – 1.0) [6]	0.4 (0.2 – 0.5) [5]
2 m	0.3 (0.1 – 0.4) [5]	0.1 (0.06 – 0.3) [7]	0.3 (0.1 – 0.4) [7]	0.4 (0.2 – 0.5) [7]	0.4 (0.1 – 0.9) [6]
4 m	0.2 (0.1 – 0.3) [5]	0.1 (0.1 – 0.2) [5]	0.2 (0.1 – 0.3) [5]	0.3 (0.1 – 0.4) [6]	0.2 (0.1 – 0.5) [5]
^{224}Ra					
Surface	0.8 (0.6 – 1.0) [3]	0.5 (N/A) [1]	0.9 (0.3 – 1.4) [2]	0.9 (0.7 – 1.1) [2]	0.7 (0.6 – 0.8) [2]
1 m	12.6 (7.2 – 18.0) [2]	N/A	10.9 (9.0 – 13.1) [4]	14.3 (3.6 – 18.4) [7]	10.9 (8.2 – 16.6) [5]
2 m	8.7 (4.6 – 14.8) [5]	5.8 (2.8 – 12.6) [7]	7.6 (4.9 – 10.9) [7]	10.8 (7.4 – 16.6) [7]	9.2 (3.0 – 13.1) [6]
4 m	3.9 (1.6 – 7.5) [5]	3.1 (1.5 – 4.7) [6]	3.6 (0.8 – 7.0) [6]	5.6 (1.6 – 8.5) [6]	3.7 (1.8 – 7.9) [6]
^{226}Ra					
Surface	0.5 (0.5 – 0.6) [3]	0.2 (N/A) [1]	0.4 (0.3 – 0.5) [2]	0.3 (0.3 – 0.4) [2]	0.17 (0.17 – 0.18) [2]
1 m	1.5 (0.6 – 2.4) [2]	N/A	2.6 (1.3 – 3.3) [4]	1.8 (1.4 – 2.8) [6]	0.9 (0.4 – 1.3) [5]
2 m	0.8 (0.5 – 1.1) [5]	0.5 (0.4 – 0.8) [7]	1.5 (1.0 – 2.2) [7]	1.2 (0.7 – 1.6) [7]	0.8 (0.1 – 1.6) [6]
4 m	0.6 (0.4 – 0.9) [5]	0.7 (0.4 – 0.9) [6]	1.2 (0.5 – 1.8) [6]	1.1 (0.4 – 1.6) [6]	0.8 (0.5 – 1.0) [6]
^{228}Ra					
Surface	0.9 (0.8 – 1.0) [3]	0.3 (N/A) [1]	0.9 (0.6 – 1.3) [2]	0.6 (0.5 – 0.6) [2]	0.3 (0.3 – 0.4) [2]
1 m	7.8 (4.4 – 11.3) [2]	N/A	10.8 (9.8 – 12.1) [4]	11.3 (8.8 – 14.8) [7]	7.5 (6.3 – 10.2) [5]
2 m	5.6 (3.4 – 11.1) [5]	4.2 (2.1 – 10.1) [7]	8.8 (6.5 – 13.2) [7]	8.4 (6.4 – 12.7) [7]	8.9 (2.0 – 10.6) [6]
4 m	2.8 (1.0 – 3.7) [5]	2.8 (0.9 – 5.3) [6]	4.6 (0.9 – 9.4) [6]	4.8 (0.9 – 9.6) [6]	3.3 (1.1 – 7.0) [6]
$^{224}Ra/^{223}Ra$					
Surface	18.8 (15.1 – 24.3) [3]	32.7 (N/A) [1]	14.6 (10.3 – 18.9) [2]	26.7 (24.1 – 29.2) [2]	19.5 (10.9 – 28.2) [2]
1 m	23.3 (22.3 – 24.4) [2]	N/A	22.1(21.6 – 23.1) [3]	27.0 (16.5 – 43.0) [6]	30.9 (18.0 – 54.5) [5]
2 m	32.8 (26.8 – 39.3) [5]	42.7 (28.1 – 84.7) [7]	29.1 (23.0 – 37.9) [7]	29.1 (21.5 – 36.1) [7]	26.8 (12.6 – 42.0) [6]
4 m	19.4 (12.7 – 30.4) [5]	26.2 (19.5 – 32.7) [5]	22.0 (5.4 – 35.0) [5]	23.1 (14.8 – 38.1) [6]	22.7 (13.3 – 33.2) [5]

Table A.3. Continued.

$^{228}Ra/^{226}Ra$					
Surface	1.7 (1.5 – 1.8) [3]	1.5 (N/A) [1]	2.1 (1.7 – 2.5) [2]	1.8 (1.7 – 1.9) [2]	1.9 (1.7 – 2.1) [2]
1 m	6.0 (4.7 – 7.3) [2]	N/A	4.7 (3.1 – 8.2) [4]	6.5 (3.1 – 8.0) [6]	10.6 (5.5 – 19.0) [5]
2 m	7.5 (5.5 – 10.1) [5]	7.6 (4.9 – 13.0) [7]	6.0 (4.6 – 8.4) [7]	7.4 (4.8 – 9.3) [7]	8.9 (5.9 – 18.5) [6]
4 m	4.4 (2.8 – 5.8) [5]	4.0 (2.4 – 5.8) [6]	3.5 (1.6 – 6.1) [6]	3.9 (2.1 – 5.8) [6]	3.8 (2.1 – 6.5) [6]

[1]Data under each sample date/location combination are the mean of all values at that location followed by the minimum – maximum (in parentheses) and finally the number of measurements that comprise the mean [in square brackets].

Table A.4: Seasonal Salinity, Temperature (°C), pH, and Redox Potential (mV) in Surface Water and Porewater[1]

Salinity	Nov 2009	Mar 2010	Jul 2010	Oct 2010	Feb 2011
Surface	31.2 (29.0 – 32.6) [3]	32.1 (N/A) [1]	35.2 (34.4 – 35.9) [2]	24.8 (19.7 – 29.9) [2]	32.4 (29.8 – 34.9) [2]
1 m	32.2 (31.7 – 32.6) [2]	N/A	34.7 (33.5 – 35.5) [4]	35.1 (27.3 – 37.6) [7]	35.2 (34.3 – 36.3) [5]
2 m	33.0 (32.2 – 34.9) [5]	33.7 (31.4 – 35.2) [7]	33.6 (25.6 – 35.9) [7]	36.2 (34.4 – 37.9) [7]	35.3 (33.7 – 36.5) [6]
4 m	32.9 (32.2 – 33.9) [5]	34.7 (34.0 – 35.5) [6]	35.0 (34.0 – 36.0) [6]	35.7 (34.2 – 36.5) [6]	35.0 (34.0 – 36.1) [6]
Temperature					
Surface	18.8 (17.7 – 20.7) [3]	18.0 (N/A) [1]	29.2 (28.3 – 30.0) [2]	25.3 (24.5 – 26.0) [2]	15.1 (14.6 – 15.6) [2]
1 m	21.8 (21.8 – 21.8) [2]	N/A	30.2 (29.5 – 30.7) [4]	26.1 (24.7 – 28.2) [7]	21.9 (18.4 – 23.6) [5]
2 m	21.7 (19.8 – 23.2) [5]	19.0 (16.4 – 22.7) [7]	26.9 (23.0 – 31.0) [7]	25.5 (24.7 – 26.7) [7]	19.1 (17.2 – 21.0) [6]
4 m	21.8 (21.4 – 22.3) [5]	18.6 (16.4 – 20.8) [6]	24.6 (22.8 – 30.5) [6]	24.2 (22.2 – 27.2) [6]	21.4 (20.0 – 22.6) [6]
pH					
Surface	7.9 (7.8 – 8.0) [3]	7.8 (N/A) [1]	7.6 (7.4 – 7.8) [2]	7.5 (7.3 – 7.7) [2]	7.6 (N/A) [1][2]
1 m	8.2 (8.1 – 8.2) [2]	N/A	6.9 (6.8 – 7.0) [4]	7.2 (6.7 – 7.7) [7]	7.4 (7.3 – 7.5) [4][2]
2 m	7.7 (7.4 – 8.0) [5]	7.7 (7.4 – 8.0) [7]	6.8 (6.6 – 7.4) [7]	6.8 (6.5 – 7.0) [7]	6.7 (6.6 – 7.0) [3][2]
4 m	7.7 (7.4 – 8.2) [5]	7.7 (7.3 – 8.1) [6]	6.8 (6.7 – 7.0) [6]	6.9 (6.6 – 7.3) [6]	7.0 (6.9 – 7.2) [5][2]
Redox Pot.					
Surface	88 (72 – 104) [3]	50 (N/A) [1]	47 (43 – 50) [2]	71 (41 – 100) [2]	46 (N/A) [1][2]
1 m	-293 (344 – 241) [2]	N/A	-310 (329 – 273) [4]	-297 (351 – 198) [7]	-284 (292 – 267) [3][2]
2 m	-258 (400 – 148) [5]	-298 (412 – 139) [7]	-314 (379 – 203) [7]	-334 (370 – 298) [7]	-281 (366 – 225) [3][2]
4 m	-300 (396 – 15) [5]	-368 (402 – 342) [6]	-333 (360 – 315) [6]	-333 (363 – 306) [6]	-319 (390 – 214) [4][2]

[1]Data under each sample date/location combination are the mean of all values at that location followed by the minimum – maximum (in parentheses) and finally the number of measurements that comprise the mean [in square brackets].

[2]Differences in [n] values due to instrument failure in the field.

Table A.5. Tide and well data used with Eq. A.3 to determine hydraulic diffusivity.

Location	a_o (m)[1]	a (m)[2]	x (m)[3]
Surface Water	0.7	--	--
EW1-4m	--	0.14	25
EW2-4m	--	0.07	57
NS2-4m	--	0.0001	88 (105)[4]
EW3-4m	--	0.04	73
EW4-4m	--	0.12	20

[1] a_o is the amplitude of the tide (m).

[2] a is the adjusted amplitude in the 4 m piezometers (m), see Appendix A text for details.

[3] x distances (m) measured along the E-W transect from the shoreline of Town Creek to the west or the small un-named creek to the east and ending at piezometer nest NS2

[4] The two different distances listed for NS2-4m reflect the measured length from the west and from the east (in parentheses).

Table A.6. Results of Tide and Well Record Harmonic Analyses[1]

		M2 Component		S2 Component		K1 Component		O1 Component	
Date Range	Location	Amp (m)	Phase (rad)	Amp (m)	Phase (rad)	Amp (m)	Phase (rad)	Amp (m)	Phase (rad)
10/21 to 12/13/07	Surf. Water	0.582	4.4	0.099	4.5	0.115	2.3	0.071	2.6
	EW1-2m	0.168	4.9	0.033	4.6	0.050	2.3	0.045	2.6
	EW1-4m	0.188	4.9	0.034	4.7	0.053	2.3	0.046	2.6
	EW4-2m	0.201	4.9	0.036	4.6	0.055	2.3	0.050	2.6
	EW4-4m	0.228	4.8	0.039	4.7	0.058	2.3	0.050	2.6
1/1 to 3/1/08	Surf. Water	0.646	4.2	0.132	4.9	0.109	2.7	0.087	2.5
	EW1-4m	0.121	4.4	0.026	5.0	0.038	2.5	0.032	2.2
	EW4-2m	0.130	4.3	0.028	4.9	0.042	2.5	0.036	2.2
	EW4-4m	0.159	4.4	0.031	5.0	0.045	2.5	0.039	2.2

[1]Results obtained using the MATLAB Program T_Tide (Pawlowicz et al., 2002). See Appendix text for details.

Table A.7. Terms used in RMS equation to determine hydraulic diffusivity and hydraulic conductivity

Date Range	Location	M2 Component			S2 Component			K1 Component			O1 Component			Dist.	D^*[4]	K[5]
		k[1] (m^{-1})	θ[2] (m^{-1})	A[3]	k[1] (m^{-1})	θ[2] (m^{-1})	A[3]	k[1] (m^{-1})	θ[2] (m^{-1})	A[3]	k[1] (m^{-1})	θ[2] (m^{-1})	A[3]	x (m)	(m^2/s)	(m/s)
10/21 - 12/13/07	EW1-2m	0.019	0.05	2.7	0.006	0.04	7.7	0.002	0.03	15.5	0.001	0.02	17.7	25	0.051	$5x10^{-5}$
	EW1-4m	0.021	0.05	2.2	0.008	0.04	5.1	0.000	0.03	93.3	0.000	0.02	176.1	25	0.058	$6x10^{-5}$
	EW4-2m	0.024	0.05	2.2	0.008	0.05	6.7	0.001	0.04	55.3	0.002	0.02	11.6	20	0.042	$4x10^{-5}$
	EW4-4m	0.020	0.05	2.3	0.009	0.05	5.2	0.001	0.03	27.7	0.003	0.02	6.1	20	0.055	$6x10^{-5}$
1/1 - 3/1/08	EW1-4m	0.007	0.07	9.5	0.002	0.06	27.7	0.009	0.04	4.9	0.013	0.04	3.1	25	0.031	$3x10^{-5}$
	EW4-2m	0.019	0.08	4.3	0.001	0.08	65.2	0.013	0.05	3.7	0.017	0.04	2.6	20	0.021	$2x10^{-5}$
	EW4-4m	0.017	0.07	4.1	0.006	0.07	13.0	0.011	0.04	4.0	0.014	0.04	2.8	20	0.027	$3x10^{-5}$

[1] k_i: wave number of the i^{th} component of the tidal signal in the well (m^{-1})
[2] θ: tidal amplitude decay constant within aquifer (m^{-1})
[3] A_i: [θ/k] tidal efficiency within the aquifer (dimensionless)
[4] D^*: hydraulic diffusivity (m^2/s)
[5] K: hydraulic conductivity (m/s)

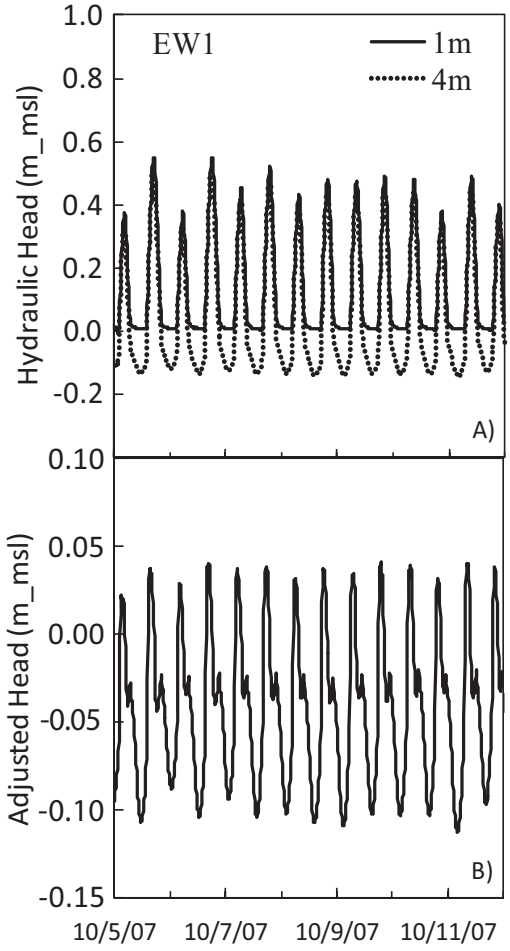

Figure A.1

Figure A.1. A) Hydraulic head at piezometer nest EW1 for a seven-day period. B) Adjusted hydraulic head for EW1-4m (see Appendix A text).

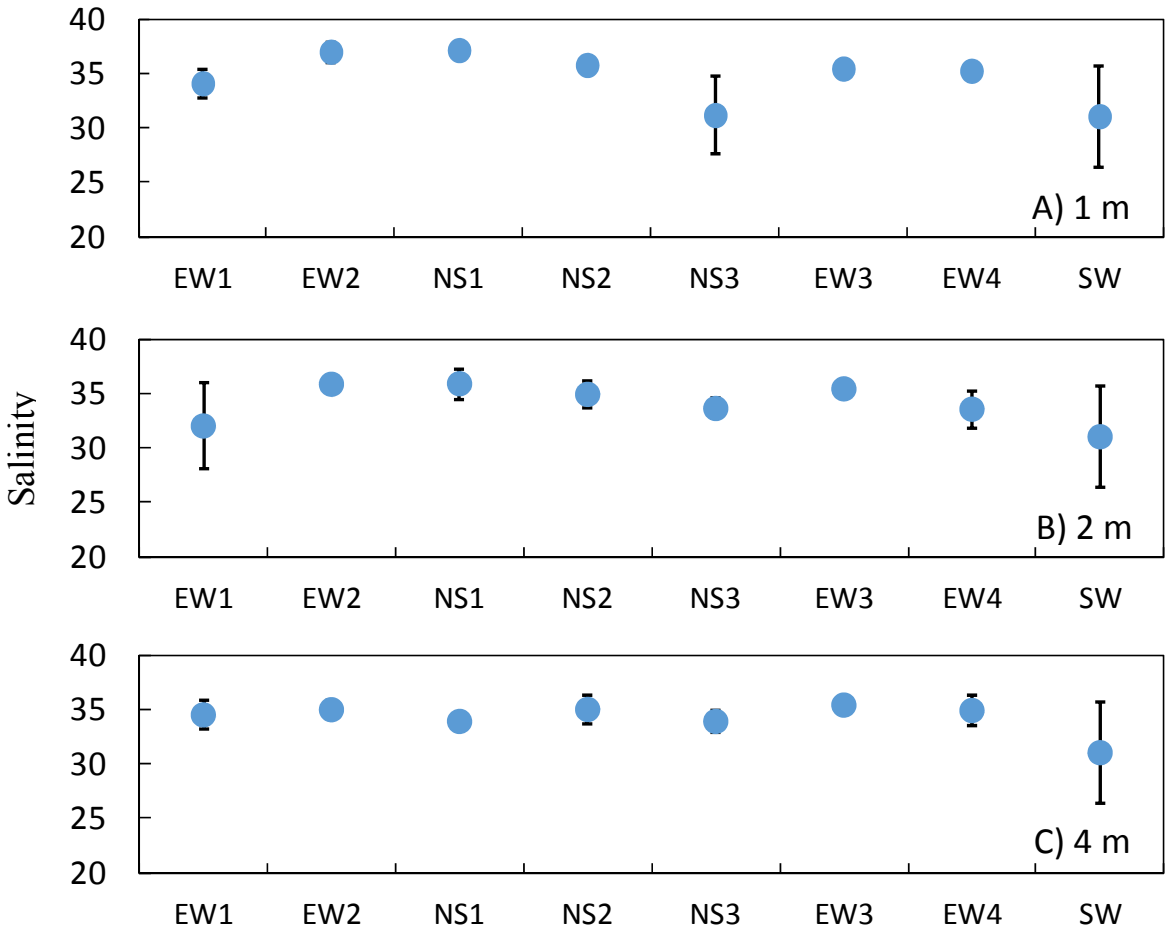

Figure A.2. Mean salinity by piezometer nest location at A) 1 m, B) 2 m, and C) 4 m. Mean surface water values are included in each plot for comparison. Symbols represent the mean at each piezoemter nest/depth combination and in the surface water over the course of the study ± 1 standard deviation.

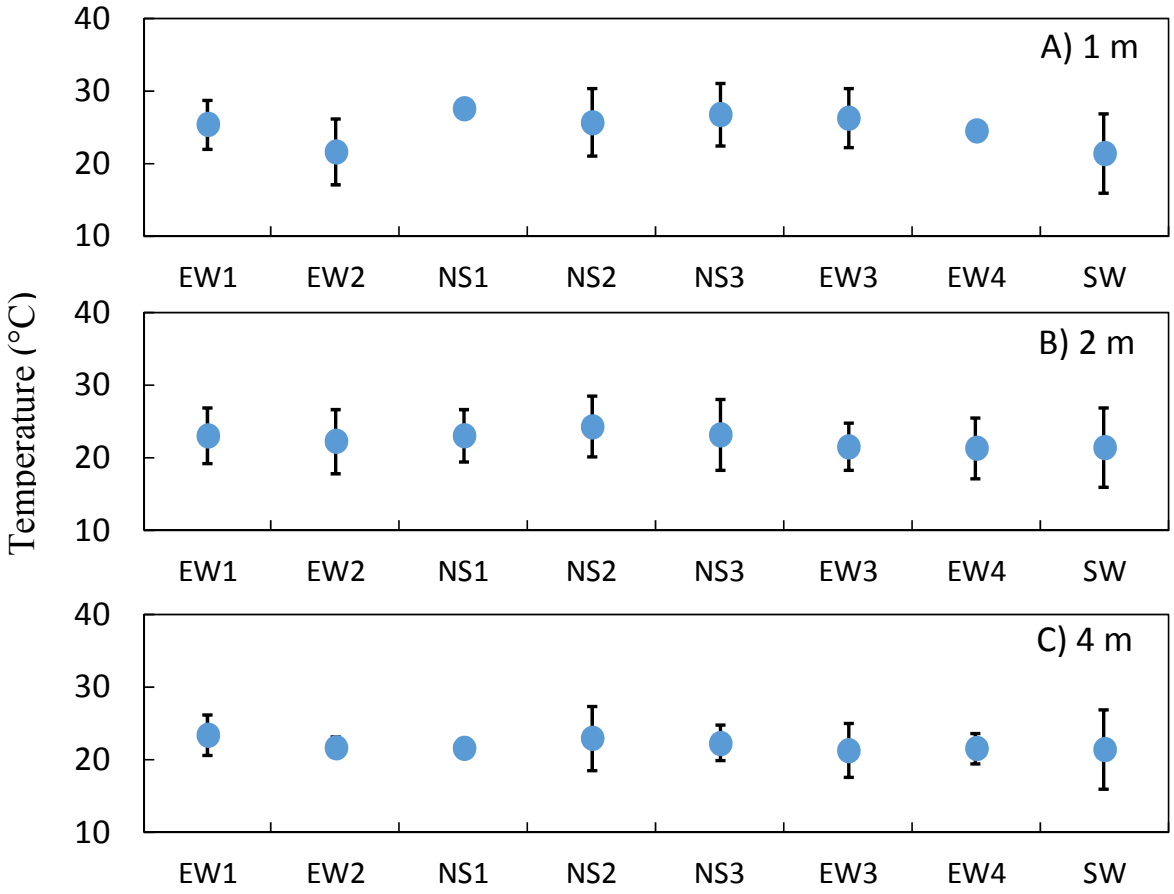

Figure A.3. Mean temperature by piezometer nest location at A) 1 m, B) 2 m, and C) 4 m. Mean surface water values are included in each plot for comparison. Symbols represent the mean at each piezoemter nest/depth combination and in the surface water over the course of the study ± 1 standard deviation.

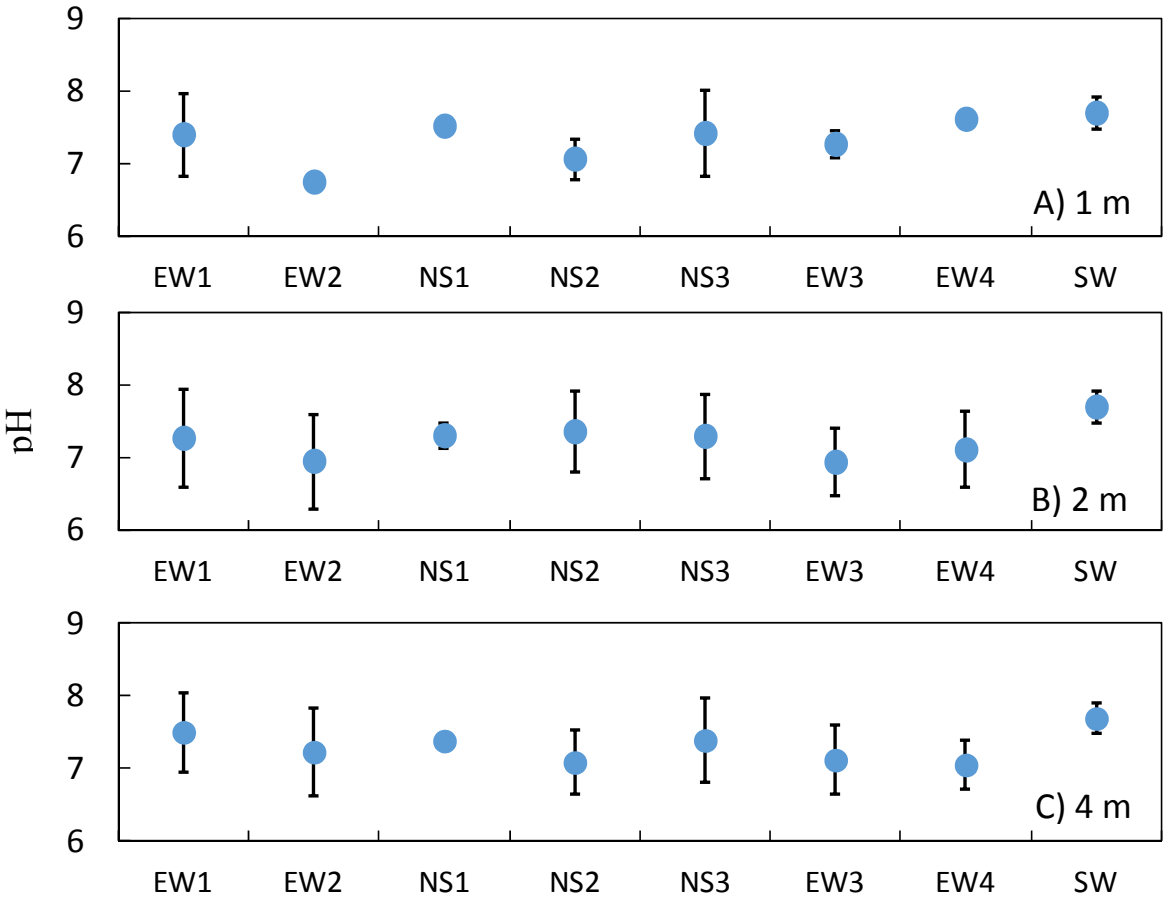

Figure A.4. Mean pH by piezometer nest location at A) 1 m, B) 2 m, and C) 4 m. Mean surface water values are included in each plot for comparison. Symbols represent the mean at each piezoemter nest/depth combination and in the surface water over the course of the study ± 1 standard deviation.

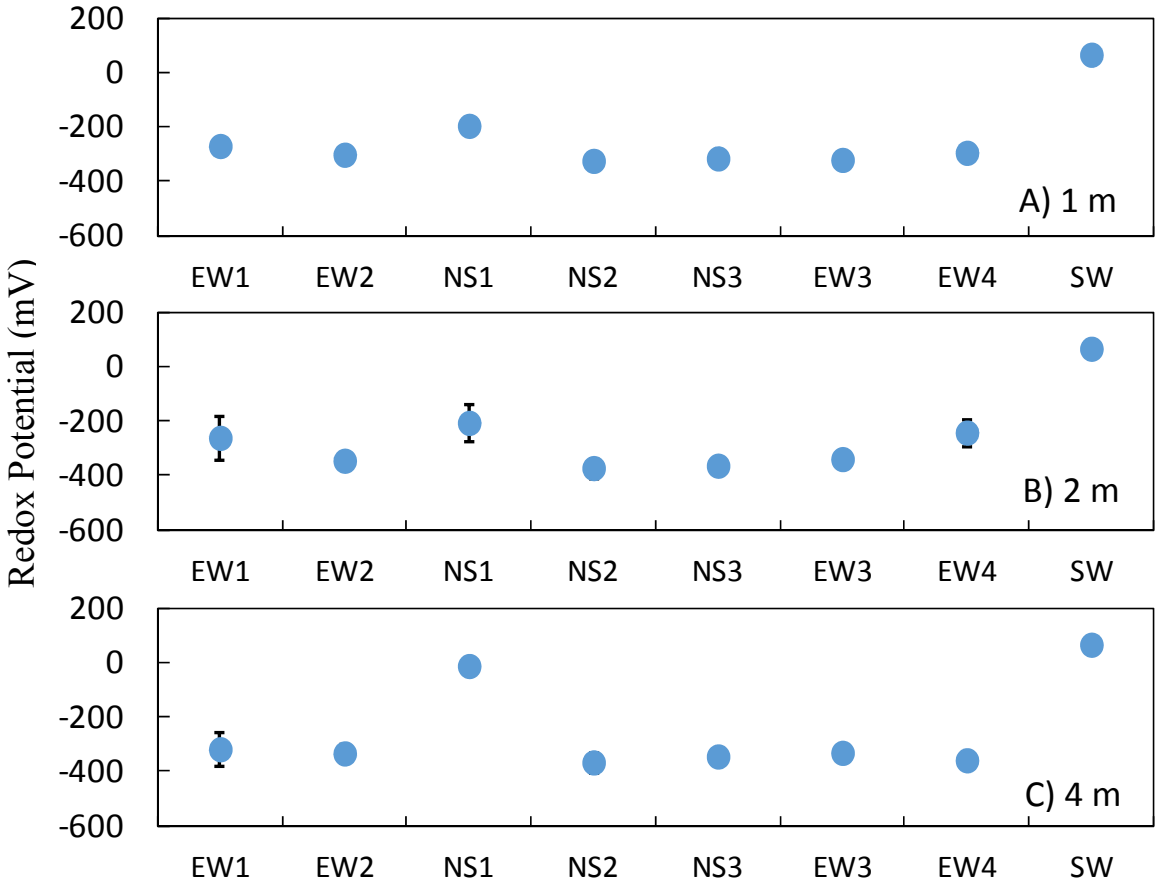

Figure A.5. Mean redox potential by piezometer nest location at A) 1 m, B) 2 m, and C) 4 m. Mean surface water values are included in each plot for comparison. Symbols represent the mean at each piezoemter nest/depth combination and in the surface water over the course of the study ± 1 standard deviation.

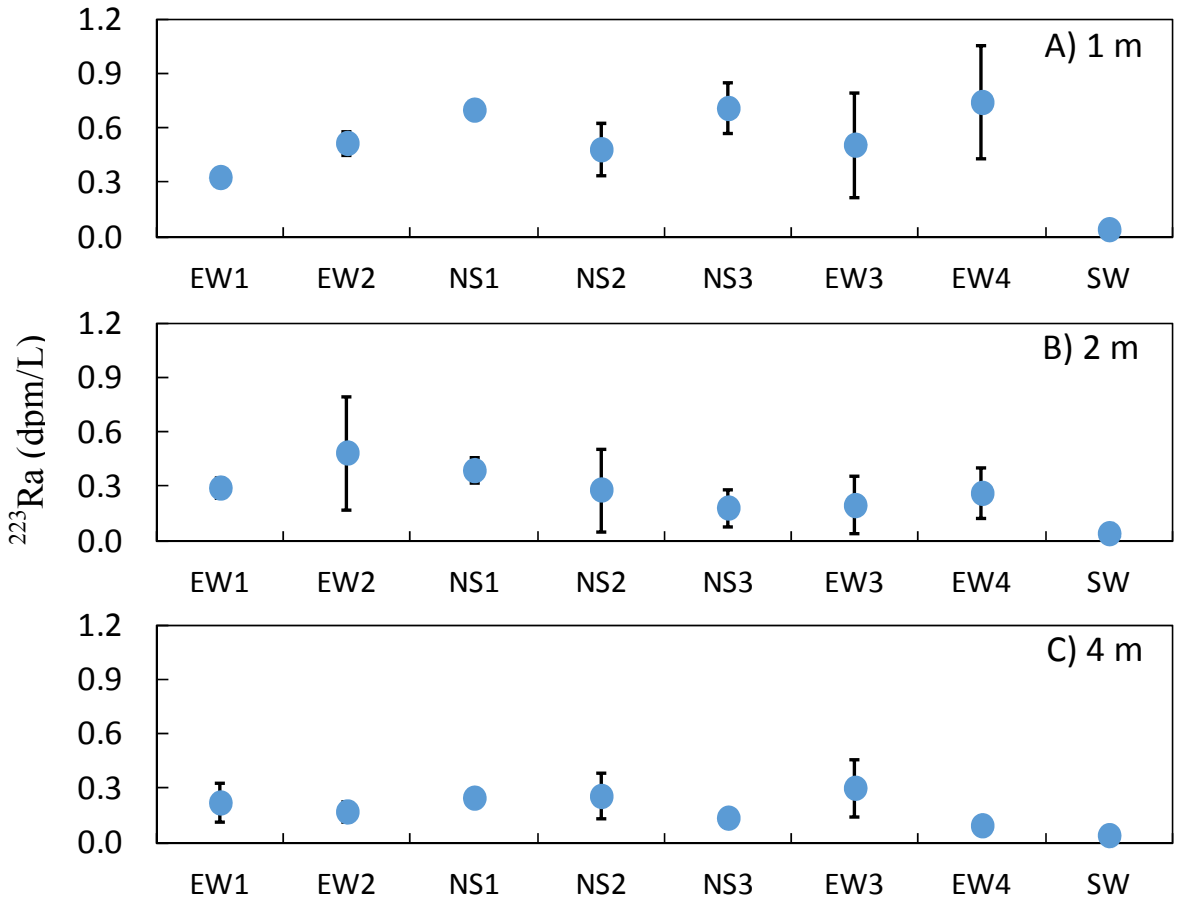

Figure A.6. Mean ^{223}Ra activity by piezometer nest location at A) 1 m, B) 2 m, and C) 4 m. Mean surface water values are included in each plot for comparison. Symbols represent the mean at each piezoemter nest/depth combination and in the surface water over the course of the study ± 1 standard deviation.

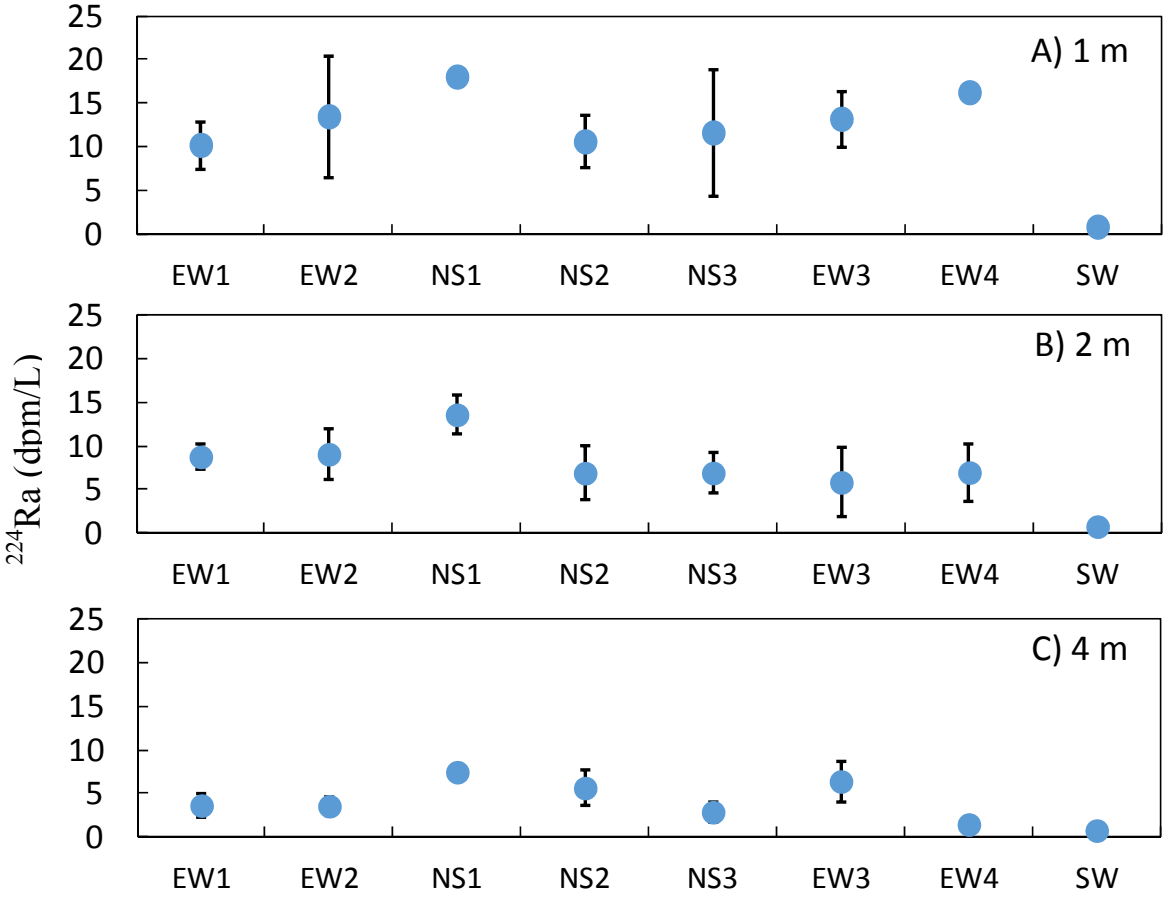

Figure A.7. Mean ^{224}Ra activity by piezometer nest location at A) 1 m, B) 2 m, and C) 4 m. Mean surface water values are included in each plot for comparison. Symbols represent the mean at each piezoemter nest/depth combination and in the surface water over the course of the study ± 1 standard deviation.

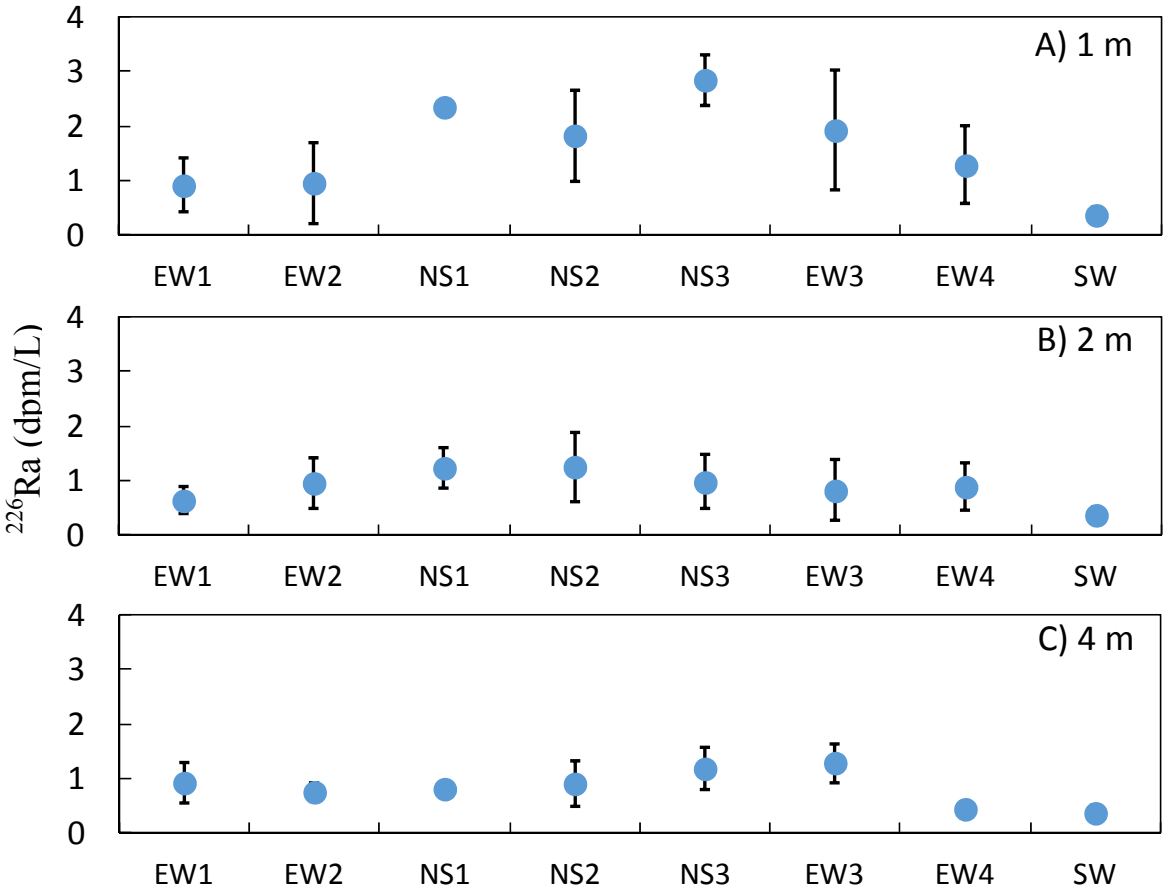

Figure A.8. Mean ^{226}Ra activity by piezometer nest location at A) 1 m, B) 2 m, and C) 4 m. Mean surface water values are included in each plot for comparison. Symbols represent the mean at each piezoemter nest/depth combination and in the surface water over the course of the study ± 1 standard deviation.

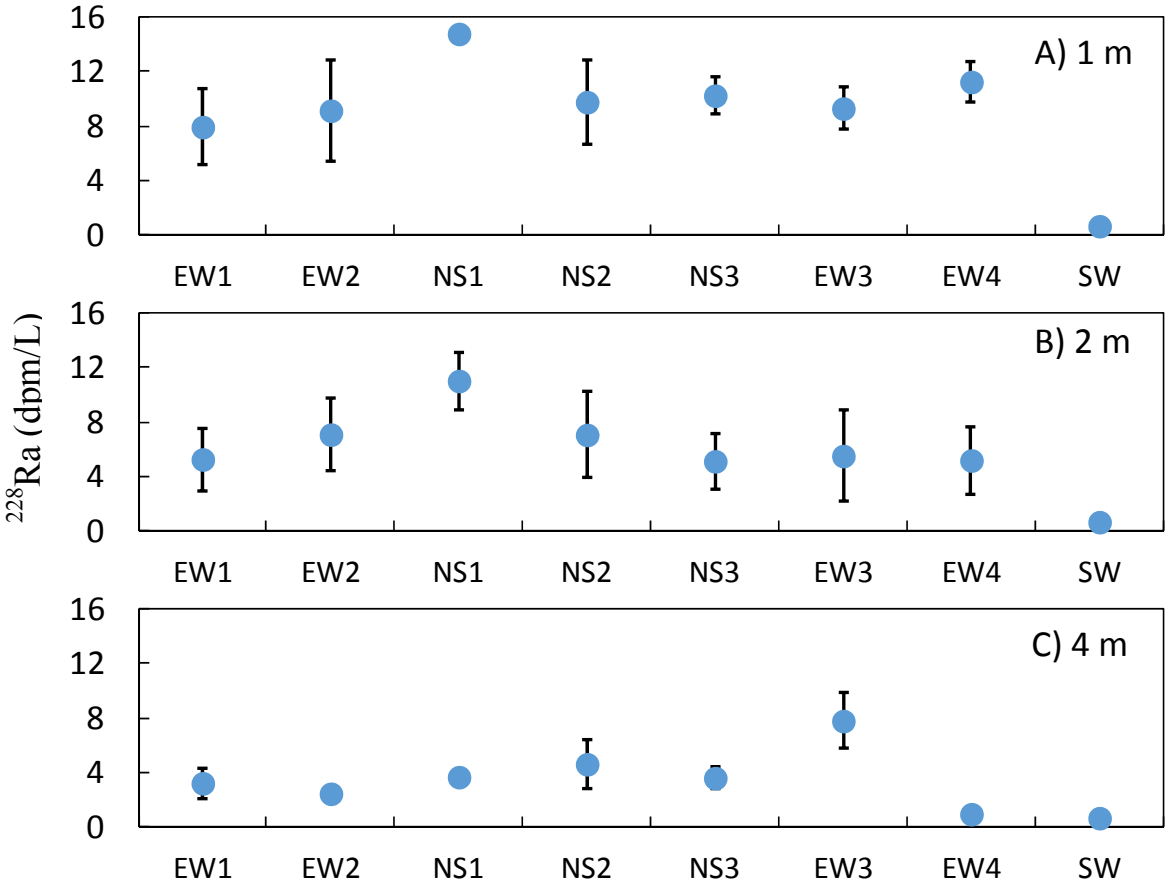

Figure A.9. Mean ^{228}Ra activity by piezometer nest location at A) 1 m, B) 2 m, and C) 4 m. Mean surface water values are included in each plot for comparison. Symbols represent the mean at each piezoemter nest/depth combination and in the surface water over the course of the study ± 1 standard deviation.

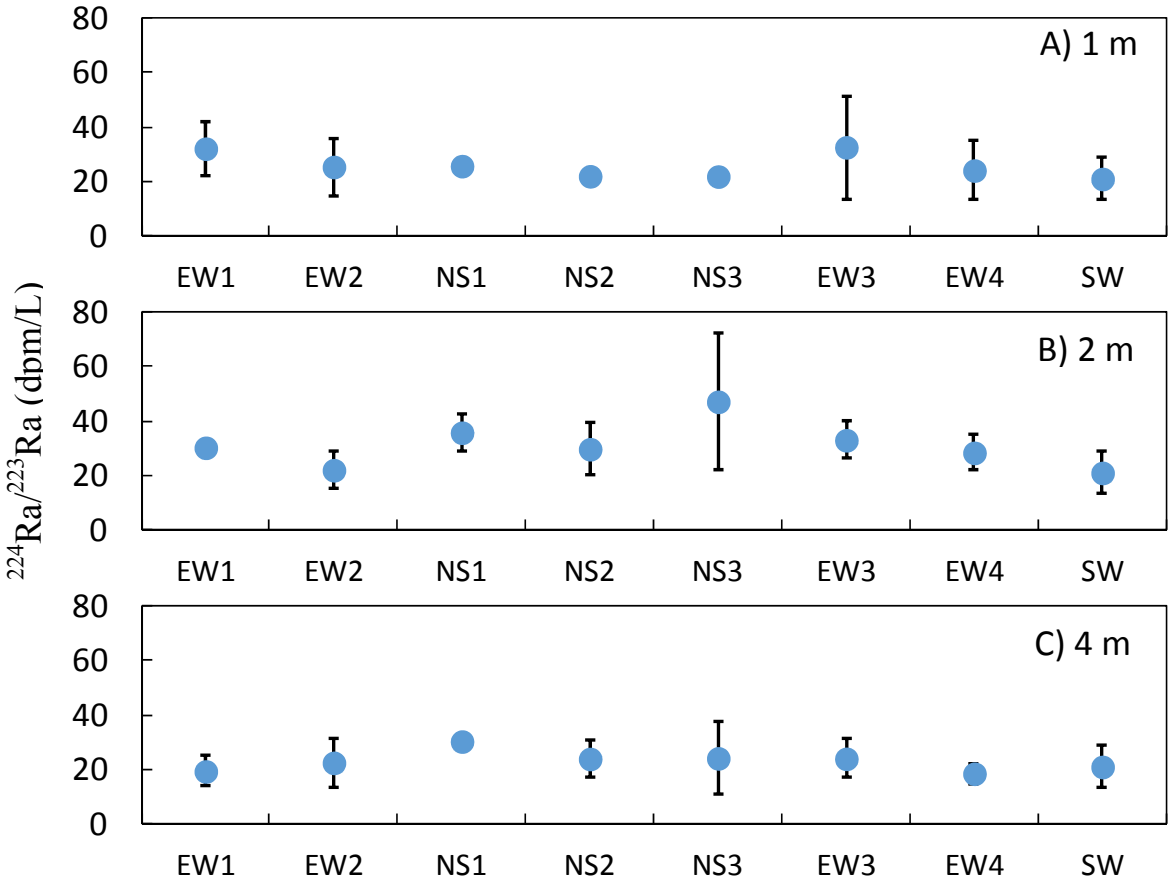

Figure A.10. Mean ^{224}Ra/^{223}Ra activity ratios by piezometer nest location at A) 1 m, B) 2 m, and C) 4 m. Mean surface water values are included in each plot for comparison. Symbols represent the mean at each piezoemter nest/depth combination and in the surface water over the course of the study ± 1 standard deviation.

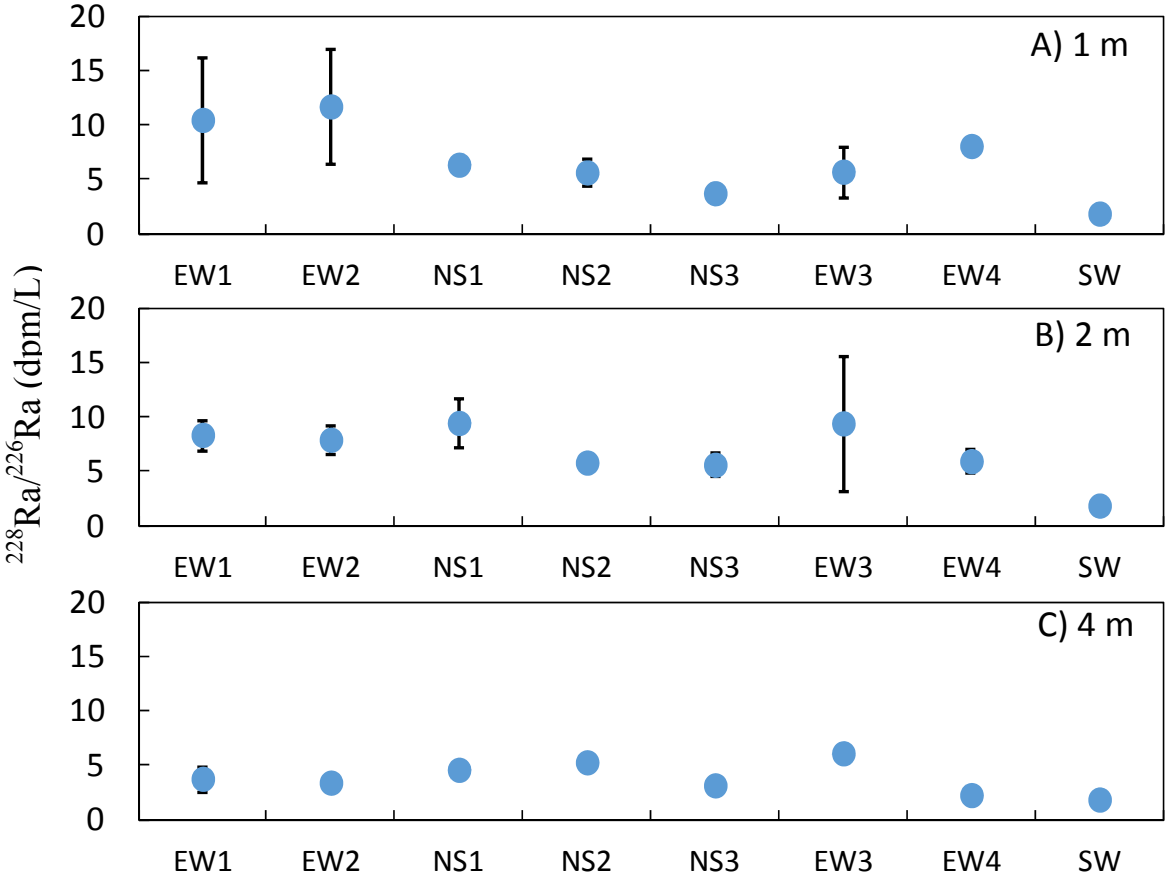

Figure A.11. Mean ^{228}Ra/^{226}Ra activity ratios by piezometer nest location at A) 1 m, B) 2 m, and C) 4 m. Mean surface water values are included in each plot for comparison. Symbols represent the mean at each piezoemter nest/depth combination and in the surface water over the course of the study ± 1 standard deviation.

APPENDIX B

DEVELOPMENT OF REGRESSION MODEL FOR K_D-TEMPERATURE RELATIONSHIP, ANALYTICAL EQUATION METHOD FOR TEMPERATURE, AND ANALYSIS OF THE RELATIVE IMPORTANCE OF THE MODEL GOVERNING EQUATION TERMS[1]

[1] Hughes, Andrea L. H., Alicia M. Wilson, and Willard S. Moore, Unpublished. Reconciling hydrologic and geochemical estimates of submarine groundwater discharge: A coupled model of groundwater flow and radium transport

B.1 Development of Regression Equation

At North Inlet salt marsh, temperature was found to control Ra distribution coefficient (K_d) values (Rama and Moore, 1996), and temperature was the only factor, along with groundwater discharge, that provided a significant control on porewater Ra activity (Hughes et al., 2015). Therefore, we developed a regression equation between the calculated Ra K_d values and the measured temperatures for each sample collected during 2009 – 2011. The distribution coefficient of Ra (m^3/kg) is the ratio of Ra activity sorbed to sediment (dps/kg) over porewater Ra activity (dps/m^3). Ra activity sorbed to sediment (A_i) was calculated as the difference between the calculated equilibrium activity of Ra (C_t) when there is no sorption to sediment and the porewater measurements of Ra activity (C_i) [$A_i = C_t - C_i$]. The equilibrium activities for ^{223}Ra, ^{224}Ra and ^{228}Ra were calculated using the following equation:

$$A_{Ra}(t) = \left(1 - e^{-\lambda_{Ra} t}\right) A_{Th} \tag{B.1}$$

where A_{Ra} is the activity of Ra in porewater, λ_{Ra} is the Ra decay constant, and A_{Th} is the activity of the parent Thorium (Th) isotope (the sediment generation rate of Ra). Figure B.1 shows the plot of calculated K_d values versus temperature measurements for all of the samples collected from 2009 – 2011. The plot also contains the regression line and equation, and the significance of the association. The resulting regression equation (Eq. 3.9) is presented in the manuscript.

B.2 USE OF ANALYTICAL SOLUTION TO HEAT TRANSPORT EQUATION

The version of SUTRA used in this study is capable of modeling either energy (heat) or solute transport—but not both. Therefore, the model code was modified to incorporate an analytical solution to the heat equation (Carslaw and Jaeger, 1959) for use in the regression equation (Eq. 3.9):

$$T(y,t) = T_{mean} + T_{amp} exp\left(-y\sqrt{\frac{\omega}{2\kappa}}\right) cos\left(\omega(t - t_0) - y\sqrt{\frac{\omega}{2\kappa}}\right) \quad \text{(B.2)}$$

where T_{mean} (20 °C) is the mean temperature in the domain, T_{amp} (10 °C) is the amplitude of the temperature variations at the surface of the domain, ω is angular frequency, κ is thermal dispersivity (1.2 x 10^{-6} m^2/s), y is the depth below the sediment surface, t is lapsed time (s), and t_0 is the time offset (155 days = -1.3392 x 10^7 s). Angular frequency is $2\pi/\tau$, where τ is the cosine wave period (365 days = 3.1536 x 10^7 s). The time offset is used to match the domain surface temperature to the average surface water temperature for the system. In other words, it sets the cosine wave so that it begins at the average surface water temperature at 1January (T(0,0)). The surface boundary condition is defined as:

$$T(0,t) = T_{mean} + T_{amp} cos\big(\omega(t - t_0)\big) \quad \text{(B.3)}$$

Figure B.2 compares measurements of and simulation results for surface water and porewater temperature at 1, 2, and 4 m below the marsh surface at the central piezometer

nest (NS2), demonstrating that the analytic solution generates a good approximation of the temperature.

B.3 Analysis of Relative Importance to Terms in Model Governing Equation

As stated in the Materials and Methods section, this version of Sutra is missing the second term $\left(C_{aq}\frac{\partial K_d}{\partial T}\frac{\partial T}{\partial t}\right)$ of Equation 3.10, which is the time-varying Ra distribution coefficient as a function of varying temperature. In order to understand how the exclusion of this term would impact modeled porewater Ra activity, Equation 3.10 was combined with Equation 3.7 (the advection-dispersion equation) resulting in 5 terms on the right-hand side: generation, decay, dispersion, advection, and the time-varying adsorption/desorption term as shown above. We excluded the dispersion term from the analysis of the relative importance of these terms because dispersion is typically orders of magnitude smaller than generation, decay, or advection. The generation and decay terms were calculated using prior sediment measurements and the known isotope decay constants. The advection term was calculated using the vertical activity gradient determined from Ra activity measurements between the 1 and 4 m piezometers $\left({\partial C_{aq}}/{\partial x}\right)$ and the average velocity at the center of the marsh island determined from the groundwater flow model. Finally, for this analysis, the time-varying K_d term was calculated using a constant value obtained from the regression equation and from the analytic solution to the heat equation discussed above. The combined advection-dispersion equation was solved on a daily time step for ^{223}Ra and ^{224}Ra and a yearly time step for ^{228}Ra and until Ra activity for all three isotopes had reached equilibrium. Table B.1 lists the values for the individual terms at equilibrium for ^{223}Ra, ^{224}Ra and ^{228}Ra. Our

results indicate that for ^{223}Ra and ^{224}Ra, the generation and decay terms are nearly equal and the advection and adsorption/desorption terms are from two to five orders of magnitude lower. For ^{228}Ra, the adsorption/desorption term is equivalent to the generation term. Therefore, the version of Sutra used for this work would produce inaccurate results for ^{228}Ra because this additional component of the adsorption/desorption equation is not included. These results mean that ^{228}Ra was excluded from the modeling work in this study.

Table B.1. Analysis of Relative Importance of Advection-Dispersion Equation Terms[1]

Isotope	Generation Term	Radium Decay Term	Radium Advection Term	Radium Adsorption/ Desorption Term
^{223}Ra	1.0	0.99854	6.25×10^{-5}	1.45×10^{-2}
^{224}Ra	22.8	22.691	5.11×10^{-3}	1.06×10^{-1}
^{228}Ra	27.9	8.06	1.71	21.51

[1]Units for each term are activity of Ra per kg of fluid [dps/kg_f]. All activities originally in dps/kg_s (kg of sediment) are converted to fluid mass units by assuming a porosity of 0.50, a sediment density of 2600 kg/m^3, and fluid density of 1026.7 kg/m^3.

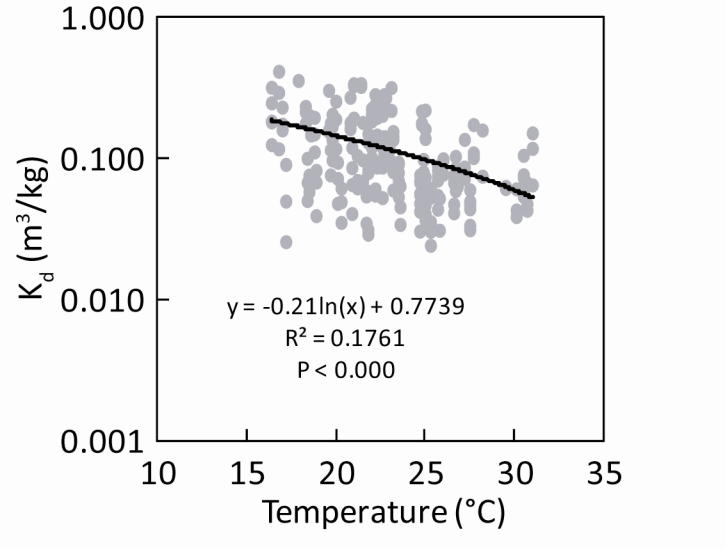

Figure B.1 Plot of Ra distribution coefficients (K_d) versus temperature for each porewater Ra sample collected during 2009 – 2011. Regression equation, r^2 value, and relationship significance are shown on the plot.

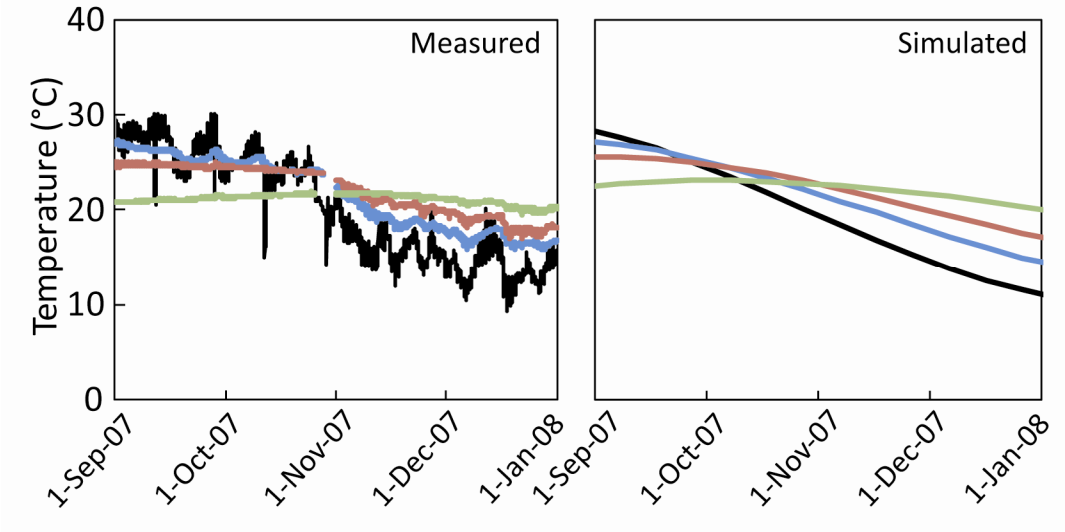

Figure B.2 Plots of measured versus simulated temperature. The temperature was measured in-situ at piezometer nest NS2, and an analytical solution to the heat equation was used to simulate temperature over the same period.

APPENDIX C

PERMISSION TO REPRINT[6]

[6] Elsevier is the publisher for Estuarine, Coastal and Shelf Science in which the first two chapters are published or in press.

C.1 COPYRIGHT E-MAIL

Department of Earth and Ocean Sciences
UNIVERSITY OF SOUTH CAROLINA

Andrea Hughes <ahughes@geol.sc.edu>

copyright permission for an article accepted but not yet typset

Permissions Helpdesk <permissionshelpdesk@elsevier.com> Tue, Jun 9, 2015 at 11:19 AM
To: Andrea Hughes <ahughes@geol.sc.edu>

Dear Ms. Hughes:

As an Elsevier journal author, you retain various rights including inclusion of the article in a thesis or dissertation (provided that this is not to be published commercially) whether in part or *in toto*; see http://www.elsevier.com/about/company-information/policies/copyright#Author%20rights for more information. As this is a retained right, no written permission is necessary provided that proper acknowledgement is given.

If I may be of further assistance, please let me know.

Best of luck with your thesis and best regards,

Hop

Hop Wechsler

Permissions Helpdesk Manager

Elsevier

1600 John F. Kennedy Boulevard

Suite 1800

Philadelphia, PA 19103-2899

Tel: +1-215-239-3520

Mobile: +1-215-900-5674

Fax: +1-215-239-3805

E-mail: h.wechsler@elsevier.com

Contact the Permissions Helpdesk:

+1-800-523-4069 x 3808 *permissionshelpdesk@elsevier.com*

From: Andrea Hughes [mailto:ahughes@geol.sc.edu]